Summer 2021

Human CST (CTC1-STN1-TEN1) Promotes TopBP1 Stability and CHK1 Phosphorylation in Response to Telomere Dysfunction and Global Replication Stress

Stephanie Michelle Ackerson

HUMAN CST (CTC1-STN1-TEN1) PROMOTES TOPBP1 STABILITY AND CHK1 PHOSPHORYLATION IN RESPONSE TO TELOMERE DYSFUNCTION AND GLOBAL REPLICATION STRESS

by

Stephanie Michelle Ackerson

Bachelor of Science
Wofford College, 2015

Bachelor of Arts
Wofford College, 2015

Submitted in Partial Fulfillment of the Requirements

For the Degree of Doctor of Philosophy in

Biological Sciences

College of Arts and Sciences

University of South Carolina

2021

Accepted by:

Jason Stewart, Major Professor

David Reisman, Committee Member

Rekha Patel, Committee Member

Alan Waldman, Committee Member

Douglas Pittman, Committee Member

Tracey L. Weldon, Interim Vice Provost and Dean of the Graduate School

DEDICATION

This work is dedicated to my incredible family and friends, without whom I would not be here today. I can't possibly name all of the people that have touched my life and helped me get here. So, thank you. From the bottom of my heart, thank you for everything.

To my parents, Marti and Michael Ackerson, my siblings, Allison, Tiffany, and Courtney, and all of my extended family. Thank you for always supporting my curiosity and passion for biology. Thank you for the support on not only my best days, but also my worst. You have always been here for me when I need you most and always reminded me that getting a PhD is difficult, so I should be proud of what I'm doing. Thank you for all the hugs, words, and gifs of encouragement. Every little thing every single day has kept me going and I will never be able to put into words how much you mean to me.

To Michelle Spigner, you are the reason I am here today. My high school magnet program superlative was "Most Likely to Emulate Mrs. Spigner in the Future" and I am proud to see that it still holds true. Your sophomore biology class was what began this all. You made biology come to life for me, and I will forever be grateful that you let me all but live in your classroom for the 2 years after that. Thank you for the day you had me take over your lecture. That was the moment I realized I wanted to teach biology and make it fun for all of my students, just like you did for me.

ACKNOWLEDGEMENTS

I would like to first thank my advisor, Dr. Jason Stewart. Thank you for taking a chance on the random college graduate that emailed asking to volunteer in your lab. We have been through so much together in the past 6 years and it has helped me become the scientist I am today. I cannot put into words how much your guidance and advice has helped me. Thank you for you unlimited patience for me and my dramatic outbursts. Thank you for replying “of course” when I dramatically said, as a tech, “Are you SURE you still want to take me on as a grad student?!” Thank you for letting me be your first graduate student. It has been an amazing journey.

To my committee members, Dr. Reisman, Dr. Waldman, Dr. Pittman, and Dr. Patel, thank you for all of your advice and feedback. You all are a wealth of knowledge and I am so appreciative that you have shared a portion of it with me. Thank you for your time, support, guidance, and for always challenging me to be the best scientist I can be.

To my fellow graduate student, Logan, thank you for putting up with me all these years. It’s been so much fun working 10 feet away from you. Thank you for the times you put treatments on my cells when I was teaching or had to go out of town you’re a life saver. Thank you for being my partner in crime. No matter how much we bicker or tease, I always knew I could count on you for support and memes. Together you and Jason made this lab my second home, so thank you.

To my minions, Caroline, Ben, Alex, Kaury, Anna, and Emma, thank you so much for always doing as I say and not as I do. I literally could not have done all of these experiments without your helping hands, emotional support, and love. The times we gathered to "spill the tea" in between incubation periods or right when we got into lab brought joy to my heart. Seeing you all grow as people and scientists just makes my heart so, so full. Continue to excel in everything you do. Your mom is proud.

To my family, go read the dedication. I love you all to the moon and back.

To the Bumble Bees plus Wasp, you have helped keep me sane (mostly). Thank you for always being here for me reminding me to eat or sleep. For sending COUNTLESS messages of love, laughter, and encouragement over the past 5 years. I couldn't have made it here without y'all, and I wouldn't have it any other way. To Bethan and Megan, thank you for being my friends for the past 16 and 12 years, respectively. We have grown up so much since middle and high school. Thank you for growing with me. To my pub family, especially Jim Daly, thank you for being my friends. Thank you for listening to my science-speak and encouraging me. Thank you for letting me work alone on days that I needed to, and for lending a listening ear when work was the last thing on my mind. Y'all are the best.

Finally, to my UofSC family, Kristen and Drew Hogan, Olivia Spead, Sam and Crystal Burnett, Kristiaän Merritt, Niti Jani, Andy Schumpert, Chad Beneker, Jessy Varghese, Jake Massey, Lindsay Sanchez, Jake Swanson, Nicole Reilly, Katie Monts, Grace Hollenbeck, Trevor Olsen, Irene Dalla Costa, Gus Martinez-Muniz, Ken Frederick, Lauren Price, Erin Anderson, Katelyn Rygel, Alissa Marchione, Alex Barth, Allie Culver, Claire Hann, Chad Simmons, Tancia Bradshaw, Maddy Janakis, Trinity Depatie,

Marj Peña, Fabienne Poulain, Deanna Smith, Shannon Davis, Josh Stone, Amanda Zeigler, Garrett Faulk, Tammi Richardson, Jeff Twiss, Mike Wyatt, Alissa Armstrong, Carolyn Banister, and Elizabeth Thames, thank you for being a wonderful part of my graduate school experience. You all have been wonderful friends and colleagues.

ABSTRACT

Genomic DNA is constantly damaged by both internal and external genotoxins and cellular processes. A consequence of unrepaired or misrepaired DNA damage is genome instability, a hallmark of cancer and numerous other diseases. Eukaryotic cells have developed complex mechanisms to repair DNA damage, which is collectively referred to as a DNA damage response (DDR). CST (CTC1-STN1-TEN1) is a heterotrimeric, RPA-like protein complex that binds to single stranded (ss)DNA. In humans, CST functions in the replication and maintenance of telomeres, structures found at the ends of linear chromosomes, as well as non-telomeric DNA. Previous studies showed that deletion of the largest CST subunit, CTC1, results in decreased cell proliferation and telomeric DNA damage signaling. However, the consequences of conditional CTC1 or STN1 knockout (KO) at the cellular level have not been fully elucidated. Consistent with previous findings, we demonstrate that CTC1 or STN1 KO results in decreased cell proliferation, G2 arrest and RPA-bound telomeric ssDNA, which should trigger a DDR through the ATR-CHK1 pathway. However, despite the increased levels of telomeric RPA-ssDNA, global ATR-dependent CHK1 and p53 phosphorylation was not detected in CTC1 and STN1 KO cells. Interestingly, we show that RPA-ssDNA still activates ATR, leading to the phosphorylation of RPA and autophosphorylation of ATR, and that G2 arrest is dependent on exhaustion of the telomere protection factor, POT1 in CTC1 KO cells. These results suggest that ATR is localized and active at RPA-bound telomeres but is unable to elicit a global checkpoint response through CHK1

Furthermore, CTC1 or STN1 KO inhibited CHK1 phosphorylation following replication stress due to decreased levels of the ATR activator TopBP1. Finally, we investigated whether the phenotypes caused by CTC1 deletion can potentially be rescued by various CTC1 mutant constructs. Preliminary studies find that TopBP1 levels can be restored with different mutant versions of CTC1, providing clues to how different CST domains may regulate the DDR. Overall, our results identify CST as a novel regulator of the ATR-CHK1 pathway.

TABLE OF CONTENTS

LIST OF TABLES

LIST OF FIGURES

LIST OF ABBREVIATIONS

9-1-1 Complex ..... RAD9-RAD1-HUS1 Complex

AAD ..... ATR Activating Domain

AND-1 ..... Acidic nucleoplasmic DNA-binding protein

ANOVA ..... Analysis of the Variance

ATM ..... Ataxia Telangiectasia Mutated

ATR ..... Ataxia Telangiectasia and Rad3 Related

ATMi ..... ATM inhibition

ATRi ..... ATR inhibition

ATRIP ..... ATR Interacting Protein

BrdU ..... Bromodeoxyuridine

CDC25A ..... Cell Division Cycle 25A

CDT1 ..... Chromatin Licensing and DNA replication factor 1

CHK1 ..... Checkpoint Kinase 1

CHK1i ..... CHK1 inhibition

CldU ..... 5'Chloro-2'-deoxyuridine

CMG ..... Cdc45-MCM-GINS4 Helicase

CP ..... Coats plus

CRMCC ..... Cerebroretinal microagiopathy with calcifications and cysts

CST CTC1-STN1-TEN1

CTC1 ..... Conserved Telomere Capping Protein 1

DAPI ..... 4’,6-diamino-2-phenylindole

DKC ..... Dyskeratosis congentia

DNA-PK ..... DNA-dependent Protein Kinase

DDR ..... DNA Damage Response

Doxy ..... Doxycycline

dsDNA ..... Double-Stranded DNA

DSBs ..... Double-Strand Breaks

EdU ..... 5-Ethynyl-2’-deoxyuridine

ETAA1 ..... Ewing’s Tumor-Associated Antigen 1

FISH ..... Fluorescent In Situ Hybridization

G4s ..... G-quadruplexes

HR ..... Homologous Recombination

HU ..... Hydroxyurea

IdU ..... Iododeoxyuridine

IF ..... Immunofluorescence

KO ..... Knockout

MCM ..... Minichromosome maintenance protein complex

MTS ..... Multiple Telomeric Signals

NHEJ ..... Non-homologous End Joining

OB-folds ..... Oligonucleotide-oligosaccharide Binding Folds

OE ..... Overexpressed

PARPi ..... poly(ADP-ribose) polymerase inhibitor

PBS ..... Phosphate-Buffered Saline

PBST .....Phosphate-Buffered Saline with Tween

PCR ..... Polymerase Chain Reaction

PIKK ..... Phosphatidylinositol-3-kinase-related kinase

POT1 ..... Protection of Telomere 1

qPCR ..... quantitative Polymerase Chain Reaction

RPA.....Replication Protein A

SEM .....Standard Error Mean

sgRNA..... Single Guide RNA

siRNA .....Small Interfering RNA

ssDNA..... Single Stranded DNA

SNPs.....Single nucleotide polymorphisms

STN1 ..... Suppressor of Cdc Thirteen

TAM.....Tamoxifen

TBST.....Tris-Buffered Saline with Tween

TEN1.....Telomere Length Regulation Protein

T-loop.....Telomere Loop

TopBP1 ..... Topoisomerase 2-Binding Protein 1

wHTH .....Winged Helix-Turn-Helix

CHAPTER 1

INTRODUCTION

1.1 DNA DAMAGE, AND THE ATR-MEDIATED DNA DAMAGE RESPONSE

DNA damage can arise from both endogenous and exogenous factors, such as replication stress, ionizing radiation and oxidation. To prevent genome instability and disease, cells have evolved elaborate signaling pathways to sense the damage, arrest the cell cycle and repair the DNA. This process, known as the DNA damage response (DDR), is primarily mediated by three members of the PIKK family, namely ATM, ATR and DNA-PK [1]. Activation of these kinases in response to DNA damage leads to the phosphorylation of downstream effectors and stabilization of the tumor suppressor, p53. p53 in turn induces transcription of downstream targets, such as p21, that facilitate cell cycle arrest and eventual apoptosis or senescence, if the damage is not resolved.

ATM and DNA-PK are primarily activated in response to double-strand breaks (DSBs), whereas ATR coordinates the repair of DNA damage arising from single stranded (ss)DNA gaps or breaks. ATR plays a primary role in managing replication stress during S-phase and is essential for the survival of dividing cells [2-4]. During S-phase, ssDNA can arise from uncoupling of the helicase from the replisome and nucleolytic processing of various replication and repair intermediates [5, 6]. Once exposed, large regions of ssDNA are quickly bound by the ssDNA binding protein, RPA (Figure 1.1) [7]. ATRIP then associates with the RPA-bound ssDNA (RPA-ssDNA), which localizes ATR [8]. Localization of ATR, however, is insufficient to fully activate ATR kinase activity.

In vertebrates, two major ATR activating proteins have been identified, TopBP1 and ETAA1 [9-12]. Both proteins contain ATR activating domains (AAD) that modulate ATR kinase activity [13]. ETAA1 was only recently discovered and less is known about

the mechanism by which it activates ATR. However, recent work suggests that ETAA1 plays only a minor role in ATR activation during the DDR [14, 15]. Instead, ETAA1 plays a primary function in proper chromosome alignment and checkpoint activation in metaphase as well as preventing untimely entry into G2. On the other hand, TopBP1 is essential for ATR activation in response to ssDNA damage [12]. Localization of TopBP1 involves interaction with RPA-ssDNA and the RAD9-RAD1-HUS1 (9-1-1) complex, which is loaded at 5' ssDNA-dsDNA junctions [16-18]. Once activated, ATR phosphorylates numerous downstream targets, including CHK1 and p53 [19-21]. CHK1 then promotes the degradation of CDC25A, leading to inactivation of cyclin-dependent kinases and inhibition of replication origin firing [22]. Failure to activate the ATR-CHK1 pathway, particularly following treatment with replication inhibitors or in cancer cells with high levels of genome instability, leads to impaired growth and cell death. Several ATR/CHK1 inhibitors are currently in clinical trials or in development as cancer therapeutics [23].

1.2 CST STRUCTURE AND DNA BINDING PROPERTIES

Human CST (CTC1-STN1-TEN1) is a conserved, ssDNA binding protein that shares homology with RPA (RPA1-RPA2- RPA3) [7]. Both RPA and CST are heterotrimeric and contain a number of oligonucleotide-oligosaccharide binding folds (OB-folds), which are used for DNA binding and protein-protein interactions. Until recently, the structures of human CST were limited to STN1 and TEN1 [24]. In a groundbreaking 2020 study, *Lim, et al*. reported the 3.0-angstrom cryo-electron microscopy structure of CST. CTC1 is characterized by 7 OB-folds which are responsible for ssDNA binding and protein interactions while STN1 and TEN1 each contain a

singular OB-Fold [25]. STN1 also contains two C-terminal winged helix-turn-helix domains, one of which interacts with CTC1 OB-fold E [25] (Figure 1.2). Structural studies demonstrate a high degree of structural homology between the OB-folds in CST and RPA [24, 25]. Like RPA, human CST binds to ssDNA in the low to sub-nanomolar range and requires multiple OB-fold for DNA binding. CST dynamically binds to ssDNA with a minimal binding site of 16-18 nucleotides and maximal binding around 48 nucleotides [26-28]. Despite their similarities RPA and CST appear to have distinct modes of binding and cellular function. [27-29]. For example, CST can stably bind an 18 nucleotide G-strand telomere sequence whereas binding is not observed on random or non-telomeric sequences until they are 32-36 nucleotides in length [28]. The preference for short G-rich sequences is facilitated in part by STN1, as mutation of key residues in the STN1 OB-fold leads to decreased binding on short G-strand sequences [26]. Interestingly, this sequence specific binding mode is related to the G-rich nature of the DNA sequence and not the telomere sequence per se [28].

Additional binding properties such as its preferential binding to ss-dsDNA junctions or its ability to bind and melt certain secondary structures (such as G4s) indicate that CST possesses a variety of DNA binding activities that allows it to function in multiple DNA replication/repair processes which will be discussed in further detail below [27].

1.3 ROLES OF CST IN TELOMERE REPLICATION

CST plays a critical role in telomere replication and less characterized functions in genome-wide replication and DSB repair [26, 27, 30-35]. The natural chromosome ends, known as telomeres, must be protected from the DDR to prevent genome instability

in the form of chromosome fusions and degradation. Telomeric DNA ranges in length from a few hundred base pairs in yeast to tens of kilobases in mammals [36, 37]. In humans, telomeres consist of short tandem 5'-TTAGGG-3' repeats on the G-rich strand and complimentary 5'-CCCTAA-3' repeats on the C-rich strand (Figure 2A). The G-rich strand also contains a 3' ssDNA region referred to as the G-overhang [38, 39]. In mammals, telomeres are protected by the shelterin complex (TRF1-TRF2-RAP1-TIN2-TPP1-POT1) [40]. Shelterin plays a critical role in telomere end protection and preventing the recognition of telomeres as DNA damage. The duplex DNA is bound by TRF1 and TRF2/RAP1 whereas the G-overhang region is protected by POT1, which complexes with TPP1 (Figure 1.3A).

During S-phase, telomeres are replicated in three distinct steps (Figure 2C) [34]. First, the duplex DNA is replicated by the conventional replication machinery. While replication on the leading strand is presumed to reach the chromosome terminus, the lagging strand machinery is unable to fully replicate the ends, a phenomenon known as the end-replication problem [41, 42]. To overcome this, telomeres are extended by telomerase, which is recruited and stimulated by TPP1/POT1 (Figure 1.3B) [43, 44]. After extension, telomerase is then dissociated from the telomere to prevent extensive G-overhang elongation and subsequent targeting by ATR for DNA repair [25, 45]. Next, DNA polymerase α-primase (pol α) converts most of the G-overhang to duplex DNA [46]. The remaining short G-overhang can then form a lariat structure called a telomere loop (t-loop) to protect the DNA terminus from being recognized as DNA damage [47].

CST promotes successful replication of the telomeric duplex region. As mentioned above, telomeres are composed of highly repetitive sequences and can form

DNA secondary structures (G4s and t-loops), which can stall replication [48, 49]. Such stalling can lead to unreplicated DNA or DNA breaks which are then targeted by the DDR for repair. Previous studies showed that disruption of CST subunits leads to a delay in telomere duplex replication and the formation of multiple telomeric signals (MTS), or fragile telomeres [34, 35, 50-53]. MTS manifest as gaps or breaks in telomere FISH signals on metaphase chromosomes and are similar to common fragile sites. MTS are proposed to arise from replication stalling and consistent with this idea, CST has been found to prevent replication failure by preventing G-4 accumulation [54] (Figure 1.4). Together, these data suggests that CST binding to the telomere DNA is required for telomere duplex replication [26].

CST also plays dual roles in telomere end processing, first, by inhibiting telomerase following telomere extension and second, by facilitating C-strand fill-in (Figure 1.3) [45]. Telomerase is suggested to elongate the telomeres through single rounds of processive elongations which is partly mediated by POT1-TPP1 [55, 56]. After telomerase extension of the telomere, CST binds to the G-overhang which prevents telomerase association [29]. Additionally, CST interferes with POT1-TPP1 dependent telomerase activity in a mechanism likely dependent on the physical interaction of CST and POT1-TPP1 [29]. CST is essential in regulating G-overhang length, and conditional CTC1 deletion results in extensive elongation of the G-overhang [57]. Next, telomere processing switches from overhang elongation to C-strand fill in by pol α. CST is proposed to facilitate this switch by stimulating DNA pol α to convert most of the G-overhang to duplex DNA, however, CST regulated fill-in does not appear to be as critical as its ability to modulate telomerase inhibition for end protection [46, 53, 58].

1.4 GENOME-WIDE ROLES OF CST

Although the role of CST at the telomeres has been more broadly studied, mounting evidence indicates that CST is a specialized genome-wide replication factor. Three key pieces of evidence supported this initial idea. First, CTC1 and STN1 were originally discovered as pol α accessory factors [59-61]. Second, only a fraction of STN1 foci (~20%) co-localize with telomeres [62]. Third, depletion of CST subunits leads to signs of general genome instability, such as non-telomeric γH2AX foci, anaphase bridges, and micronuclei [63]. In recent years, several studies have analyzed the various roles of CST in DNA helping to facilitate replication rescue, preventing genome instability, and promoting DNA damage repair.

During unperturbed DNA replication, multiple studies indicate a role for CST as a multifaceted player in genome-wide replication. Previous work indicated that CST promotes origin firing in response to genome-wide replication stress [34]. Additionally, CST has been shown to recruit RAD51 to stalled replication forks to rescue replication at GC-rich DNA [33]. Recently, we discovered that STN1 directly interacts with two subunits of the replicative helicase, MCM4 and MCM7, and is involved in proper origin licensing. By interacting with the MCM complex, CST disrupts MCM and CDT1 interaction which limits over licensing of DNA replication origins [30]. Additionally, CST interacts with AND-1, which couples pol α to the replisome [30, 64]. Together, these studies suggest that CST helps to regulate DNA replication origin licensing and replisome assembly, and thereby contributes to overall genome stability.

In addition to its roles in unperturbed DNA replication, CST prevents genome instability in response to replicative stress. Cells with depleted levels of CST show

reduced cell viability after diverse forms of DNA damage such as HU, aphidicolin, or methanseulphonate treatment [65]. CST also promotes dormant origin firing to rescue stalled replication forks (Figure 1.5A) [30]. On the other hand, CST overexpression increases cell fitness after these different damages, suggesting that CST levels are limiting and overexpression can facilitate recovery from many types of DNA damage [65].

In recent groundbreaking studies, CST was found to also function in DSB repair [31, 66]. DSBs are considered to be the most deleterious types of DNA damage and are repaired mainly through two pathways, non-homologous end joining (NHEJ) and homologous recombination (HR) [67, 68]. HR is considered to be the more accurate method by which DSBs are repaired, however, it is limited to S and G2 phases of the cell cycle where a sister chromatid is present for homology directed repair [69, 70]. NHEJ, on the other hand, is fast, highly mutagenic, and selective for two-ended DSBs [71]. Therefore, many studies have targeted HR as a way to combat cancer and the accurate repair of DSBs in these cells. There are multiple decision points during DSB repair that can help determine whether a DSB is repaired by NHEJ versus HR. For HR, the DSB are resected to facilitate homology search and DNA synthesis to repair the break. On the other hand, resection must be inhibited for NHEJ so that blunt ends of the DSB can be ligated together. CST was found to play a role in promoting NHEJ by preventing DNA end resection in combination with Shieldin and pol α [31, 32]. 53BP1 can help recruit Shieldin through RIF1 which localizes CST/pol α to the resected DNA. CST/pol α then convert the ssDNA back to duplex DNA, shifting repair towards NHEJ (Figure 1.5B) [31, 66]. The highly mutagenic nature of NHEJ versus HR provides possible targets for cancer

therapies whereby promoting DSBs can provide synthetic lethality when HR is blocked. PARP inhibitors (PARPi) are able to induce such lethality in HR-deficient cells, such as those lacking BRCA1. In conjunction with this, 53BP1 was found to promote PARPi sensitivity with the help of Shieldin/CST/pol α. In BRCA1 deficient cells, CST helps to inhibit DSB end resection to promote NHEJ and increased cell death. However, in BRCA1 and CST deficient cells, DSBs can be repaired through accurate HR [32]. Together, these studies indicate an essential role for CST in protecting DSBs from end resection to promote NHEJ, and thus, creating a pathway for the synthetic lethal effects of PARPi.

1.5 CST AND TELOMEROPATHIES

Coats plus (CP), also known as CRMCC, is a pleiotropic, autosomal recessive disorder that is typically diagnosed in infancy or early childhood and carries high mortality and morbidity rates [72, 73]. Loss of stem cell compartments appears to underlie the disease. CP has common features including intrauterine growth retardation, intracranial calcifications, retinopathy, neurological defects and gastrointestinal bleeding. Penetrance and expression of symptoms is wide-ranging and the cause of death varies greatly between patients, underscoring the complexity of CP. In 2012, CTC1 mutations were identified in a number of CP patients with additional cases later reported [74-81]. Biallelic mutations in either STN1 or the shelterin component POT1 have also been shown to cause CP [82-85]. Interestingly, characterization of cells from the CP patient harboring POT1 mutations were shown to affect CST recruitment and positioning at the telomere, suggesting that CST misregulation also underlies CP in this patient [84]. CTC1 mutations were also found in patients with dyskeratosis congentia (DKC) [86, 87]. DKC

is in a class of short telomere spectrum disorders, often referred to as telomeropathies. These disorders encompass a variety of diseases ranging from childhood bone marrow failure disorders to adult-onset pulmonary fibrosis and liver disease [88-91]. Like CP, the loss of stem cell compartments is thought to cause telomeropathies. CP shares common features with DKC and other childhood telomeropathies, including bone marrow failure, sparse and graying hair, nail dystrophy and osteopenia. Furthermore, in a case report by Keller et al. a patient diagnosed with DKC showed intracranial calcifications and early signs of retinopathy, indicating overlap with CP [86]. The fact that mutations in CST subunits cause both DKC and CP suggest a common molecular etiology. Several groups have proposed telomere shortening as the common denominator [74, 92, 93]. However, there have been conflicting reports on whether all CP and DKC patients with mutations in CTC1 or STN1 have shortened telomeres. At present, it is unclear whether these differences arise from the methods used to measure telomere length and/or variations in disease pathology from specific mutations.

Several studies have sought to determine the molecular consequences of CP mutations. CTC1 mutations occur as compound heterozygotes with one allele typically harboring a frameshift or nonsense mutation and the other allele a missense mutation. Expression of the equivalent nonsense and frameshift mutants in mice produced truncated proteins that either express poorly or not at all, suggesting that these alleles are non-functional [92]. Indeed, these mutants are unable to bind telomeric DNA, localize to telomeres or interact with STN1. Analysis of CTC1 missense mutants showed hypomorphic phenotypes in CST, with some affecting DNA binding activity and telomeric association, while others led to changes in nuclear localization or decreased

interaction with pol alpha [93]. Yet, no common telomeric phenotype was observed across the mutants, opening the possibility that these mutations also affect the non-telomeric roles of CST. In agreement with this idea, cells from CP patients, with STN1 mutation, had telomere dysfunction as well as signs of general genomic instability and DNA replication defects [85]. Together, these results argue that defects in both telomeric and non-telomeric functions of CST contribute to CP, which may help explain the diversity of symptoms and their expression. To date no molecular studies of DKC patient-derived cells harboring CTC1 mutations have been performed. However, stromal cells collected from one patient showed severe premature senescence [86], which was also observed in CP patient cells with STN1 and POT1 mutations. The authors of this study suggest that expression of both DKC and CP features may relate to environmental or genetic modifiers. Thus, further characterization of CP and DKC patient-derived cells will be critical to understand CST and help in the treatment and management of these diseases.

1.6 CST AND CANCER

Alteration in the expression of CST subunits has been linked to increased cancer risk and poor prognosis of survival [94-97]. For example, decreased CTC1 or STN1 (also known as OBFC1) gene expression leads to decreased survival in breast, lung and gastric cancer patients [98]. SNPs in CTC1 and STN1 have also been associated with an increased risk of cancer development. These findings are consistent with the fact that depletion of CST subunits leads to hallmarks of cancer, including telomere dysfunction and increased genome instability (anaphase bridges, micronuclei, DNA damage) [29, 33, 34, 51, 52, 63]. Furthermore, increased CTC1 expression leads to radioresistance in

melanoma cancer cell lines by preventing telomere shortening and apoptosis [96]. While further analysis is required, these results indicate that CST levels are tightly regulated to preserve genome stability and suggest that CST may be a promising target for cancer therapy.

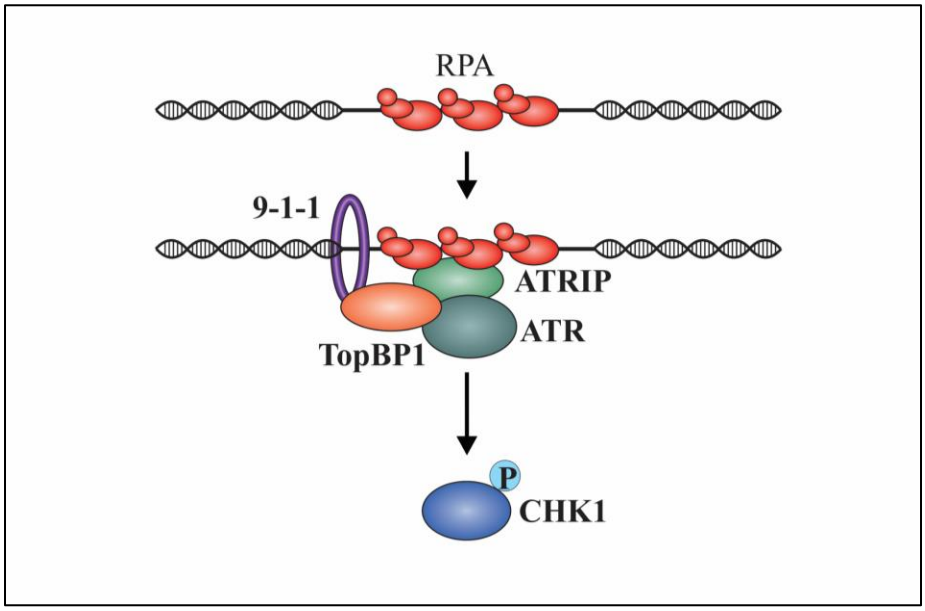

Figure 1.1 Model of ATR activation in response to ssDNA. In the event of ssDNA damage, the DNA is quickly bound by RPA. ATRIP then associates with RPA-ssDNA which localizes ATR to the damage site. Independently, the 9-1-1 complex binds at the ds-ssDNA junction and localizes TopBP1 to the damage site. TopBP1 interacts and activates ATR which will then phosphorylate CHK1 and other downstream targets.

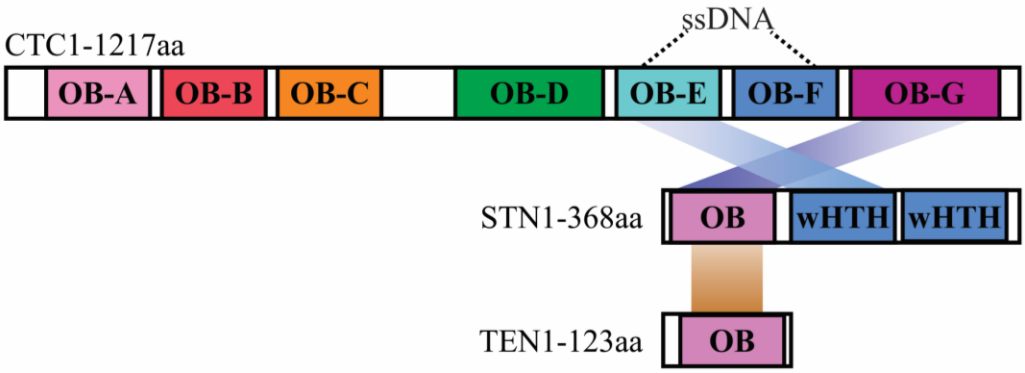

Figure 1.2 Schematic representation of domain structures of the CST complex. CST is a ssDNA binding protein characterized by multiple OB-folds. CTC1 is 1217 amino acids (aa) long and contains 7 OB-folds. OB-E and OB-F contain the ssDNA binding domains. CTC1 interacts with the 368aa protein, STN1, through binding of OB-E of CTC1 to the single STN1 OB-fold and OB-G of CTC1 to the first wHTH domain of STN1. STN1 acts as the bridge between CTC1 and TEN1 (123aa) by interacting with the single OB-fold of TEN1.

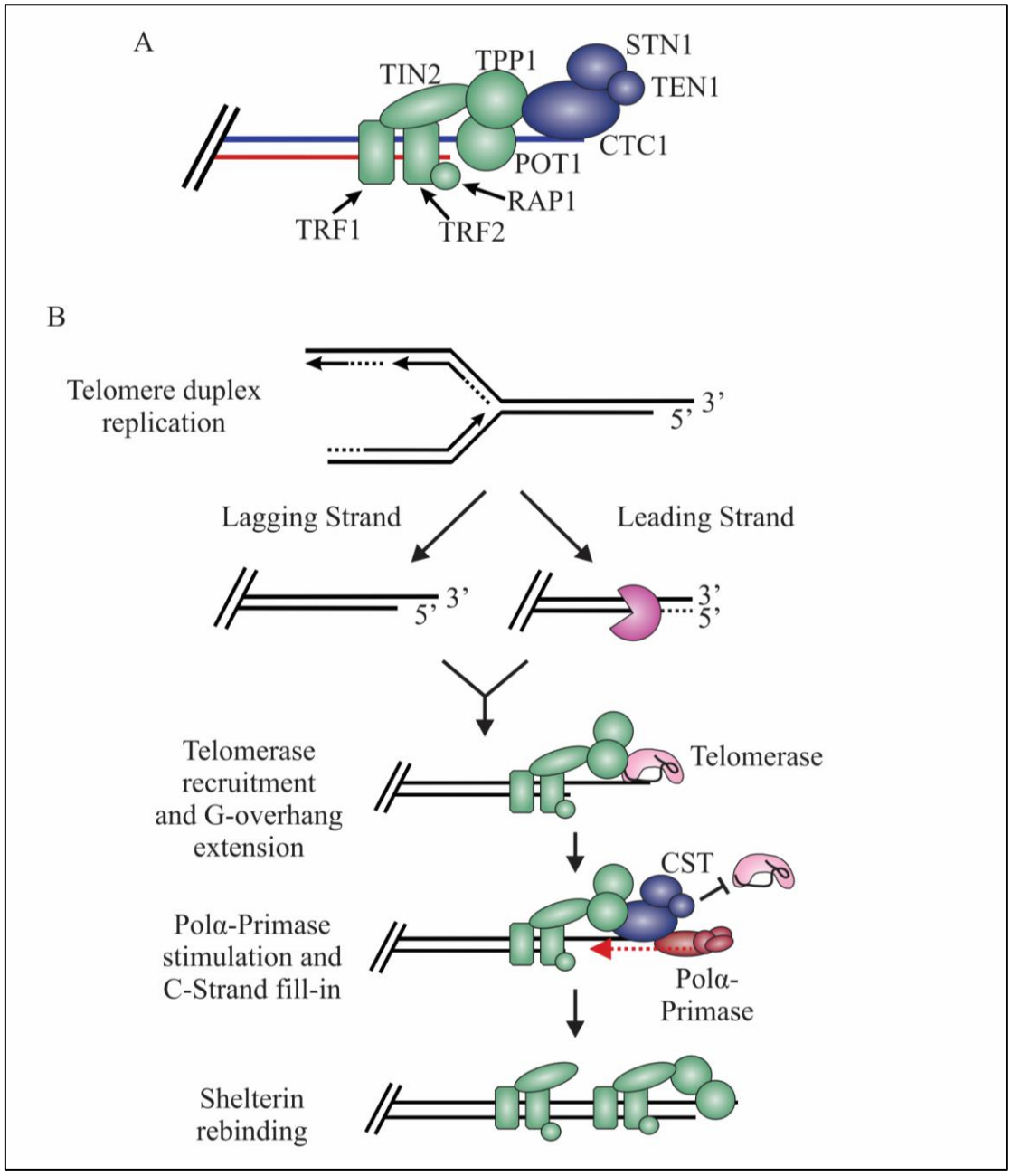

Figure 1.3 Overview of the roles of CST at telomeres. (A) Telomeres are bound by the shelterin complex (TRF1-TRF2-RAP1-TIN2-TPP1-POT1) and the 1236 CST complex (CTC1-STN1-TEN1), which aid in telomere maintenance. **(B)** After telomere duplex replication the leading strand is processed to produce a G-overhang. Telomerase then extends the G-overhangs. To prevent G-overhang hyperextension, CST is localized to telomeres by TPP1 and inhibits telomerase activity. Additionally, CST promotes C-strand fill-in by stimulating pol α. After telomere processing, the shelterin complex rebinds.

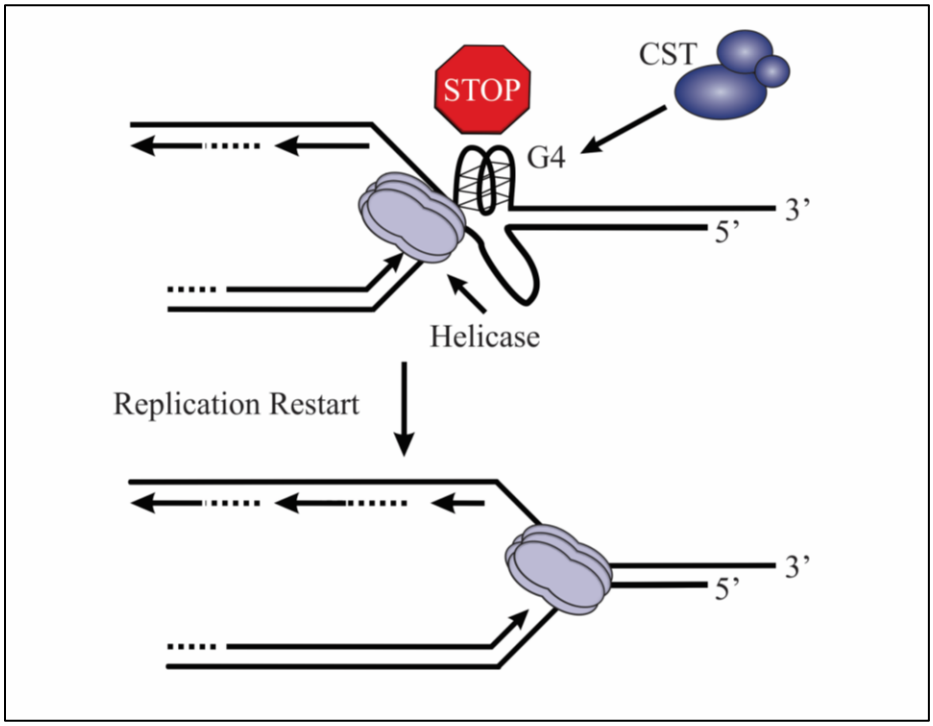

Figure 1.4 Model of G-quadruplex (G4) melting and fork restart during telomere duplex replication. The G4 secondary structure can form in G-rich sequences of DNA such as the telomeres. In the absence of CST, replication is stalled. CST resolves or prevents G4 formation to promote replication restart.

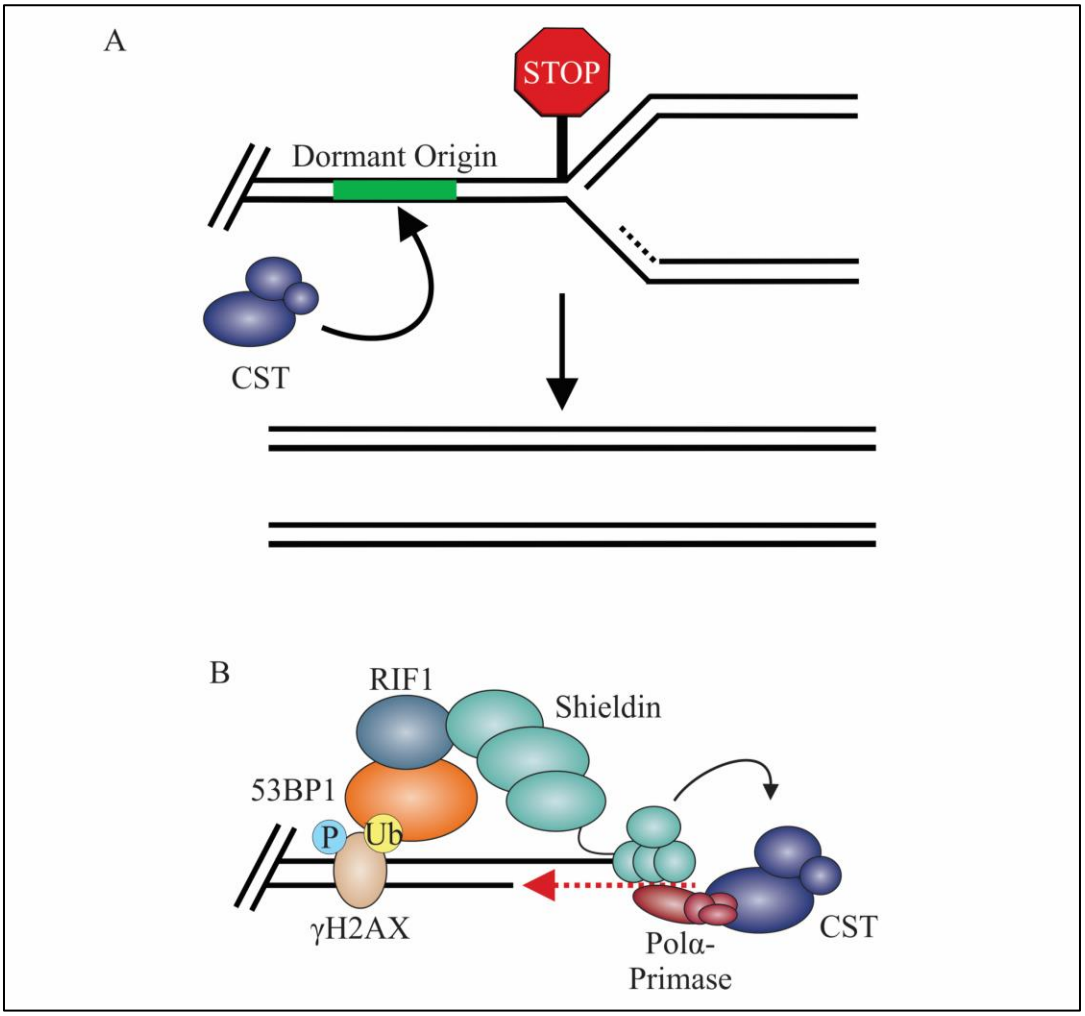

Figure 1.5 Roles of CST in genome wide replication and the DNA damage response. (A) In the event of replication stalling, CST promotes the firing of dormant or unfired origins which rescue the stalled replication fork and promotes DNA replication. **(B)** In response to DSBs, 53BP1 is localized through its interaction with γH2AX. 53BP1 then interacts with RIF1, which localizes the Shieldin complex. Shieldin inhibits long-range resection by preventing access to the resected DNA and reverses resection through its interaction with CST-pol α, which can mediate fill-in of the resected DNA. This promotes repair of the break by NHEJ. (P: phosphorylation; Ub: ubiquitination).

CHAPTER 2

CST IS A REGULATOR OF CELL CYCLE PROGRESSION BY PROMOTING TELOMERE PROTECTION

2.1: INTRODUCTION

Previous work demonstrated that conditional deletion of human CTC1 leads to growth inhibition and unregulated lengthening of the G-overhang by telomerase as well as shortening of telomeres from the inability to perform C-strand fill-in [57]. Since telomeres resemble DNA breaks, they must be protected from recognition by the DDR. Telomere G-overhangs are typically protected by POT1, a member of the shelterin complex. However, these extended G-overhangs in CTC1 deleted cells exhaust the cellular pools of POT1, leading to telomeric RPA-ssDNA and telomeric γH2AX, a marker of DNA damage. While this accumulation of RPA-ssDNA is predicted to elicit activation of the ATR-CHK1 pathway, this was not directly tested in previous studies [57, 99].

To more precisely examine the effects of conditional CTC1 KO, we performed time course analysis of the cell cycle in HCT116 conditional CTC1 KO ($CTC1^{-/-}$). The HCT116 $CTC1^{-/-}$ cell line was previously generated by the addition of loxP sites surrounding exon 5 of both endogenous CTC1 alleles ($CTC1^{F/F}$) [57]. Cells were then stably selected for expression of a Cre recombinase linked to the estrogen receptor (Cre-ER). Addition of TAM results in localization of Cre-ER to the nucleus and removal of exon 5 by Cre-induced recombination. Gene disruption was confirmed by Western blot and PCR analysis following the addition of TAM, as previously described (Figure 2.1) [57]. To control for possible off-target effects, a stable cell line was developed, expressing Flag-CTC1 in the $CTC1^{F/F}$ line ($CTC1^{F/F}$+Flag-CTC1) [57]. Following the addition of TAM ($CTC1^{-/-}$+Flag-CTC1), the endogenous CTC1 is disrupted, while the exogenous Flag-CTC1 expression remains unchanged (Figure 2.1).

2.2: RESULTS

2.2A: CTC1 DELETION INDUCES G2 ARREST AND APOPTOSIS BUT DOES NOT ALTER S-PHASE PROGRESSION

Previous studies found that CTC1 deletion led to decreased proliferation and an accumulation of G2/M arrested cells [35, 57]. In agreement with these studies, we observed decreased cell proliferation (Figure 2.2A) and the accumulation of G2/M cells starting around six days after conditional CTC1 deletion, which became more severe 10-12 days after TAM addition (Figure 2.2B-C).

In addition to its role in telomere replication, CST aids in several aspects of genome-wide replication, including replication of G-rich DNA, dormant origin activation following replication stress and origin licensing [30, 34, 54, 100]. Since past studies focused on telomere and not genome-wide replication, we tested whether CTC1 deletion affected global replication rates. To test this, we examined the levels of DNA synthesis in $CTC1^{-/-}$ cells by flow cytometry and DNA combing. Flow cytometry revealed a significant decrease in the number of S-phase cells following CTC1 deletion (Figure 2.2B). However, the cells within S-phase retained similar levels of DNA synthesis (i.e. EdU intensity per cell) compared to controls (Figure 2.2C). Additionally, the number of S-phase EdU negative cells was not substantial increased (Figure 2.2B), suggesting that global replication is not inhibited in the $CTC1^{-/-}$ cells under normal conditions. To confirm this result, we performed DNA fiber analysis on day 11 after TAM addition (Figure 2.3A-C). Again, we failed to detect any significant changes in DNA synthesis or replication events following CTC1 deletion. These findings indicate that S-phase progression and global DNA synthesis are not significantly altered following CTC1

removal, which is in line with the idea that CST acts as a specialized, not general, replication factor to promote replication at G-rich DNA or dormant origin activation following replication stress [34, 100].

Since CTC1 deletion induces the accumulation of G2/M phase cells, we sought to distinguish between G2 versus M-phase. Accordingly, IF was performed to assess the number of phosphorylated Histone H3 S10 positive cells, as a readout of the mitotic index [101]. The percentage of mitotic cells was not increased in the $CTC1^{-/-}$ cells compared to controls, indicating that CTC1 deletion causes an accumulation of G2 rather than M-phase cells (Figure 2.4). In addition, we observed an increase in the sub-G1 population (Figure 2.2C), which could arise from increased apoptosis. Indeed, we found that CTC1 deletion led to increased apoptosis, as measured by increased caspase 3/7 activity (Figure 2.4B). Conditional CTC1 deletion also leads to increased senescence in human and mouse cells, suggesting that both apoptosis and senescence contribute to overall growth inhibition in $CTC1^{-/-}$ cells [35, 52, 57].

2.2B: CTC1 KO DOES NOT INDUCE GLOBAL ATR-CHK1 SIGNALING

Since CTC1 deletion leads to an increased number of G2 arrested cells, we next wanted to determine the cause of this arrest. Previous work determined that loss of CTC1 increases G-overhang length, leading to RPA binding and presumably activation of the DDR through ATR-CHK1 [57]. Nevertheless, whether the ATR-CHK1 pathway is activated following CTC1 deletion was not directly tested. Following the accumulation of RPA-ssDNA, ATR should be recruited leading to the phosphorylation of several downstream ATR targets, including H2AX, CHK1 and p53. As a readout of ATR activation, we measured the phosphorylation of CHK1 (pCHK1) S317 and S345, and p53

S15 (p-p53 S15) in whole cell lysates collected at days 8, 11 and 13 after TAM addition (Figure 2.5A-B). Additionally, global γH2AX levels were measured by IF (Figure 2.5C). However, CTC1 KO did not result in detectable pCHK1 S317/S345 or p-p53 S15, suggesting that the ATR-CHK1 pathway is not globally activated in CTC1$^{-/-}$ cells under these conditions. Total γH2AX levels were also not increased, implying that cells do not contain high levels of DNA damage signaling. Interestingly, while p53 S15 phosphorylation was not observed, total p53 levels were increased in the CTC1$^{-/-}$ cells, suggesting activation of a DDR (Figure 2.5A). In agreement with p53 activation, p21 levels also increased starting at eight days after TAM addition (Figure 2.6A), which corresponds to the partial G2 arrest and growth inhibition in the CTC1$^{-/-}$ cells (Figure 2.2). Finally, CTC1$^{-/-}$ cells were treated with siRNA to p53 to determine whether the G2 arrest was p53-dependent (Figure 2.6B). However, p53 knockdown did not suppress the accumulation of G2 cells following CTC1 deletion, suggesting that p53-independent mechanisms also promote G2 arrest following CTC1 deletion (Figure 2.6C)

2.2C ATR IS ACTIVATED AND PHOSPHORYLATES TELOMERE-BOUND RPA IN CTC1$^{-/-}$ CELLS

As mentioned previously, CTC1 KO leads to telomeric RPA and γH2AX staining on metaphase chromosomes [57]. Under normal conditions, excess RPA-ssDNA should lead to ATR activation and CHK1 phosphorylation. Since pCHK1 was not detected following CTC1 deletion, we determined whether ATR was active and localized to RPA-bound telomeres. First, we confirmed that RPA-ssDNA was present at telomeres following CTC1 deletion by IF-FISH to measure chromatin-bound RPA at telomeres. In agreement with previous findings, RPA foci were increased in interphase CTC1$^{-/-}$ cells

and these foci were almost exclusively at telomeres (~80%) (Figure 2.7) [57]. Interestingly, increased RPA foci typically corresponded to enlarged nuclei in CTC1$^{-/-}$ cells (Figure 2.8A). The increased levels of chromatin-bound RPA in the CTC1$^{-/-}$ cells was also confirmed by flow cytometry of pre-extracted cells (Figure 2.8B). Recruitment of ATRIP-ATR to RPA-ssDNA typically leads to ATR-dependent phosphorylation of RPA32 S33 (pRPA) [102]. Since pCHK1 was not detected in cell extracts but RPA was increased at telomeres, pRPA was measured as a readout of ATR activation (Figure 2.9). Similar to total chromatin-bound RPA, we observed a significant increase in pRPA. This suggested that, although pCHK1 is not present in CTC1$^{-/-}$ cells, ATR is active and present at telomeres. To confirm this, CTC1$^{-/-}$ and control cells were treated with ATRi for 24 hours and pRPA and RPA determine (Figure 2.7B and 2.9B). Treatment with ATRi suppressed the pRPA foci in CTC1$^{-/-}$ cells. However, total RPA foci remained unchanged, indicating that the phosphorylation of RPA in the CTC1$^{-/-}$ cells is ATR-dependent. A previous study also found telomeric γH2AX in CTC1$^{-/-}$ cells on metaphase spreads [57]. In agreement with this study, we found that RPA-foci co-localized with γH2AX in interphase CTC1$^{-/-}$ cells (Figure 2.10A-B). Nevertheless, these foci were difficult to distinguish from background γH2AX foci in the control cells without RPA staining, which likely precluded their detection in the global γH2AX analysis in Figure 2.5C. To more directly test ATR activation, Western blot analysis was performed to measure the levels of autophosphorylated ATR at T1989 (pATR). In contrast to pCHK1, pATR was significantly increased in CTC1$^{-/-}$ cells (Figure 2.10C). Additionally, there was an overall increase in total ATR levels, which suggest that CTC1 deletion may alter ATR gene expression. Together, these results indicate that ATR

localizes to telomeric RPA-ssDNA and is activated in CTC1$^{-/-}$ cells. However, ATR activation is insufficient to induce detectable levels of pCHK1 S317/S345 or p-p53 S15 in the absence of CTC1 (Figure 2.5A-B).

2.2D: ATR BUT NOT ATM OR CHK1 PROMOTES G2 ARREST IN CTC1 DELETED CELLS

To assess whether ATR activation contributes to the accumulation of G2 arrested cells following CTC1 KO, we performed flow cytometry on cells treated with the ATR inhibitor (ATRi) VE-821 for 24 h or siRNA to ATR (Figures 2.11 and 2.12 and Tables 2.1-2). ATR inhibition or knockdown prevented the accumulation of G2/M cells following CTC1 deletion. ATR inhibition also resulted in increased apoptosis in CTC1$^{-/-}$ cells, as measured by caspase 3/7 activity (Figure 2.4B). As a control, cells were also treated with siRNA to ATM or CHK1 to confirm that the increased number of G2 cells were ATR-dependent (Figures 2.13 and 2.14 and Tables 2.3-2.4). Unlike knockdown of ATR, depletion of ATM was unable to suppress the increase in G2 arrested cells following CTC1 deletion. Depletion of CHK1 was also unable to suppress the increase in G2 cells. However, these results are somewhat complicated by the fact that CHK1 knockdown leads to an overall increase in G1 and decrease in G2/M phase cells across all cell lines (Figure 2.14C and Table 2.4). Despite alterations in the cell cycle, comparison of the fold increase in G2/M cells between CTC1$^{-/-}$ and control cells was similar following treatment with siNT (CTC1$^{-/-}$/CTC1$^{F/F}$/:1.39, CTC1$^{-/-}$/CTC1$^{-/-}$+Flag-CTC1:1.29) and siCHK1 (CTC1$^{-/-}$/CTC1$^{F/F}$:1.30, CTC1$^{-/-}$/CTC1$^{-/-}$+Flag-CTC1:1.26) (see Tables 2.1-4). Still, our results do not exclude the possibility that CHK1 may be partially

responsible for the G2 arrest. Together, these results indicate that the accumulation of G2 arrested cells following CTC1 KO is ATR-dependent.

2.2E STN1 DELETION INDUCES G2 ARREST AND ATR SIGNALING AT TELOMERES

Next, we evaluated the effect of conditional STN1 KO using an inducible Cas9 (iCas9) system in HeLa cells. This allowed us to confirm whether the phenotypes observed with CTC1 deletion are due to CST function as a whole rather than specific to CTC1 alone or HCT116 cells. To date, no human STN1 KO line has been reported, therefore we developed a conditional STN1 KO cell line in HeLa cells. To create this cell line, HeLa cells with Cas9 under an inducible doxycycline (Doxy) promoter were obtained from Dr. Iain Cheeseman [103, 104]. sgRNA to STN1 were transfected into HeLa iCas9 cells, clones were isolated, and STN1 gene disruption was measured by Western blot (Figure 2.15A). In agreement with our results using the HCT116 CTC1$^{F/F}$ cell line, we found that STN1$^{-/-}$ cells showed a growth defect starting around day 12 after the addition of Doxy, which is similar in timing to the CTC1$^{-/-}$ cells (Figure 2.15B). Additionally, we found an accumulation of G2/M cells and a sizable increase in sub-G1 cells 12 days after Doxy addition (Figure 2.16) indicating an increase in cell death and cell cycle arrest. HeLa cells are p53 deficient, therefore this further supports our idea that the accumulation of G2 cells following CTC1 deletion is promoted by p53-independent mechanisms.

In CTC1$^{-/-}$ cells, the G2 arrest is induced in response to the accumulation of telomeric RPA, which results in ATR activation. We are currently investigating if this holds true in STN1$^{-/-}$ cell, but preliminary results have suggest that STN1 KO leads to

similar defects in telomere maintenance and DNA damage signaling. First, RPA-foci appear to co-localize with telomere-FISH signals (~70%) (Figure 2.17A). Second, we measured γH2AX localization to RPA-ssDNA as a readout of DDR activation. Similar to what we saw in CTC1$^{-/-}$ cells, we found increased RPA foci and RPA co-localization with γH2AX in STN1$^{-/-}$ cells (Figure 2.17B-C). As a more direct measurement of ATR activation, we measured pRPA32 S33 foci in response to STN1 KO and saw increased number of nuclei with 3 or more pRPA32 foci, which corresponded to the timing of cell proliferation decrease and G2 arrest following STN1 removal (Figure 2.17D). These results suggest that both CTC1 and STN1 are required for the protection of telomeres from ATR-dependent DNA damage signaling. However, it is still possible that CTC1 and STN1 have different roles in the binding and localization of the CST complex to different areas of the genome. For example, at the telomeres CTC1 and STN1 both interact with TPP1, however only CTC1 appears to bind POT1 [29, 105]. Additionally, STN1, but not CTC1 or TEN1, was found to interact with different subunits of the CMG helicase to suppress origin licensing [30]. Thus, additional studies, using the CTC1 and STN1 conditional KO cells and a newly developed TEN1 KO cell line, are needed and will prove instrumental in our understanding of how CST subunits work together to promote the diverse functions of the complex as a whole.

2.2F POT1 OVEREXPRESSION PREVENTS RPA-ssDNA AND RESCUES CELL GROWTH IN CTC1$^{-/-}$ CELLS

POT1 is a ssDNA binding protein and a member of the six-subunit telomere protection complex, shelterin. One of the primary roles of POT1 is to prevent ATR-dependent DNA damage signaling at telomeres through the inhibition of RPA binding to

G-overhangs [57]. Previous work demonstrated that POT1-OE partially rescues the telomeric DDR induced following CTC1 knockout (i.e. telomeric RPA and γH2AX) [57]. However, POT1-OE was not able to rescue the elongated G-overhangs, indicating that POT1 is unable to substitute for CST in telomerase inhibition or C-strand fill-in. Furthermore, it suggests that endogenous POT1 levels are insufficient to outcompete RPA for the hyperextended G-overhangs caused by CTC1 deletion. To test the effects of POT1-OE on cell cycle progression and cell growth, we performed flow cytometry and growth curve analysis on $CTC1^{-/-}$ cells overexpressing Flag-POT1 ($CTC1^{-/-}$ +POT1) (Figure 2.18A). In agreement with the previous study, POT-OE prevented RPA as well as pRPA S33 foci formation in the $CTC1^{-/-}$ cells (Figure 2.18B-C) [57]. Flow cytometry and cell growth analysis revealed that not only did POT1-OE rescue G2 arrested cells but also the growth delay associated with CTC1 deletion (Figure 2.19 and 2.20). These results indicate that increased telomeric RPA-ssDNA, caused by G-overhang elongation, is the primary cause of decrease proliferation following CTC1 KO and that the non-telomeric roles of CST do not significantly affect proliferation in unperturbed cells. Furthermore, they highlight the essential role of POT1 in telomere end protection and indicate that POT1 exhaustion due in an abundance of telomeric ssDNA has a profound impact on cell cycle progression and cell growth (Figure 2.21)

2.3 DISCUSSION

One of the major questions we sought to address in this chapter was the underlying cause(s) of decreased cell proliferation associated with CTC1 removal. In agreement with previous studies, we find that conditional deletion of CTC1 and STN1 both lead to a partial G2 arrest, which is primarily caused by telomeric RPA-ssDNA [35,

57]. Unexpectedly, we demonstrate that, while ATR is actively recruited to telomeric RPA-ssDNA, ATR dependent CHK1 phosphorylation is not detectable in the event of CTC1 deletion. Instead, we suggest that the primary cause of cell death and checkpoint activation following loss of CTC1 or STN1 is the accumulation of telomeric RPA due to POT1 exhaustion.

Our results combined with previous findings indicate that CST plays multiple functions in the DDR at telomeres. First, it prevents ATR-mediated checkpoint activation by inhibiting telomerase from hyperextending G-overhangs, leading to RPA-ssDNA (Figures 2.7 and 2.17) [29, 57]. Second, it promotes ATR-CHK1 signaling once telomeres are bound by RPA. Despite significant ATR activity at RPA-bound telomeres in both CTC1$^{-/-}$ and STN1$^{-/-}$ cells, our results suggest that this is insufficient to induce global CHK1 phosphorylation (Figures 2.5-2.10). While it is possible that low levels of pCHK1 are present at telomeres but not detectable by Western blot, this seems unlikely, as a significant portion of the CTC1$^{-/-}$ cells (~25%) contain three or more large RPA foci and ATR is clearly activated (Figures 2.7-10). Furthermore, attempts to detect pCHK1 at telomeres were unsuccessful. Previous work also found that replication fork stalling at a single defined repeat sequence is sufficient to induce detectable ATR-dependent CHK1 phosphorylation [106]. Thus, the significant levels of RPA-ssDNA from elongated G-overhangs in CTC1$^{-/-}$ cells should induce CHK1 phosphorylation, as previously observed following POT1 deletion in mice and chicken cells [107, 108].

Why CHK1 is not activated in CTC1$^{-/-}$ cells is unclear. Yet, a recent study in mouse cells showed that CST is required to override POT1b-mediated telomere protection in S/G2, suggesting that CST may activate ATR-CHK1 signaling at telomeres

in mice [109]. However, despite the lack of pCHK1, ATR activation from telomere RPA-ssDNA is sufficient to induce cell cycle arrest, suggesting an alternate ATR pathway is activated. Determining whether or not these extended G-overhangs are recognized as DDR and then repaired or shortened, what DDR pathway is activated and the interplay between POT1 and CST in ATR regulation will require further investigation. However, our work provides novel insight into ATR-CHK1 signaling at telomeres.

In the absence of CTC1, a previous study found that the G-overhangs because severely over-extended [57]. We predicted that this incredible amount of ssDNA results in exhaustion of POT1 and therefore, telomere ends cannot be protected from RPA localization and ATR activation. Indeed, POT1 overexpression was sufficient to completely rescue cell growth and block ATR activation following CTC1 removal. Thus, telomere length regulation/protection not genome-wide replication is the primary function of CST in unstressed cells.

In summary, we establish CST as a regulator of cell cycle progression by promoting telomere protection. In the absence of CST, telomeres become over elongated [57] and thus RPA binds telomeric ssDNA which results in ATR checkpoint activation. Additionally, overexpression of the shelterin complex component, POT1, can rescue the cell proliferation and cell cycle defects.

Table 2.1 Percentage of cells in each cell cycle phase following ATR inhibition.

	G1 Phase	S Phase (Edu+)	G2 Phase	S Phase (Edu-)
$CTC1^{F/F}$ DMSO	33.83	40.80	20.40	4.97
$CTC1^{-/-}$ DMSO	40.63	15.17	30.00	14.19
$CTC1^{-/-}$+Flag-CTC1 DMSO	32.97	44.20	18.23	4.60
$CTC1^{F/F}$ ATRi	40.93	30.27	19.63	9.17
CTC1-/- ATRi	45.87	16.23	20.60	17.30
$CTC1^{-/-}$+Flag-CTC1 ATRi	40.07	31.90	17.03	11.00

Table 2.2 Percentage of cells in each cell cycle phase following siATR.

	G1 Phase	S Phase (Edu+)	G2 Phase	S Phase (Edu-)
$CTC1^{F/F}$ siNT	38.83	35.23	22.83	3.16
$CTC1^{-/-}$ siNT	39.53	22.03	31.63	6.75
$CTC1^{-/-}$+Flag-CTC1 siNT	40.03	30.13	24.53	5.33
$CTC1^{F/F}$ siATR	41.17	30.77	23.30	4.77
CTC1-/- siATR	39.77	27.00	26.97	6.27
$CTC1^{-/-}$+Flag-CTC1 siATR	42.47	26.00	24.27	7.28

Table 2.3 Percentage of cells in each cell cycle phase following siATM.

	G1 Phase	S Phase (Edu+)	G2 Phase	S Phase (Edu-)
$CTC1^{F/F}$ siNT	36.67	36.10	23.10	4.16
$CTC1^{-/-}$ siNT	38.47	21.87	30.80	8.84
$CTC1^{-/-}$+Flag-CTC1 siNT	37.70	31.87	24.67	5.79
$CTC1^{F/F}$ siATM	32.23	35.40	27.40	4.93
CTC1-/- siATM	35.30	20.07	36.10	8.54
$CTC1^{-/-}$+Flag-CTC1 siATM	35.50	28.07	29.30	7.07

Table 2.4 Percentage of cells in each cell cycle phase following siCHK1.

	G1 Phase	S Phase (Edu+)	G2 Phase	S Phase (Edu-)
$CTC1^{F/F}$ siNT	38.83	35.23	22.83	3.16
$CTC1^{-/-}$ siNT	39.53	22.03	31.63	6.75
$CTC1^{-/-}$+Flag-CTC1 siNT	40.03	30.13	24.53	5.33
$CTC1^{F/F}$ siCHK1	54.13	25.07	16.53	4.27
CTC1-/- siCHK1	56.83	16.57	21.57	5.06
$CTC1^{-/-}$+Flag-CTC1 siCHK1	59.33	18.13	17.07	5.44

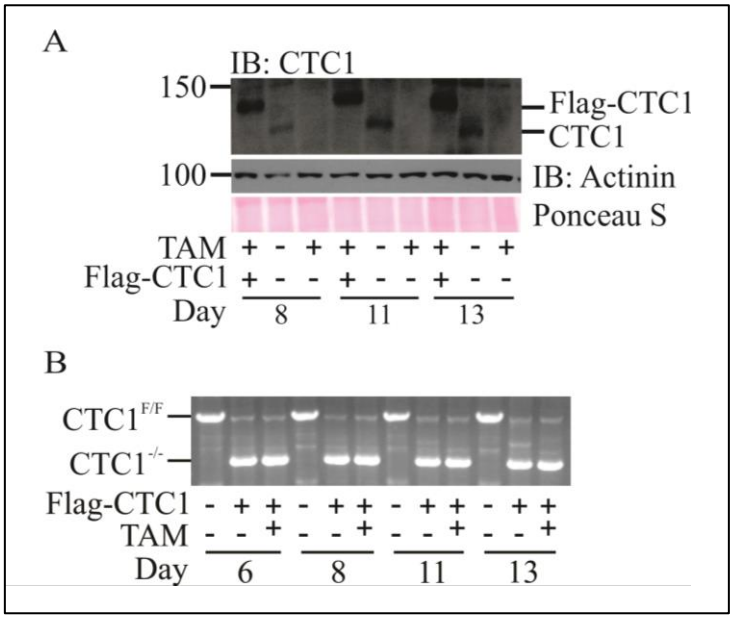

Figure 2.1 Verification of CTC1 KO in HCT116 cells. TAM was added to $CTC1^{F/F}$ and $CTC1^{F/F}$ + Flag-CTC1 cell lines at day 0 to disrupt *CTC1* ($CTC1^{-/-}$) **(A)** Western blot of CTC1 KO in HCT116 cells. Representative gel showing days 8, 11, and 13. Actinin and Ponceau S staining are loading controls. **(B)** Agarose gel of truncated CTC1 PCR product in $CTC1^{-/-}$ and $CTC1^{-/-}$ + Flag-CTC1 samples. Representative gel showing days 6, 8, 11, and 13.

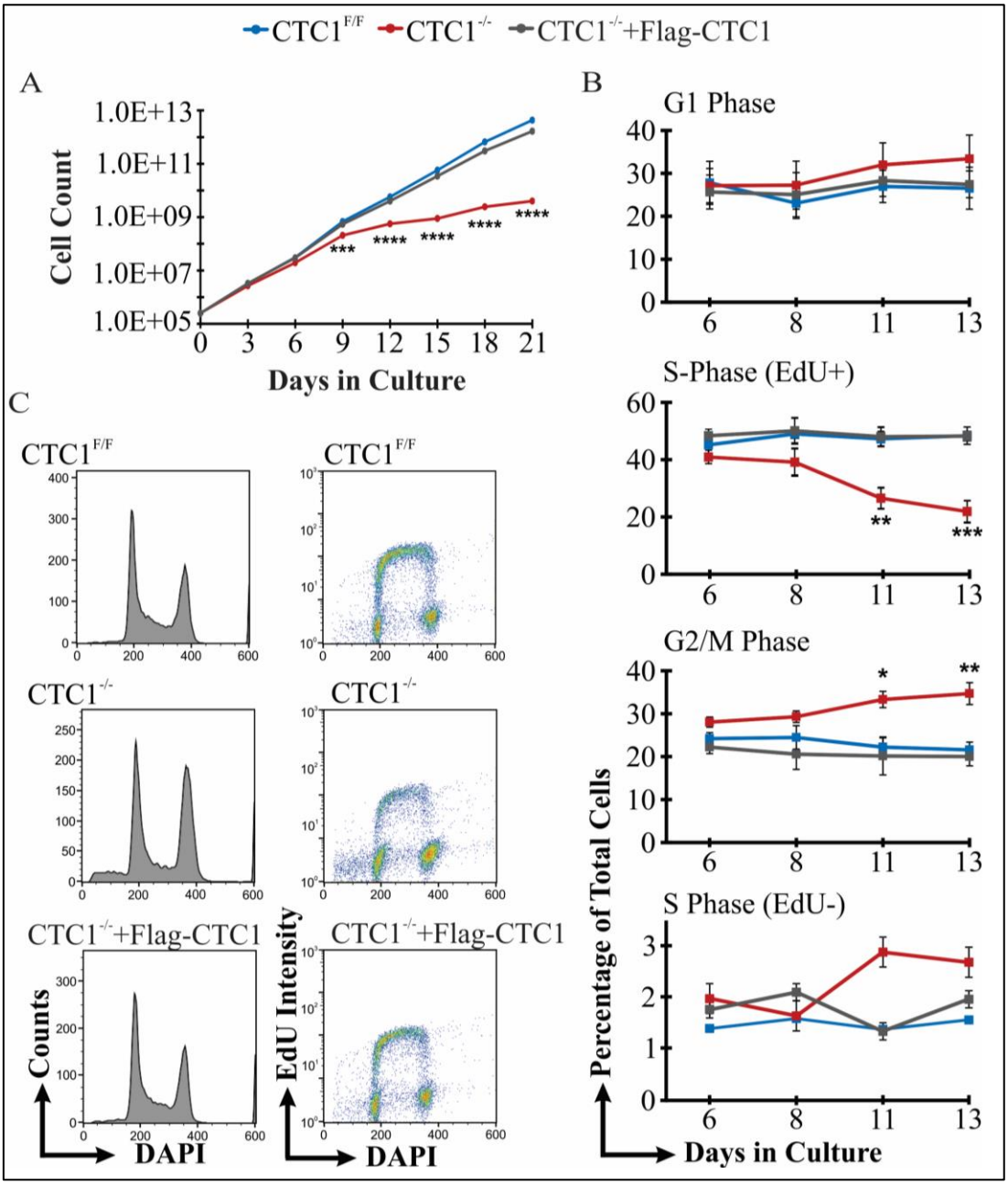

Figure 2.2 CTC1 deletion results in proliferation decrease and a partial G2 arrest. (A) Representative growth curve of three independent, biological replicates. **(B-C)** Flow cytometry analysis of HCT116 CTC1F/F, CTC1-/-, and CTC1-/- + Flag-CTC1 cells. **(B)** Representative histograms from flow cytometry analysis. Left panel: DNA content (DAPI) versus cell count. Right panel: DNA content versus replicating cells (EdU+). **(C)** Percentage of cells in each cell cycle phase, as indicated. (n=3 independent, biological replicates). Error bars indicate ±SEM. P-values were calculated by one-way ANOVA test (*$P \leq 0.05$, **$P \leq 0.01$, ***$P \leq 0.001$).

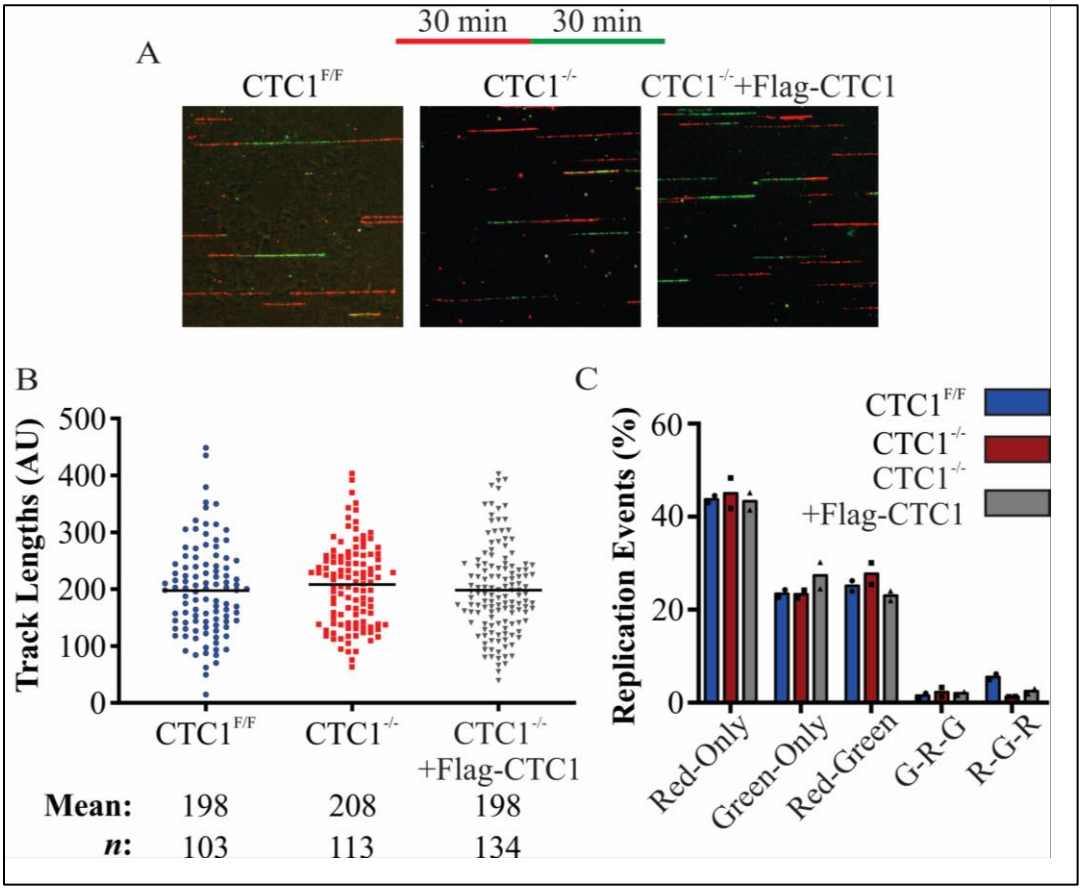

Figure 2.3 CTC1 deletion does not alter replication speed or percentage of replication events. (A) Image shows representative fibers used for DNA fiber analysis. Red: IdU labeling. Green: CldU labeling. **(B)** Dot plot of track length for elongating forks (Red-Green). Black line and numbers below the graph indicate the mean length in arbitrary units (AU). *n* indicates the number of total tracks scored. **(C)** Percentage of replication events. Red-only: stalls or terminations, Green-only: origins fired during second label (CldU), Red-Green: elongating forks, G-R-G (Green-Red-Green): origins fired in first label (IdU), R-G-R (Red-Green-Red): terminations. Number of events scored: $CTC1^{F/F}$: 451, $CTC1^{-/-}$: 393, $CTC1^{-/-}$+Flag-CTC1: 572.

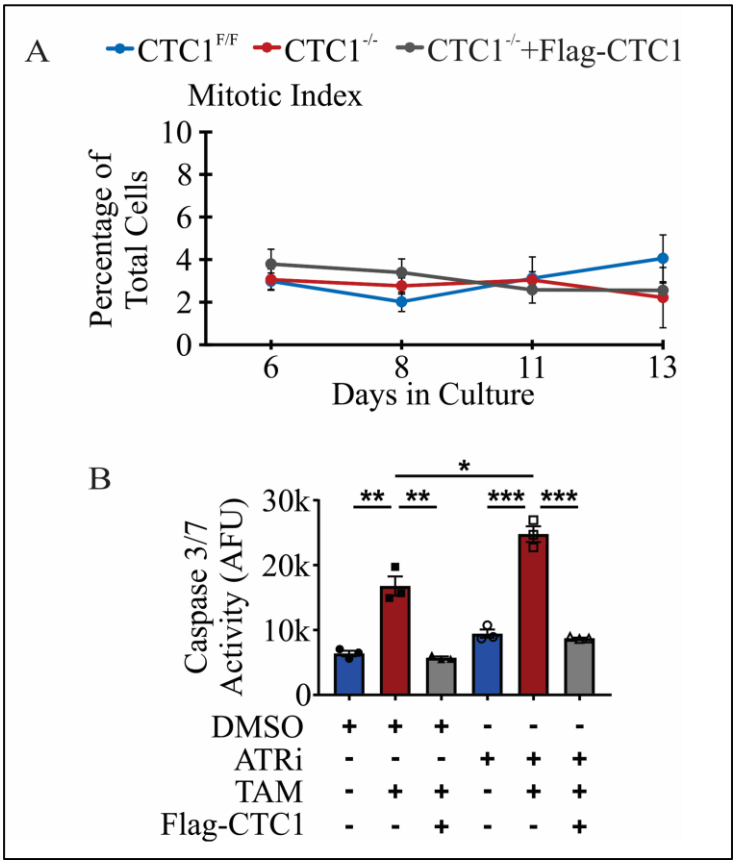

Figure 2.4 CTC1 deletion is G2 specific and induces apoptosis. (A) Mitotic index is based on the levels of phosphorylated Histone H3 as measured by immunofluorescence. (n=3 independent, biological replicates) Error bars indicate ±SEM. **(B)** Fold change of apoptosis as measured by the Caspase-Glo 3/7 assay. The ATR inhibitor (5μM, VE-821) was added for 24 h prior to measurement. (n=3 independent biological experiments.) Error bars indicate the ±SEM. P-values were calculated by an unpaired, two tailed *t* test (*$P \leq 0.05$, **$P \leq 0.01$, *** $P \leq 0.001$).

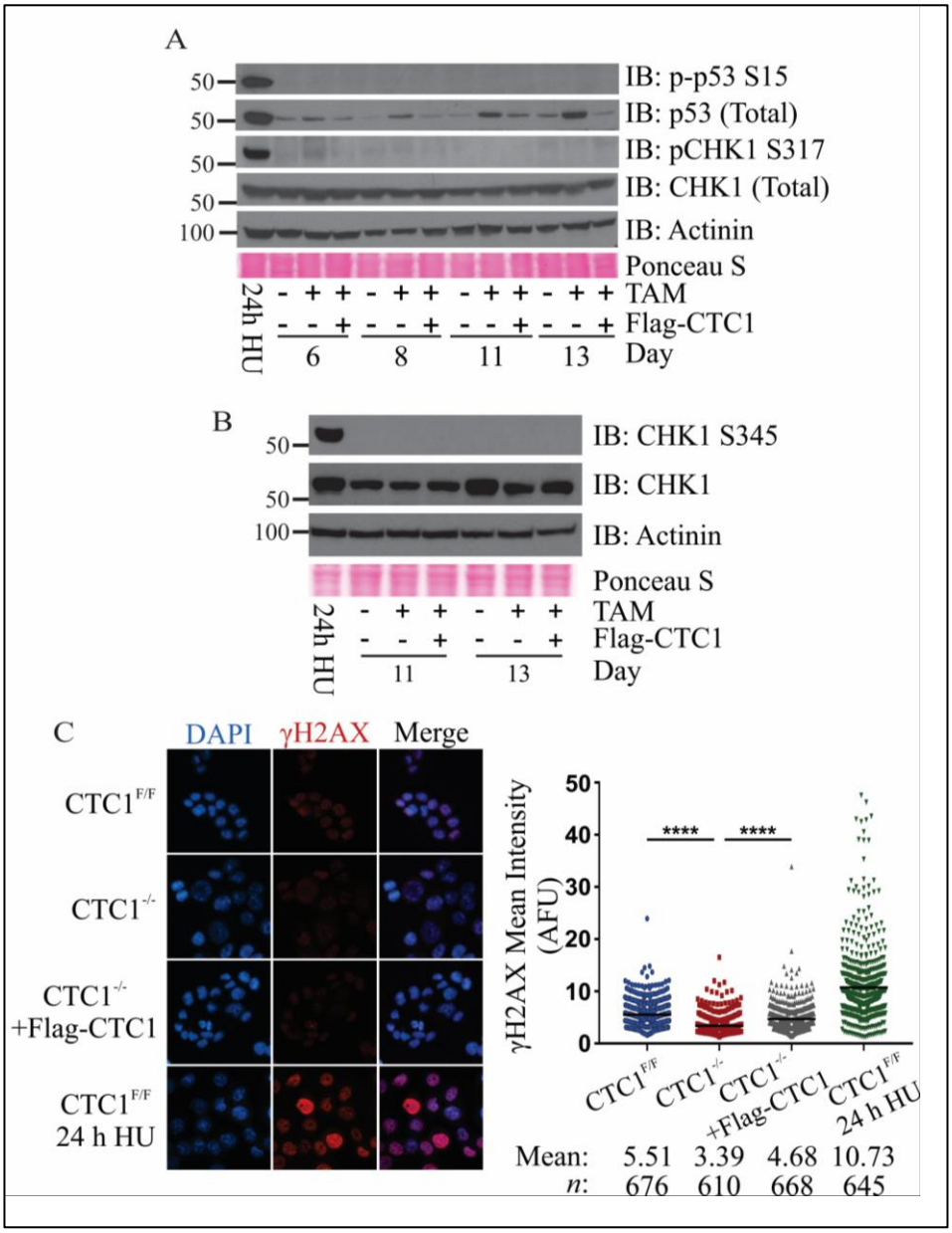

Figure 2.5 CTC1 deletion does not activate ATR-mediated p53 or CHK1 phosphorylation or global γH2AX response. (A) Levels of phosphorylated p53 S15 (p-p53 S15), or CHK1 S317 (pCHK1S317) and total CHK1 or p53, as indicated. **(B)** Levels of phosphorylated CHK1 S345 (pCHK1 S345) and total CHK1 as indicated. **(A-B)** For Western blots, Actinin and Ponceau S staining serve as loading controls. 24 h HU indicates CTC1F/F cells treated for 24 h with 2 mM HU and were used as a control for activation of the DDR. **(C)** Left: Representative images of γH2AX levels at 13 days after addition of TAM. DAPI: blue, γH2AX: red. Right: Dot plots of mean γH2AX intensity per nucleus in arbitrary fluorescent units (AFU).

Figure 2.5 CTC1 deletion does not activate ATR-mediated p53 or CHK1 phosphorylation or global γH2AX response. **(Continued)** Black lines and numbers below the graph indicate the mean AFU and number of nuclei scored (*n*). 24 h HU sample serves as a positive control for γH2AX. (n=3 independent, biological experiments). P-values were calculated by an unpaired, two tailed Mann-Whitney test (*$P \leq 0.0001$).

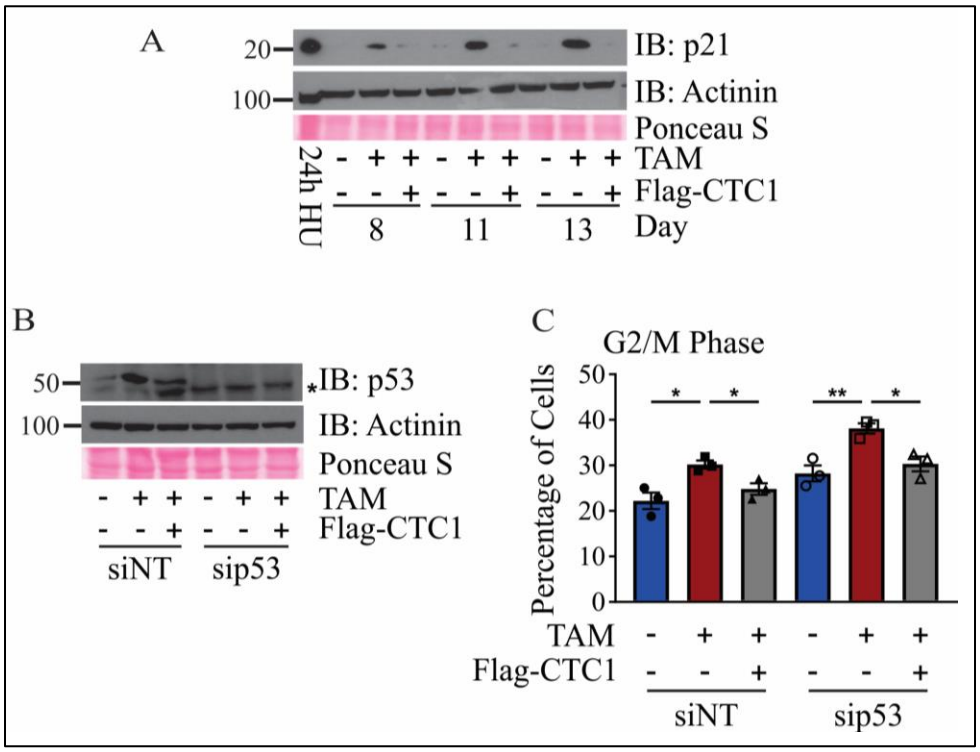

Figure 2.6 CTC1 deletion increases p53/p21, but p53 knockdown does not suppress the accumulation of G2 cells. (A) Levels of p21, as indicated. **(B-C)** Cells were treated with siRNA to a non-targeting control (siNT) or p53 (sip53) for 72 h prior to collection starting on day 8 after TAM addition. **(B)** Levels of p53 following siRNA knockdown, as indicated. * indicates non-specific bands. **(C)** Percentage of G2/M cells following siRNA knockdown of p53 (n=3 independent, biological replicates. For Western blots, Actinin and Ponceau S staining serve as loading controls. 24 h HU indicates CTC1F/F cells treated for 24 h with 2 mM HU and were used as a control for activation of the DDR. Error bars indicate the ±SEM. P-values were calculated by an unpaired, two tailed *t* test (**P* ≤0.05, ***P* ≤0.01).

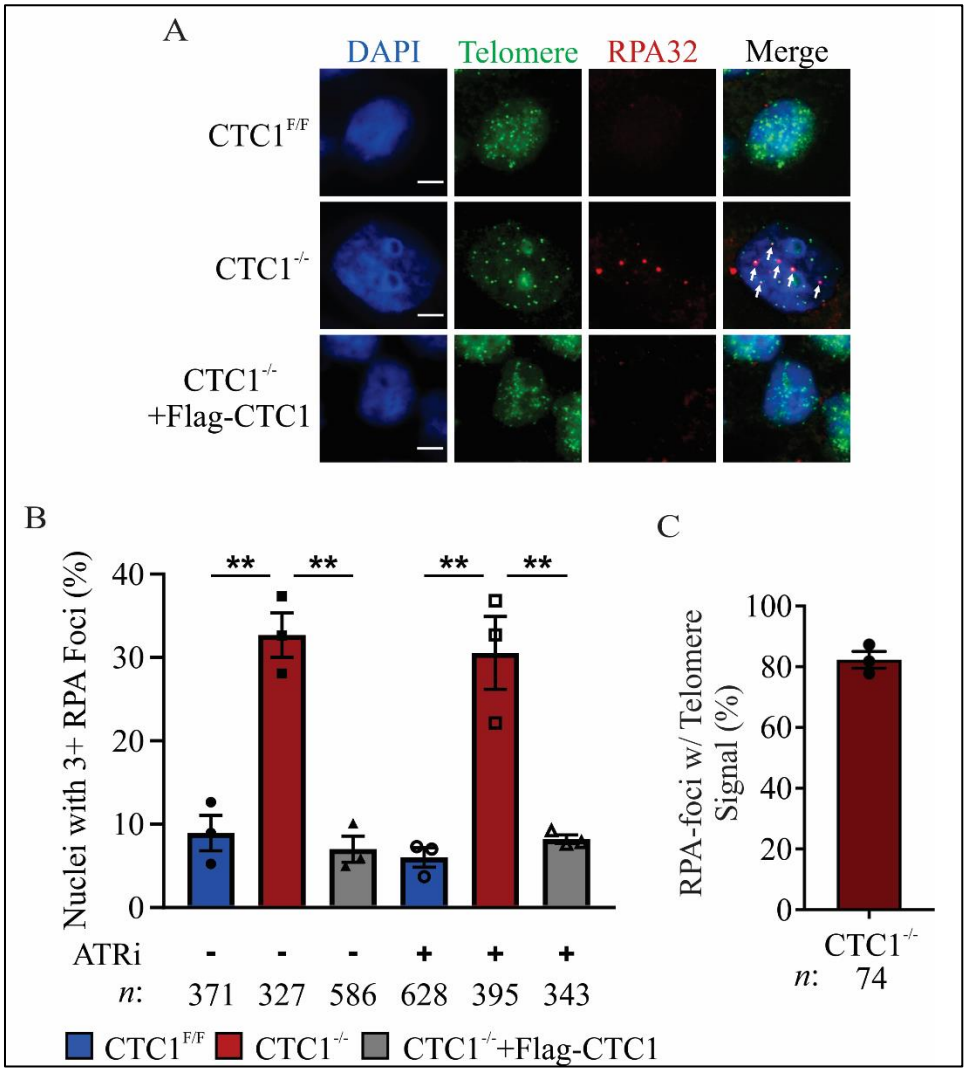

Figure 2.7 Telomeric phosphorylated RPA levels increase in response to CTC1 KO. (A) Representative images of RPA foci and telomere FISH signal on day 13 after TAM addition. Cells were pre-extracted prior to fixation to identity chromatin-bound RPA. DAPI: blue, RPA32: red, Telomere ($TTAGGG_3$); green. Scale bar represents 5 µm. **(B)** Percentage of nuclei with three or more RPA foci. (n=3 independent, biological replicates). **(C)** Percentage of RPA-foci containing telomere signal in CTC1-/- cells. (n=3 independent, biological replicates). *n* indicates the number of total nuclei scored. Error bars indicate the ±SEM. P-values were calculated by an unpaired, two tailed *t* test (**$P \leq 0.01$)

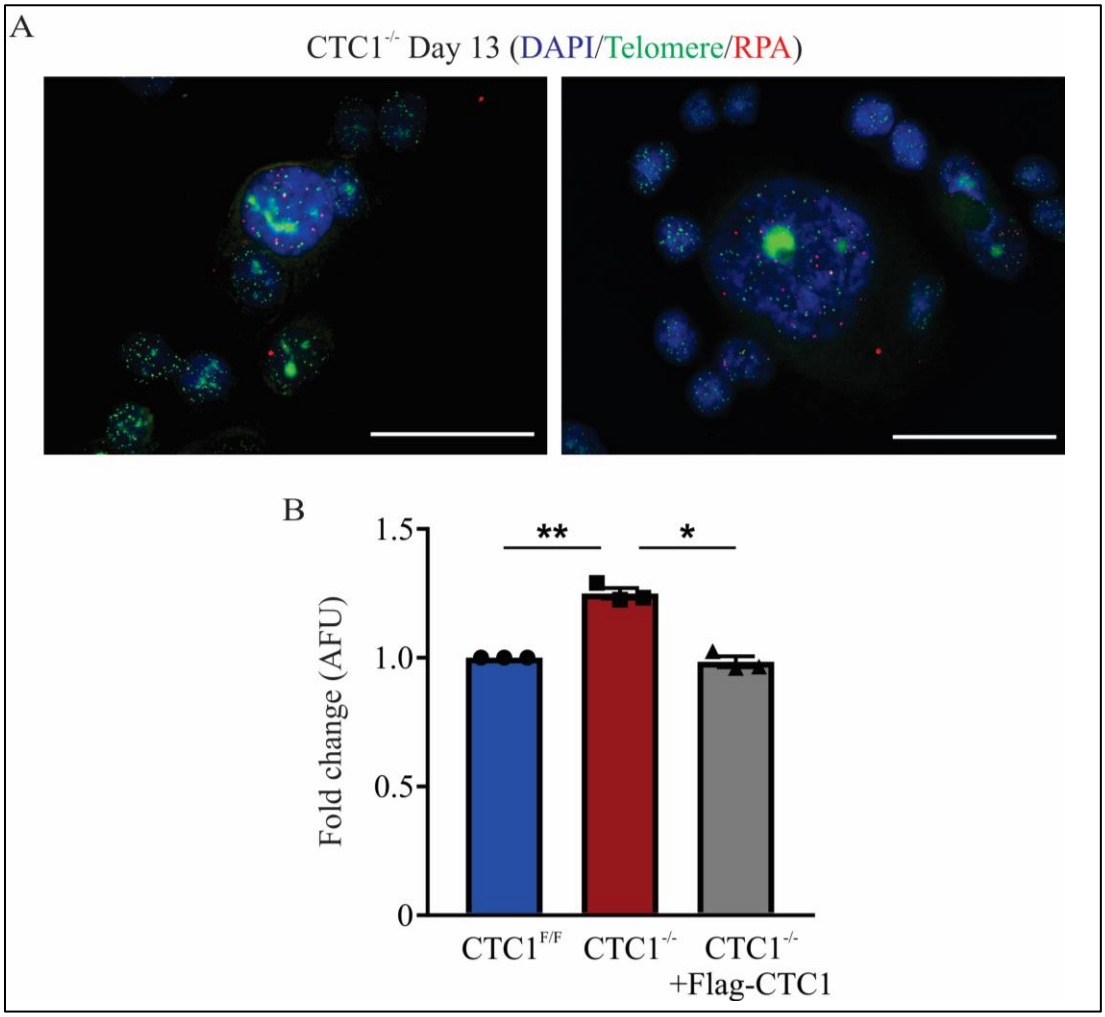

Figure 2.8 CTC1 deletion results in increased chromatin bound and telomeric RPA. (A) Representative images of CTC1-/- cells at day 13 after TAM addition. Scale bar represents 50 µm. **(B)** Flow cytometry analysis of fold change in chromatin-bound RPA32 in pre-extracted cells. (n=3 independent, biological replicates). Error bars indicate the ±SEM. P-values were calculated by an unpaired, two tailed *t* test (**P* ≤0.05, ***P* ≤0.01).

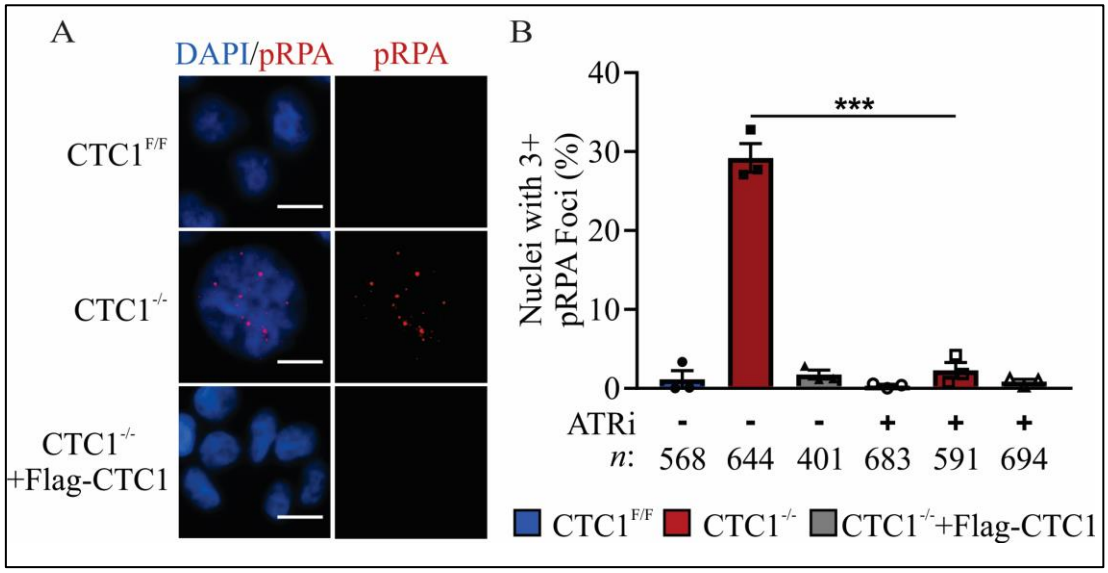

Figure 2.9 Phosphorylated RPA levels are increased in response to CTC1 KO and are ATR-dependent. (A) Representative images of phosphorylated RPA32 S33 (pRPA) foci on day 13 after TAM addition, as indicated. Scale bar represents 25 µm. **(B)** Percentage of cells with greater than three pRPA foci. (n=3 independent biological replicates). ATRi: treatment with the ATR inhibitor VE-821 for 24 h. *n* indicates the number of total nuclei scored. Error bars indicate the ±SEM. P-values were calculated by an unpaired, two tailed *t* test (***$P \leq 0.001$).

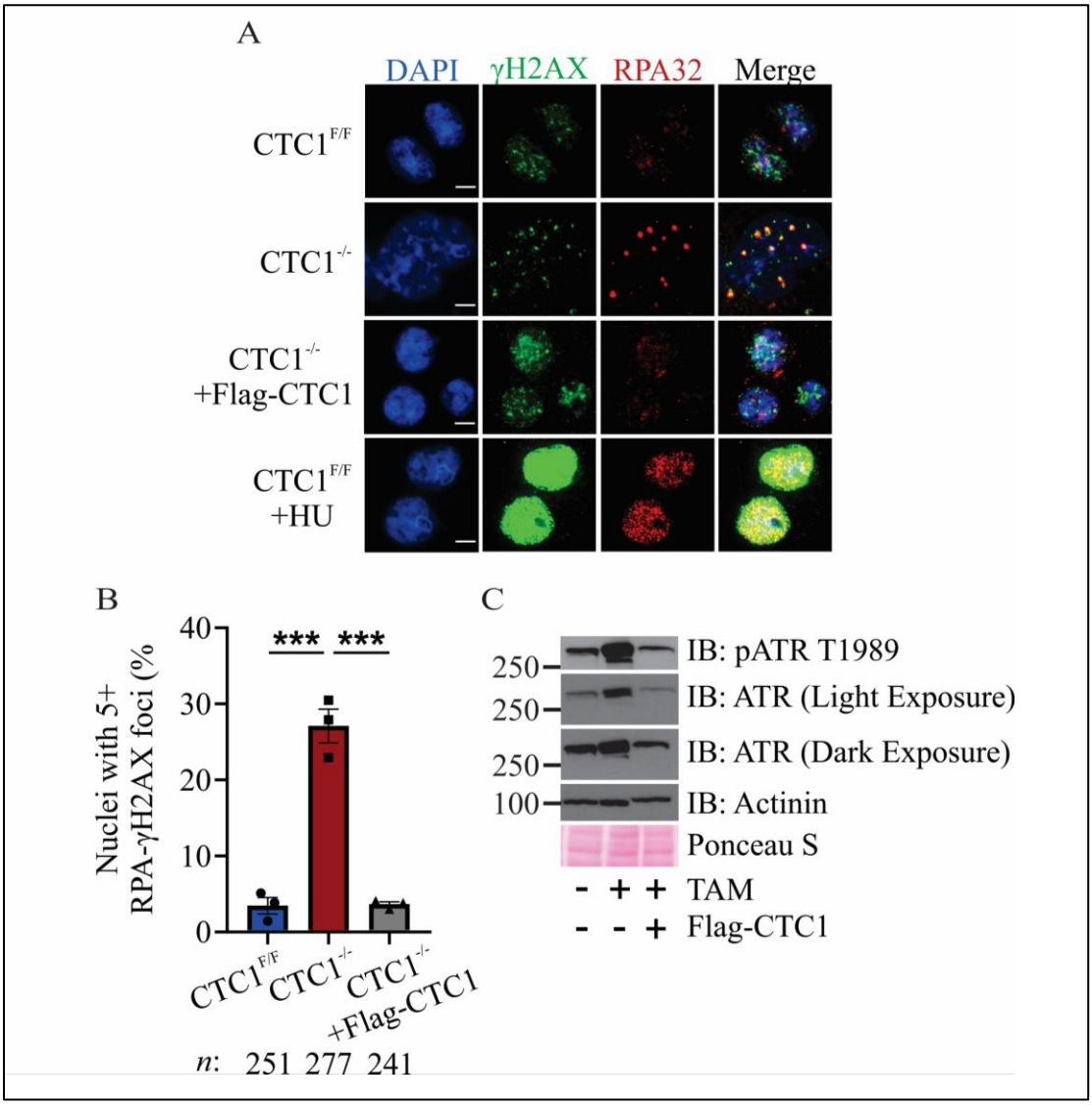

Figure 2.10 RPA localizes with γH2AX DNA damage foci, and ATR is activated in response to CTC1 KO. (A) Representative images of co-localization of RPA and γH2AX foci, as indicated. CTC1$^{-/-}$ +HU samples were treated with HU for 24 h prior to fixation and are used as a control to show the intensity of γH2AX foci in the presence of global replication stress. Scale bar represents μm. **(B)** Percentage of nuclei with greater than 5 co-localizing RPA-γH2AX foci. *n* indicates the number of nuclei scored. (n=3 independent, biological experiments). Error bars indicate the ±SEM. P-values were calculated by an unpaired, two tailed *t* test (***$P \leq 0.001$). **(C)** Levels of total and phosphorylated ATR T1989 (pATR), as indicated. Actinin and Ponceau S staining are loading controls.

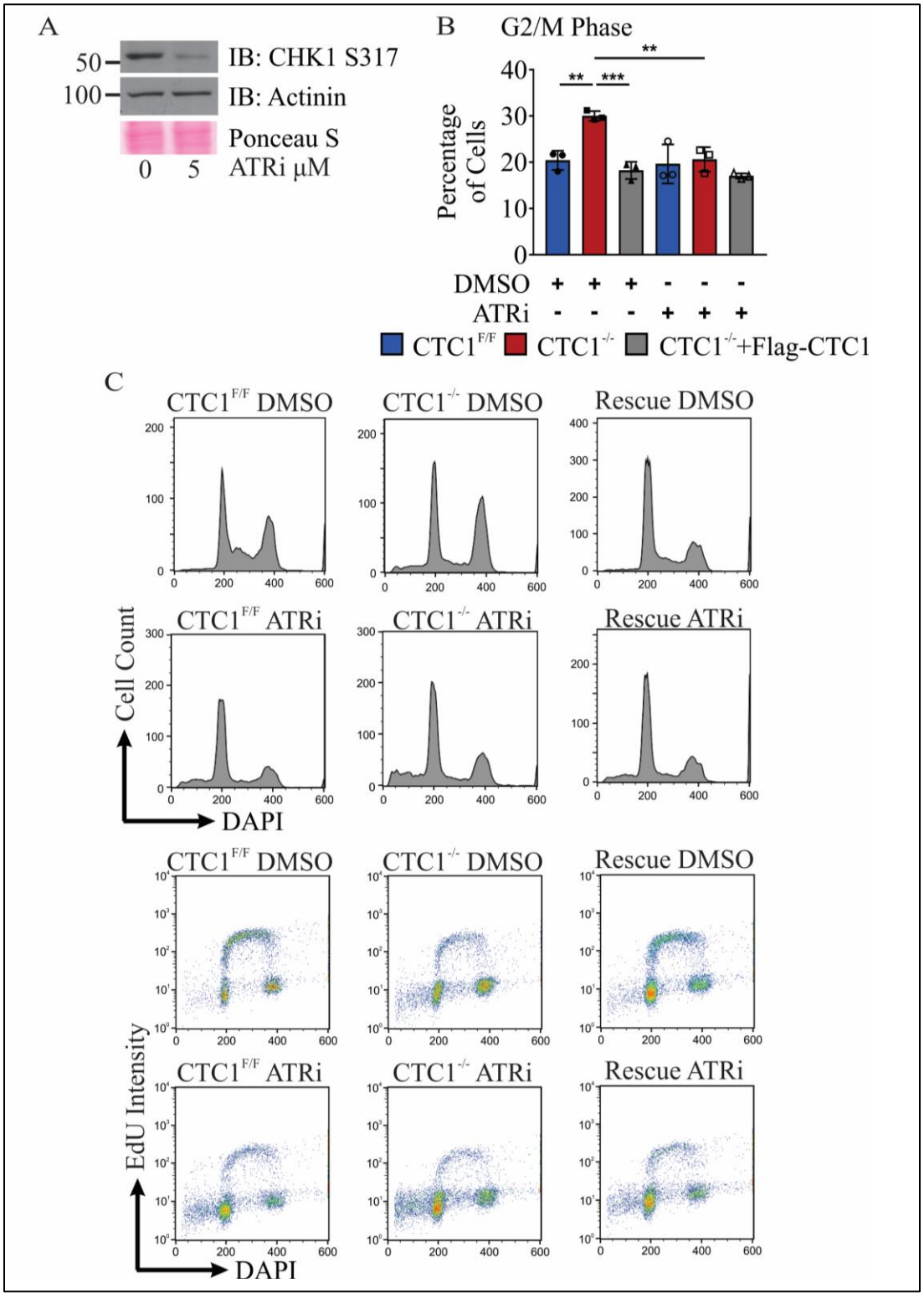

Figure 2.11 G2 arrest following CTC1 KO is ATR-dependent shown by ATRi. (A) Western blot analysis of CTC1$^{F/F}$ cells treated with 5 μM ATRi (VE-82) for 24 h to confirm ATR inhibition.

Figure 2.11 G2 arrest following CTC1 KO is ATR-dependent shown by ATRi (Continued). 2 mM HU was added 2 h prior to collection to induce CHK1 S317 phosphorylation. Actinin and Ponceau S staining serve as loading controls. **(B)** Graph of the percentage of G2/M cells at 13 days after TAM addition with DMSO or ATRi treatment for h. (n=3 independent biological replicates). Error bars indicate the ±SEM. P-values were calculated by an unpaired, two tailed *t* test (***P* ≤0.01, ****P* ≤0.001). **(C)** Representative histograms of cell cycle data for ATRi. Top: DAPI versus cell count. Bottom: DAPI versus EdU signal intensity.

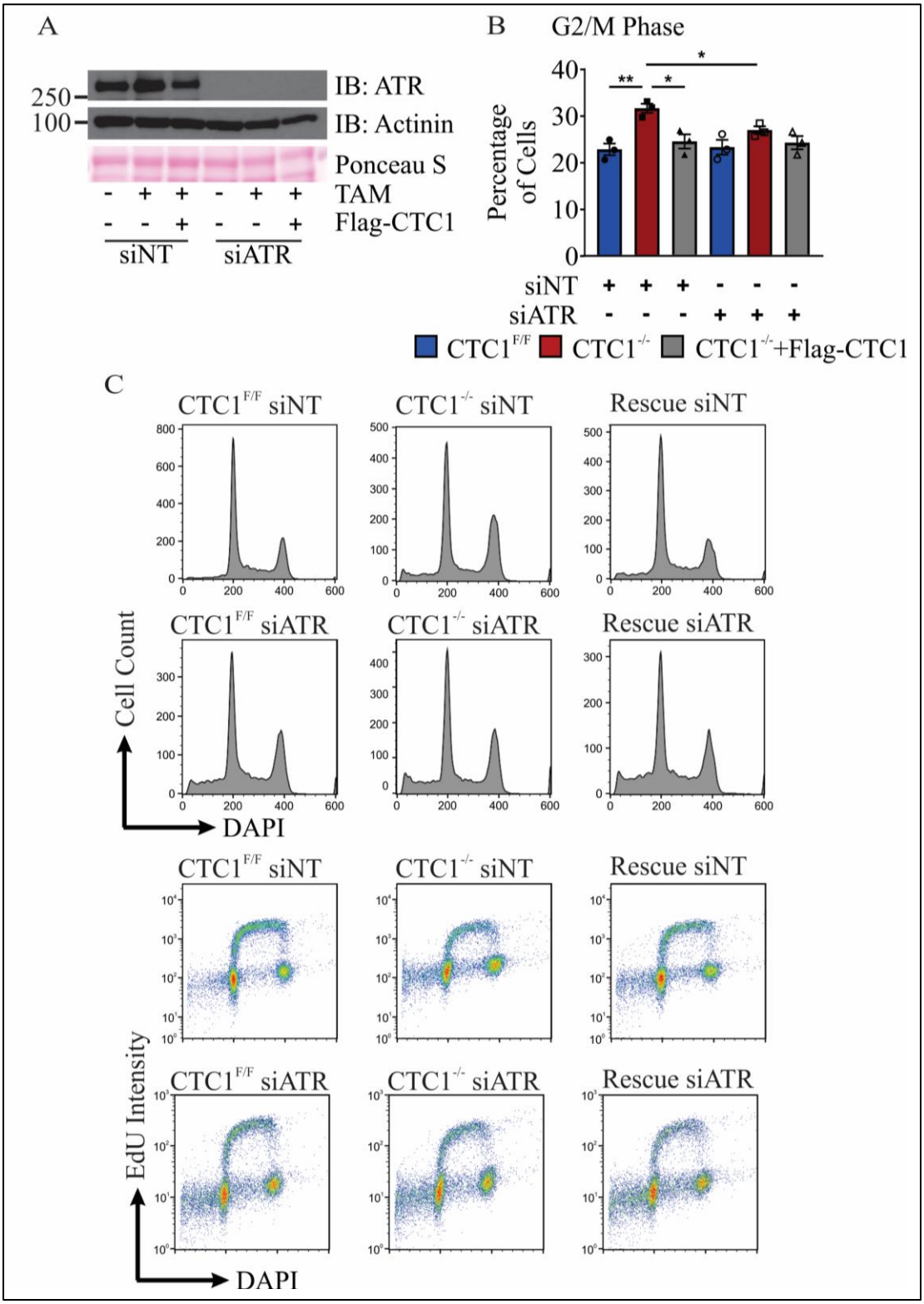

Figure 2.12 G2 arrest following CTC1 KO is ATR-dependent shown by ATR knockdown by siRNA. (A) Western blot analysis of CTC1$^{F/F}$ cells treated with siRNA targeting ATR (siATR) for 72 h prior to collection starting on day 8.

Figure 2.12 G2 arrest following CTC1 KO is ATR-dependent shown by ATR knockdown by siRNA (Continued). Cells were collected on day 11 after TAM addition and tested for knockdown efficiency. siNT: non-target control. Actinin and Ponceau S staining serve as loading controls. **(B)** Graph of the percentage of G2/M cells following siATR. (n=3 independent, biological replicates). Error bars indicate the ±SEM. P-values were calculated by an unpaired, two tailed *t* test (**P* ≤0.05, ***P* ≤0.01). **(C)** Representative histograms of cell cycle data for siNT and siATR. Top: DAPI versus cell count. Bottom: DAPI versus EdU signal intensity.

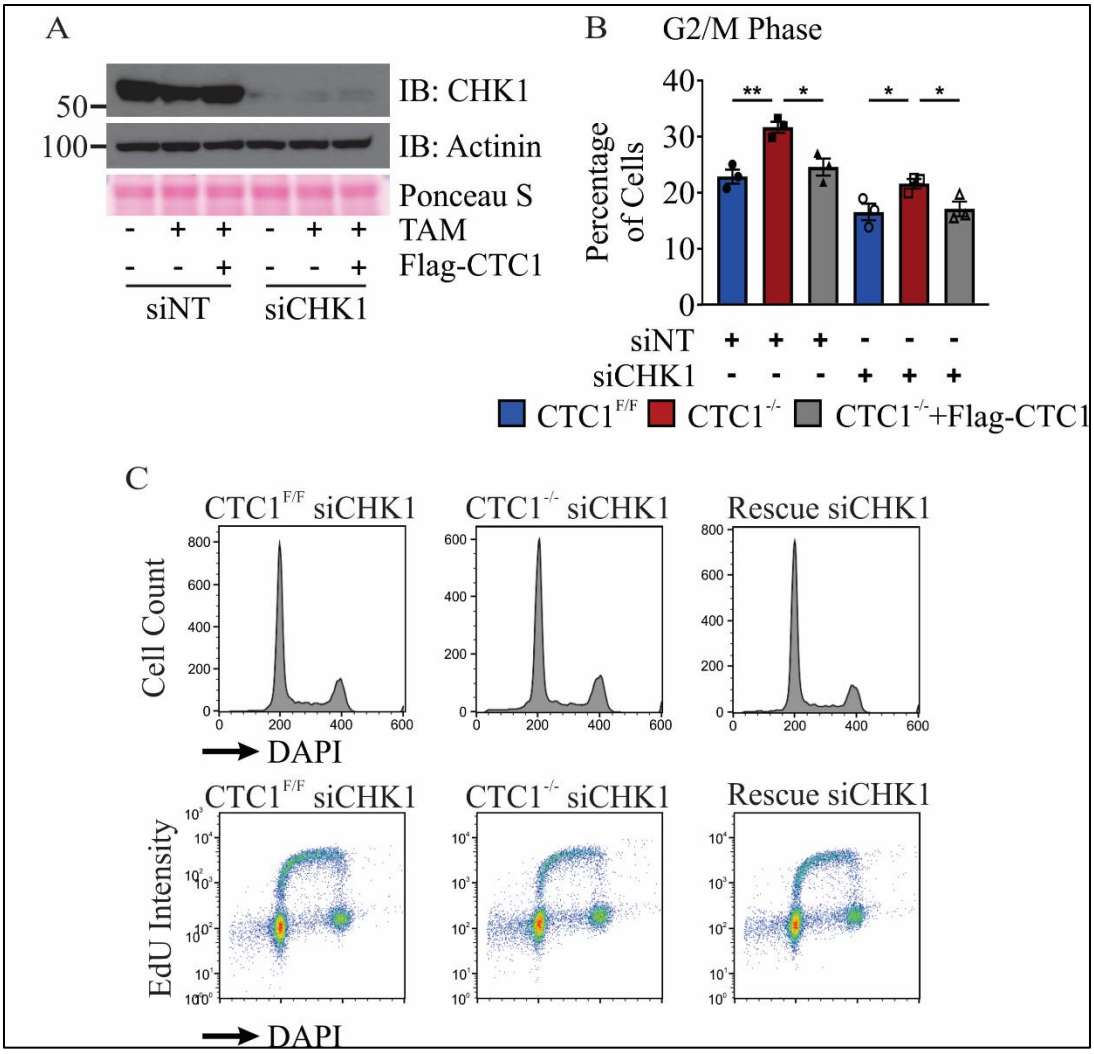

Figure 2.13 G2 arrest following CTC1 KO is CHK1-independent shown by CHK1 knockdown by siRNA. (A) Western blot analysis of CTC1$^{F/F}$ cells treated with siRNA targeting CHK1 (siCHK1) for 72 h prior to collection starting on day 8. Cells were collected on day 11 after TAM addition and tested for knockdown efficiency. siNT: non-target control. Actinin and Ponceau S staining serve as loading controls. **(B)** Graph of the percentage of G2/M cells following siCHK1. (n=3 independent, biological replicates). Error bars indicate the ±SEM. P-values were calculated by an unpaired, two tailed *t* test (**P* ≤0.05, ***P* ≤0.01). **(C)** Representative histograms of cell cycle data for siCHK1. Top: DAPI versus cell count. Bottom: DAPI versus EdU signal intensity.

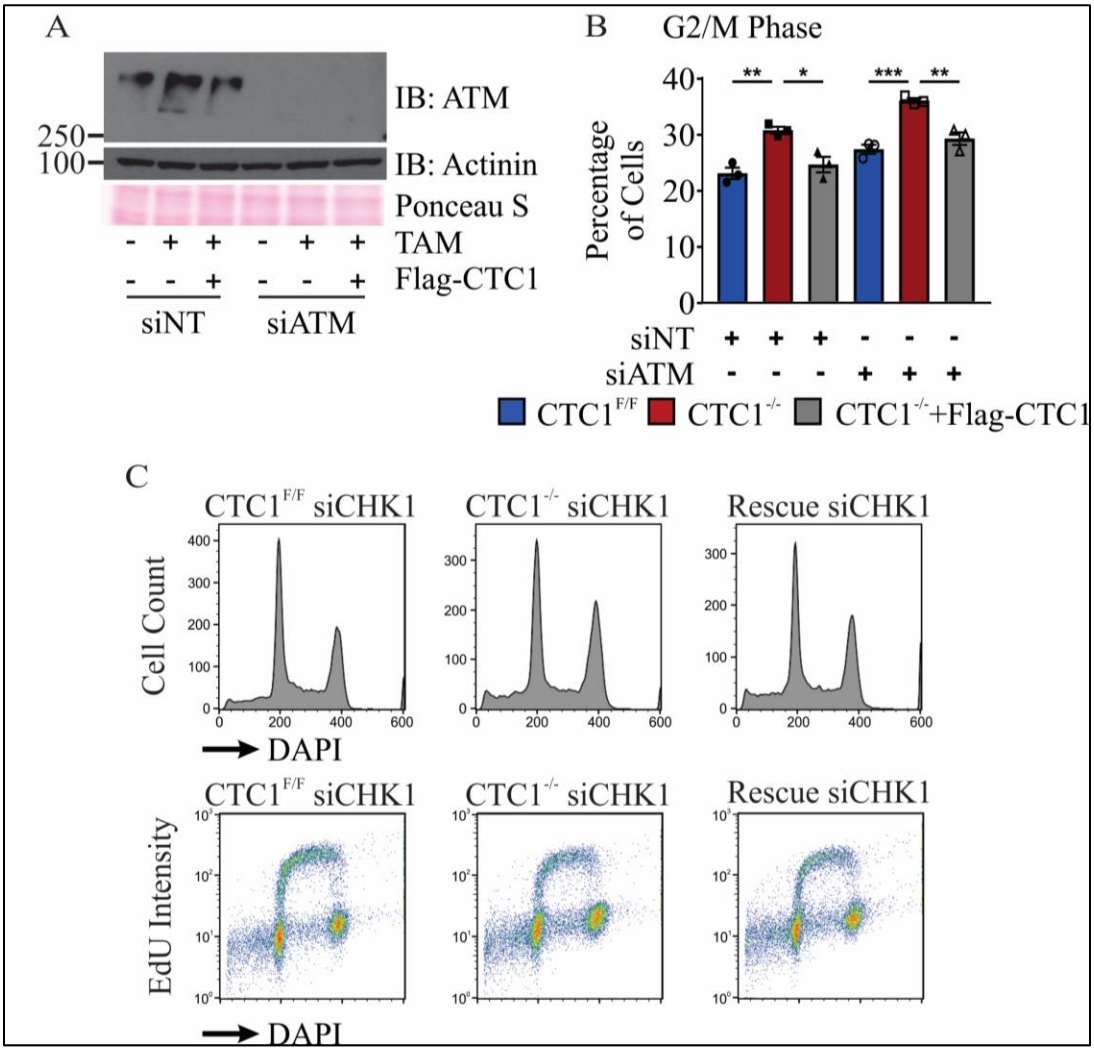

Figure 2.14 G2 arrest following CTC1 KO is ATM-independent shown by ATM knockdown by siRNA. (A) Western blot analysis of CTC1$^{F/F}$ cells treated with siRNA targeting ATM (siATM) for 72 h prior to collection starting on day 8. Cells were collected on day 11 after TAM addition and tested for knockdown efficiency. siNT: non-target control. Actinin and Ponceau S staining serve as loading controls. **(B)** Graph of the percentage of G2/M cells following siATM. (n=3 independent, biological replicates). Error bars indicate the ±SEM. P-values were calculated by an unpaired, two tailed *t* test (*$P \leq 0.05$, **$P \leq 0.01$, **$P \leq 0.001$). **(C)** Representative histograms of cell cycle data for siATM. Top: DAPI versus cell count. Bottom: DAPI versus EdU signal intensity.

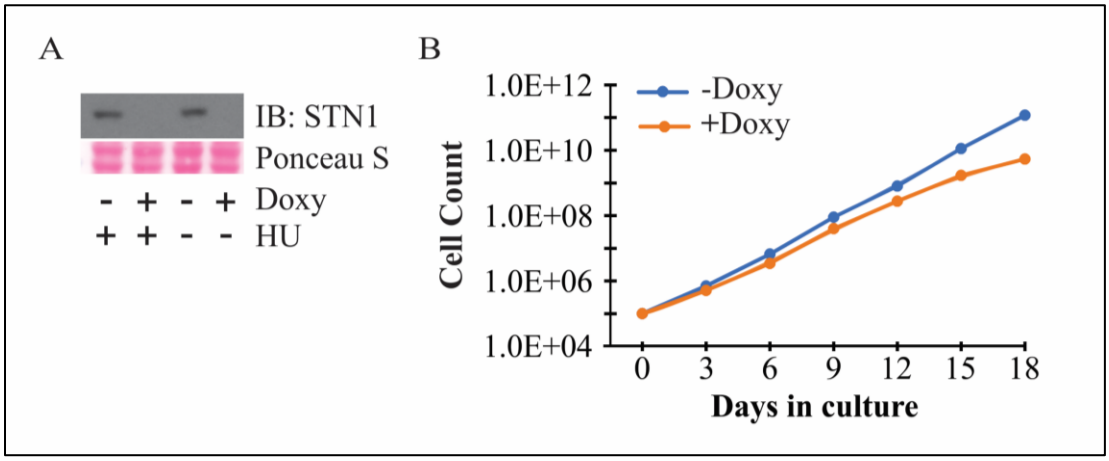

Figure 2.15 STN1 deletion results in a decrease in cell proliferation. (A) Doxy was added to HeLa iCas9 sgSTN1 cells at day 0 to disrupt STN1. Western blot of STN1 KO (+Doxy) on days 12 and 15 after Doxy treatment. Ponceau S staining is a loading control. **(B)** Representative growth curve of three independent, biological replicates.

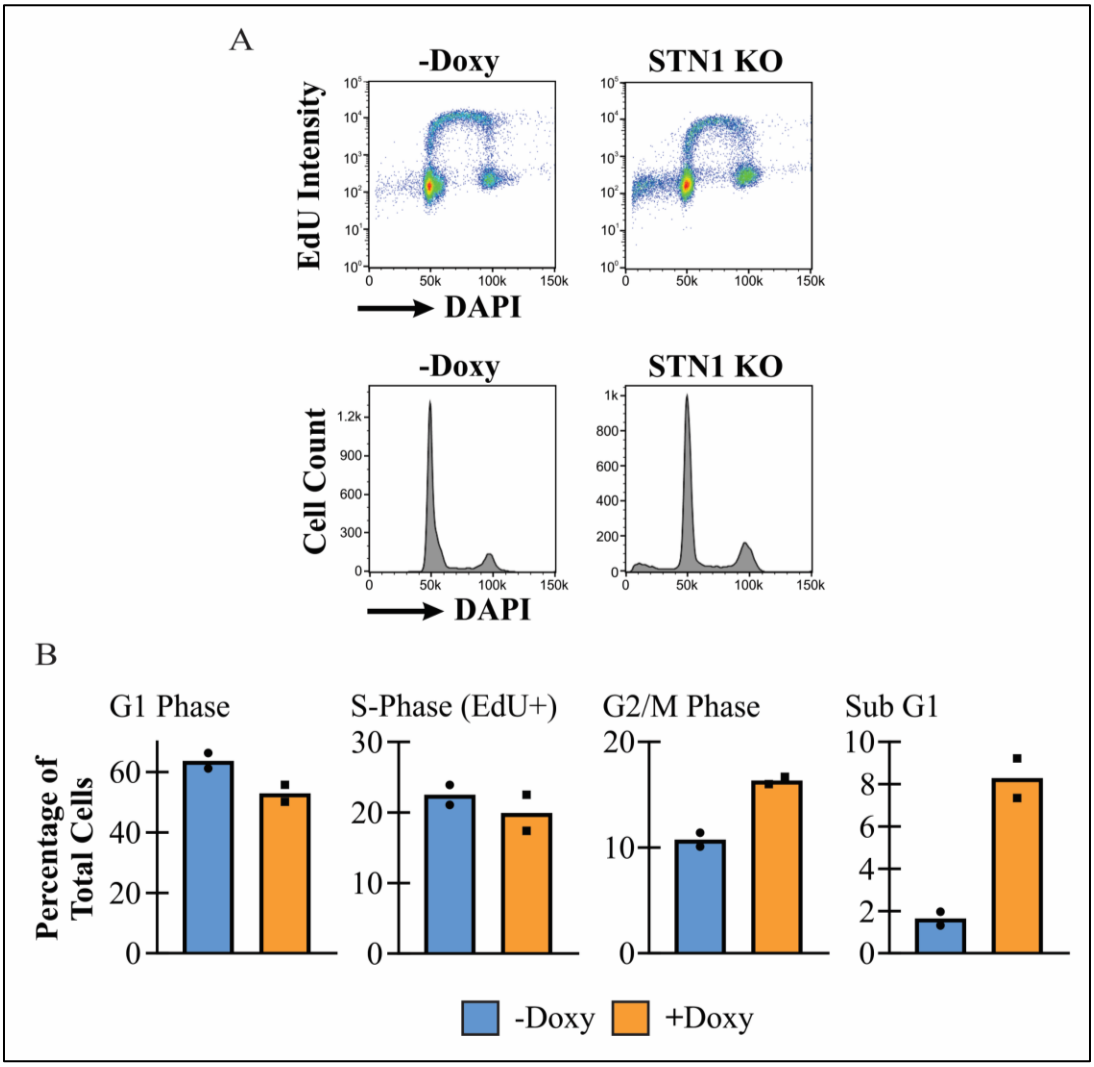

Figure 2.16 STN1 deletion results in partial G2 arrest and increased Sub G1 population. **(A)** Representative histograms from flow cytometry analysis. Top panel: DNA content versus replicating cells (EdU+). Bottom panel: DNA content (DAPI) versus cell count. **(C)** Percentage of cells in each cell cycle phase, as indicated. (n=2 independent, biological replicates). -Doxy indicates untreated cells, +Doxy indicates STN1 KO.

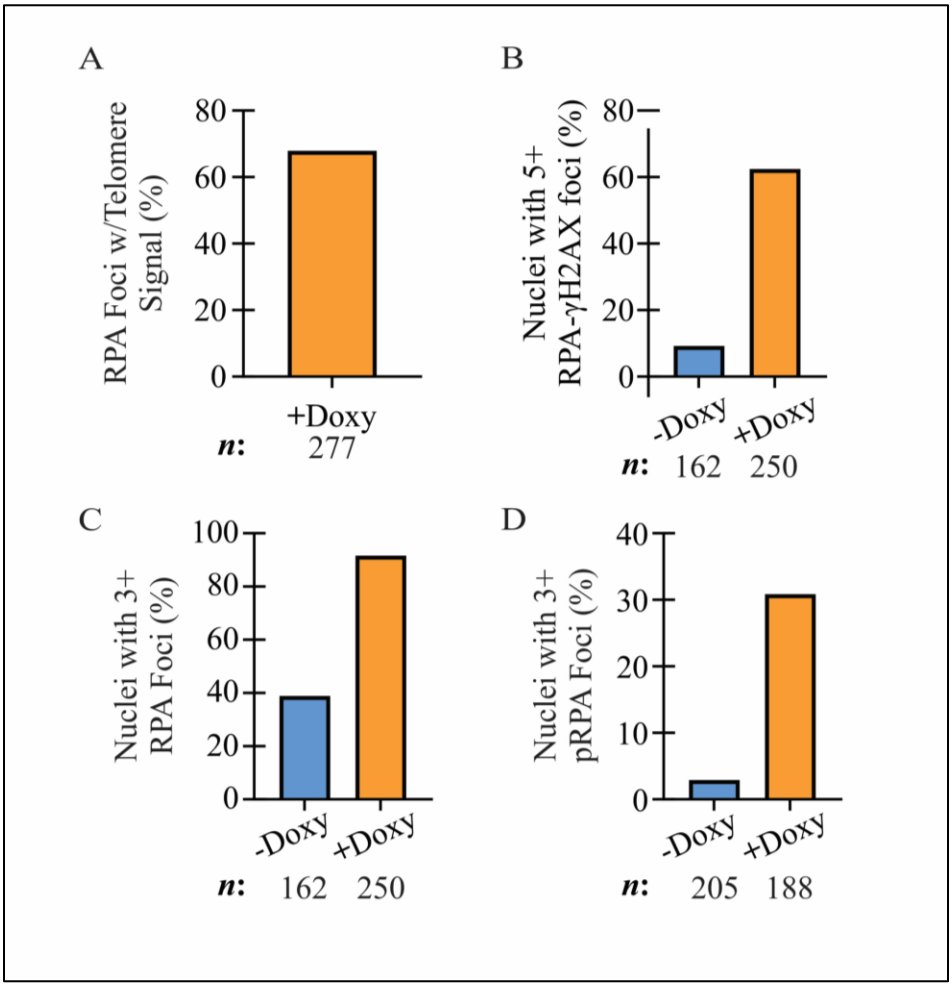

Figure 2.17 STN1 deletion results in increased telomeric RPA foci and RPA phosphorylation. A) Percentage of RPA foci containing telomere signal in STN1 KO cells, *n* indicates the number of total nuclei scored. **(B)** Percentage of nuclei with greater than 5 co-localizing RPA-γH2AX foci. *n* indicates the number of nuclei scored. **(C)** Percentage of nuclei with 3 or more RPA foci, *n* indicates the number of nuclei scored. **(D)** Percentage of nuclei with 3 or more pRPA foci, *n* indicates the number of nuclei scored. (For all, n=1 biological replicate and were analyzed at 15 Days after doxy addition).

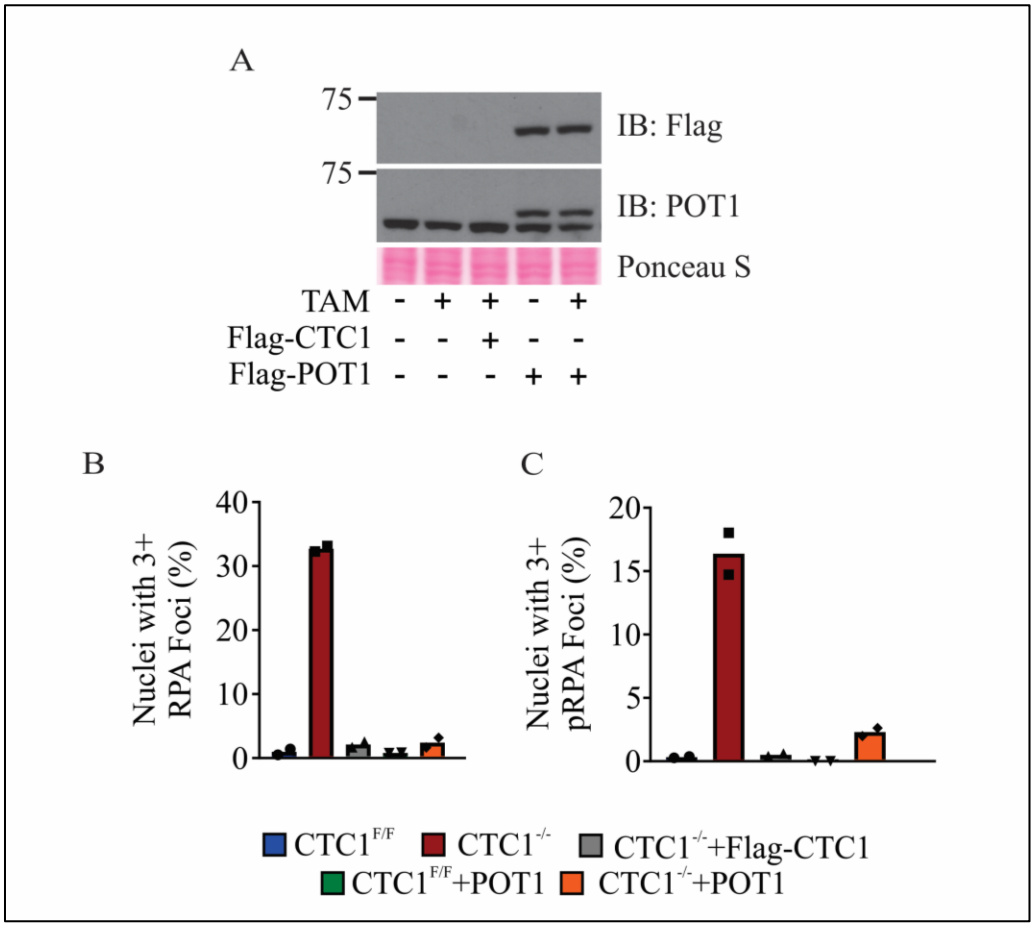

Figure 2.18 POT1 over expression rescues RPA and pRPA levels after CTC1 deletion (A) Western blot of POT1 and Flag-POT1 levels at 11 days in culture, as indicated. Ponceau S serves as a loading control. **(B)** Percentage of nuclei with three or more RPA **(B)** or pRPA **(C)** foci 11 days after CTC1 deletion (n=2 independent biological experiments).

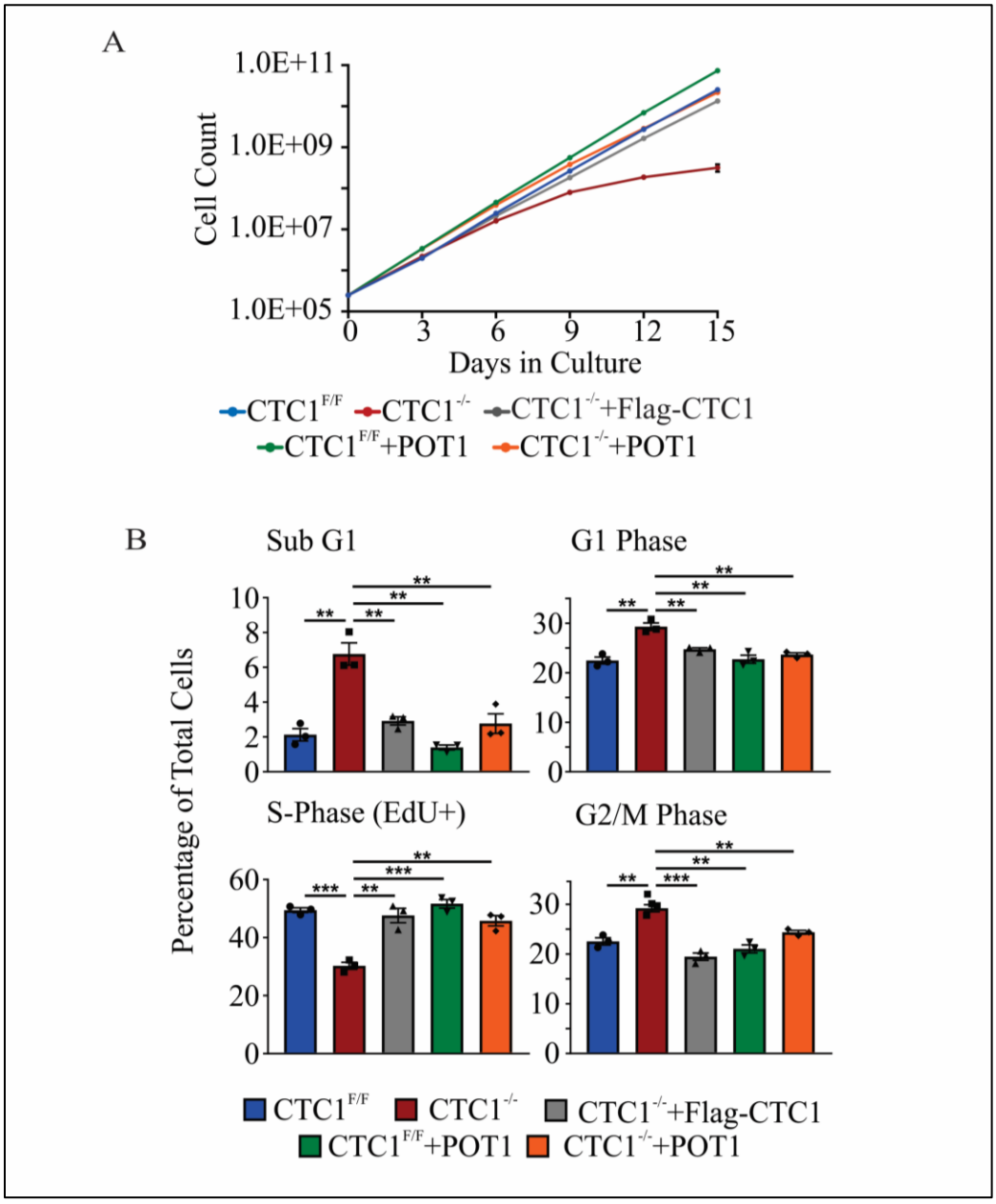

Figure 2.19 Over expression of POT1 rescues the CTC1 KO induced growth defect and cell cycle arrest (A) Representative growth curve of two independent biological replicates, as indicated. **(B)** Flow cytometry was used to assess cell cycle phases, as indicated (n=3 independent biological replicates). Error bars indicate the ±SEM. P-values were calculated by an unpaired, two tailed *t* test (**P* ≤0.05, ***P* ≤0.01, ****P* ≤0.001).

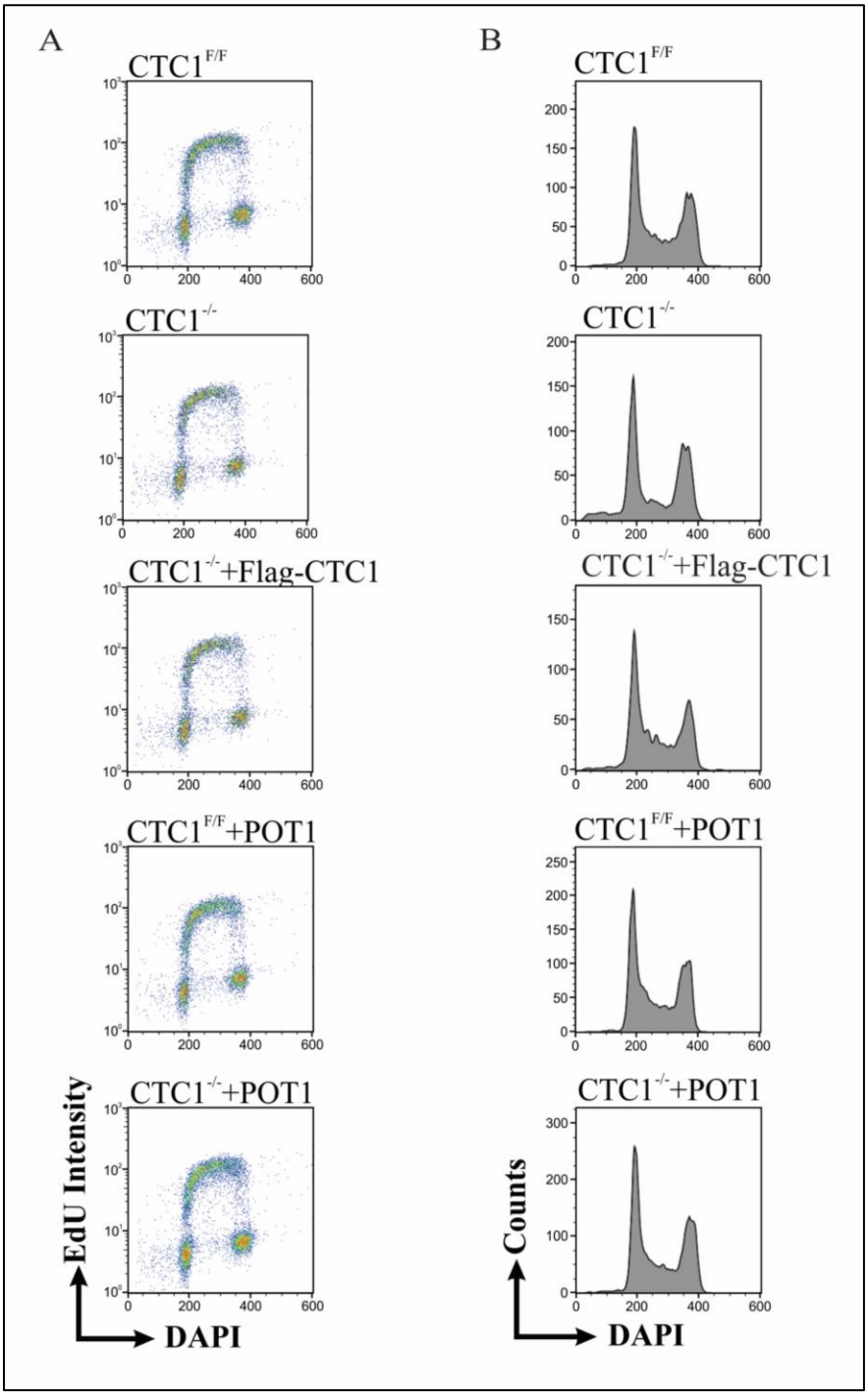

Figure 2.20 Cell cycle profile of CTC1$^{-/-}$ cells with POT1 OE. **(A)** Representative graphs from flow cytometry analysis showing DNA content (DAPI) versus replicating cells (EdU+). **(B)** Representative histograms from flow cytometry analysis showing DNA content versus cell count.

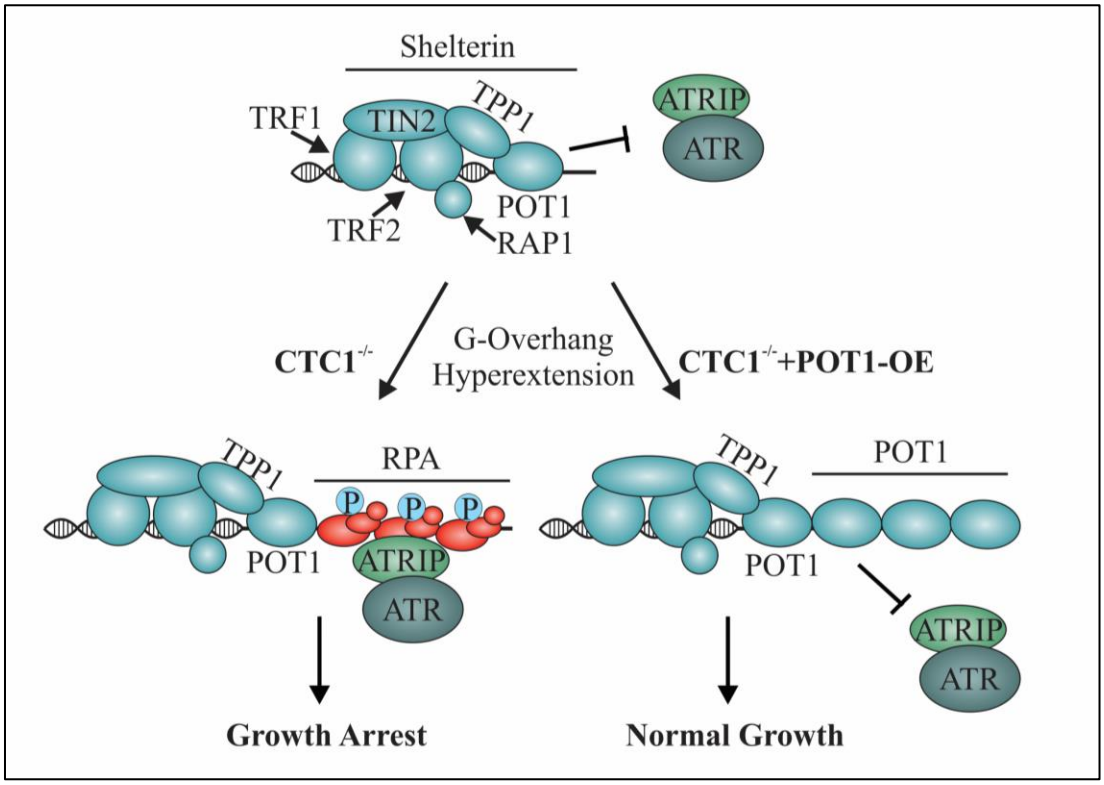

Figure 2.21 Model of telomere damage signaling after CTC1 deletion with or without POT1 OE. POT1 prevents telomeric RPA binding and thus inhibits ATR activation at telomeres. In the absence of CTC1 ($CTC1^{-/-}$), the telomeric G-overhand is hyperextended, leading to the exhaustion of POT1 in the cell and telomeric RPA binding. This in turn leads to ATR localization and G2 arrest. However, when POT1 is overexpressed in the absence of CTC1 ($CTC1^{-/-}$+POT1), the G-overhangs are coated by POT1, blocking RPA binding and G2 arrest.

CHAPTER 3

CST IS A NOVEL REGULATOR OF TOPBP1 AND THE ATR-CHK1 SIGNALING PATHWAY

3.1 INTRODUCTION

As seen in previous studies and in Chapter 2, CTC1 or STN1 KO results in G-overhang elongation to the point that endogenous POT1 is insufficient to protect the ssDNA. In mammals, POT1 prevents RPA from binding the G-overhang, which in turn suppresses ATR activation and unwanted "repair" of the telomeres by HR. ATR is the predominant kinase which responds to ssDNA damage genome-wide. RPA-bound ssDNA serves as a platform for localization of ATR to the damage site through interaction with ATRIP. However, localization alone is not sufficient for ATR activation. To date there are two known activators of ATR, ETAA1 and TopBP1. Whether ATR activation occurs via ETAA1 versus TopBP1 is dependent on cell cycle phase and the presence of DNA damage. ETAA1 plays a primary role in ATR activation during normal DNA replication and mitosis, and is suggested to play only a minor role in the DDR (30139873 and 30755469). On the other hand, TopBP1 is essential for activation of ATR in response to ssDNA damage [12].

For TopBP1 localization to ssDNA damage, it engages the 9-1-1 complex at ds-ssDNA junctions [2, 16, 17]. TopBP1 interacts with and activates ATR in a mechanism which is both necessary and sufficient for stimulating ATR-ATRIP [12]. Once activated, ATR then phosphorylates a number of downstream substrates. In particular, ATR phosphorylates CHK1 at residues S317 and S345 activating this effector kinase [19, 20]. CHK1 then phosphorylates additional effectors which contribute to G2 arrest as well as intra S-phase inhibition of origin firings [110-112]. Although ATR is activated and induces a partial G2 arrest in $CTC1^{-/-}$ cells (Figures 2.7-11), CHK1 is not activated.

Therefore, we were interested to see if TopBP1-dependent ATR signaling to CHK1 is defective in response to exogenous stress.

3.2 RESULTS

3.2A CTC1 KO LEADS TO DECREASED LEVELS OF TopBP1

Since TopBP1 recruitment is independent of ATR recruitment to DNA damage, we examined whether defects in TopBP1 recruitment and protein expression could explain why CHK1 is not phosphorylated (Figure 2.5) despite significant levels of RPA-ssDNA and ATR activation after CTC1 deletion (Figures 2.7-2.9). TopBP1 protein levels were measured at days 8, 11 and 13 following TAM addition (Figure 3.1). Surprisingly, we observed a decrease in TopBP1 following conditional CTC1 KO starting at day 11 after TAM addition. These findings are significant as the timing of TopBP1 decline corresponds to the increase in RPA-ssDNA and accumulation of G2 cells following CTC1 removal. This suggested to us that ATR-mediated CHK1 signaling could be defective due to decreased cellular and chromatin-bound TopBP1. We also examined the levels of the other major ATR activator ETAA1 and found that it was also decreased in the CTC1-/- cells (Figure 3.1). Since ETAA1 appears to play a minor role in ATR-mediated CHK1 activation following DNA damage, it is unclear how this might affect checkpoint signaling. However, it is possible that decreased ETAA1 could contribute to changes in cell cycle progression. We next examined whether decreased TopBP1 was due to changes in gene expression. We performed qPCR to measure TopBP1 mRNA levels but did not observe any significant changes at day 8 and only minor changes at days 11 and 13 that were not statically significant, suggesting that decreased protein stability and not gene expression is likely responsible for the changes in TopBP1 (Figure 3.1D).

3.2B CTC1 PROMOTES ATR-MEDIATED CHK1 SIGNALING FOLLOWING EXOGENOUS REPLICATION STRESS THROUGH TopBP1

Since TopBP1 is important for ATR-CHK1 activation, we hypothesized that CST promotes CHK1 phosphorylation in the presence of exogenous replication stress by stabilizing TopBP1. This would be consistent with previous findings demonstrated that shRNA depletion of TopBP1 results in reduced pCHK1 S317/S345 following replication stress [113]. To test our hypothesis, we measured CHK1 phosphorylation in cells following treatment with HU, which is known to induce global replication fork stalling, create excess ssDNA and activate the ATR-CHK1 pathway [114]. Cells were treated with HU for 2 h before collection to generate ssDNA but not cause fork collapse and DSBs [115]. Phosphorylation of CHK1 and γH2AX staining were then assessed by Western blot and IF, respectively (Figure 3.2 and 3.3). In line with our hypothesis, we observed a decrease in the levels of pCHK1 S317/S345 and γH2AX in CTC1 deleted cells compared to controls.

To see whether we could rescue pCHK1 levels, Flag-tagged TopBP1 was exogenously expressed in $CTC1^{-/-}$ and control cell lines at day 8 after TAM addition. At day 11, cells were treated with HU for 2 h and then collected for Western blot analysis. Transfection with exogenous TopBP1 resulted in similar levels of TopBP1 in the $CTC1^{F/F}$, $CTC1^{-/-}$ and $CTC1^{-/-}$+Flag-CTC1 cells (Figure 3.4A). pCHK1 S317 was then measured as a readout of ATR-dependent CHK1 activation (Figure 3.4A). While CHK1 phosphorylation was inhibited in the CTC1-/- cells, we found that expression of exogenous TopBP1 rescued CHK1 phosphorylation in response to HU treatment. A possible explanation for the decreased pCHK1 is that it arises from the lower number of

S-phase cells following CTC1 KO (Figure 2.2B). To exclude this possibility, we determined the number of S-phase cells with and without expression of Flag-TopBP1 (Figure 3.5). In both cases, the number of S-phase cells is decreased in CTC1$^{-/-}$ cells, however, pCHK1 S317 is rescued with TopBP1 expression after HU treatment. These findings strongly suggest that the lower level of S-phase cells do not account for the decreased levels of pCHK1 observed in the CTC1$^{-/-}$ cells after HU treatment. Interestingly, while addback of TopBP1 rescued pCHK1 following replication stress, it did not rescue global pCHK1 in CTC1$^{-/-}$ cells in the absence of HU treatment. Thus, restoration of TopBP1 levels alone is not sufficient to rescue ATR-CHK1 signaling arising from telomere-bound RPA and additional factors likely contribute to the telomere DNA damage response in the absence of CST.

3.2C STN1 KO PREVENTS CHK1 PHOSPHORYLATION DUE TO DECREASED TopBP1 LEVELS IN THE CELL

To further validate the role of CST in TopBP1 expression and ATR-CHK1 signaling, we assessed TopBP1 and pCHK1 levels in HeLa iCas9 STN1 KO cells. In agreement with the experiments in CTC1$^{-/-}$ cells, we found that STN1 deletion results in severe loss of TopBP1 (Figure 3.6). Furthermore, CHK1 phosphorylation is absent in untreated cells, and upon HU induction, CHK1 is not activated in STN1$^{-/-}$ cells. Unlike CTC1 deletion, STN1 KO also showed decreased levels of total CHK1 (Figure 3.6). The mechanism behind this still unclear but could be due to differences in the cell type used or possible non-overlapping functions of CTC1 versus STN1. Overall, these results indicate that both CTC1 and STN1 are required to regulate TopBP1 and fully activate the

ATR-CHK1 pathway in response to genome-wide replication stress (Figure 3.7). These results could in part explain how CST promotes recovery from replication stress.

3.3 DISCUSSION

Here, we further investigated the surprising results from Chapter 2 in which ATR activation does not result in CHK1 phosphorylation after CTC1 deletion. Upon further analysis, we discovered that CST regulates the ATR activator TopBP1 and that removal of CTC1 or STN1 leads to a substantial decrease in CHK1 phosphorylation following global replication stress. Together, these findings highlight an unanticipated function of human CST in maintaining genome stability through the regulation of CHK1 phosphorylation.

As seen in Chapter 2, POT1 overexpression was able to rescue the G2 arrest in $CTC1^{-/-}$ cells (Figure 2.19). In a similar vein, we propose that CST could both stabilize TopBP1 and override telomere protection pathways to induce "repair" or shortening of the G-overhang. It is also possible that hyperextension of the G-overhang activates protection mechanisms that lead to TopBP1 degradation as a means to prevent recognition of the RPA-coated G-overhang as recombination intermediates.

In regard to genome-wide ATR activation following replication stress, our results determined that regulation of TopBP1 by CST contributes to ATR-CHK1 signaling. Unlike untreated $CTC1^{-/-}$ cells, with HU-induced fork stalling, CHK1 activation is fully rescued by overexpression of TopBP1 (Figure 3.4). In the event of genome-wide replication stress, decreased TopBP1 levels short-circuit TopBP1-dependent ATR activation (Figure 3.7). However, while ATR was active at telomeres (i.e. pRPA), ATR-

CHK1 signaling was compromised not only due to decreased TopBP1 levels, but also some yet undiscovered mechanism.

TopBP1 is integral to both checkpoint activation and DNA replication origin firing [116], so why is DNA replication and origin firing not inhibited in these cells? We propose that it is due to the decreased but not complete absence of TopBP1 (Figure 3.1). In this case, while there is enough TopBP1 for origin activation, these levels are insufficient to fully activate ATR-mediated CHK1 signaling. This suggests that it may be possible to separate TopBP1 functions through regulating its protein expression and would also explain why pCHK1 levels are decreased but not absent following global fork stalling in the $CTC1^{-/-}$ cells. Furthermore, it implies that TopBP1 is regulated through multiple pathways.

While the mechanism of ATR activation by TopBP1 has been closely examined, how TopBP1 levels are regulated remains poorly understood. Previous work has shown that TopBP1 is post-transcriptionally regulated by two E3 ubiquitin ligases, UBR5 (also known as EED1 and hHYD) and HUWE1 (also known as HECTH9 and MULE) [117-119]. Interestingly, TopBP1 when not chromatin associated is targeted for degradation by the ubiquitin ligase, HUWE1 [117]. This protection is at least partly facilitated by the transcriptional repressor Miz1. In a similar manner, CST could stabilize TopBP1 by recruiting it to the chromatin. As to the mechanism of CST recruitment to stalled forks, we recently showed that CST interacts with the MCM2-7 helicase [30]. Thus, CST could be recruited to stalled forks by MCM2-7 and then recruit TopBP1 to prevent degradation, stimulating ATR-mediated CHK1 phosphorylation. However, whether CST directly or indirectly stabilizes TopBP1 will require further studies.

In addition to TopBP1, ATR can also be activated by ETAA1. However, several studies suggest that TopBP1 is the dominant pathway for ATR-CHK1 activation following replication stress [10, 120]. Recent work from the Cortez lab showed that, in HCT116 cells, deletion of the AAD of ETAA1 did not inhibit ATR activation. Yet, attempts to delete the AAD of TopBP1 resulted in cell death, indicating that, at least in HCT116 cells, TopBP1 is the major activator of ATR [14]. Accordingly, it is unlikely that ETAA1 could compensate for decreased TopBP1. In addition, we find that ETAA1 levels are also decreased after CTC1 KO, suggesting this potential secondary pathway is not even available for ATR-mediated CHK1 activation (Figure 3.1). Why ETAA1 levels are decreased following CTC1 deletion is unclear. However, it is possible that TopBP1 and ETAA1 are regulated through similar mechanisms. In summary, we establish CST as a regulator of ATR-CHK1 signaling in response to global replication stress through maintenance of TopBP1 levels. While further studies are essential to delineate the mechanism by which CST regulates TopBP1 levels, this is a ground breaking first step in understanding the regulation of TopBP1 activity.

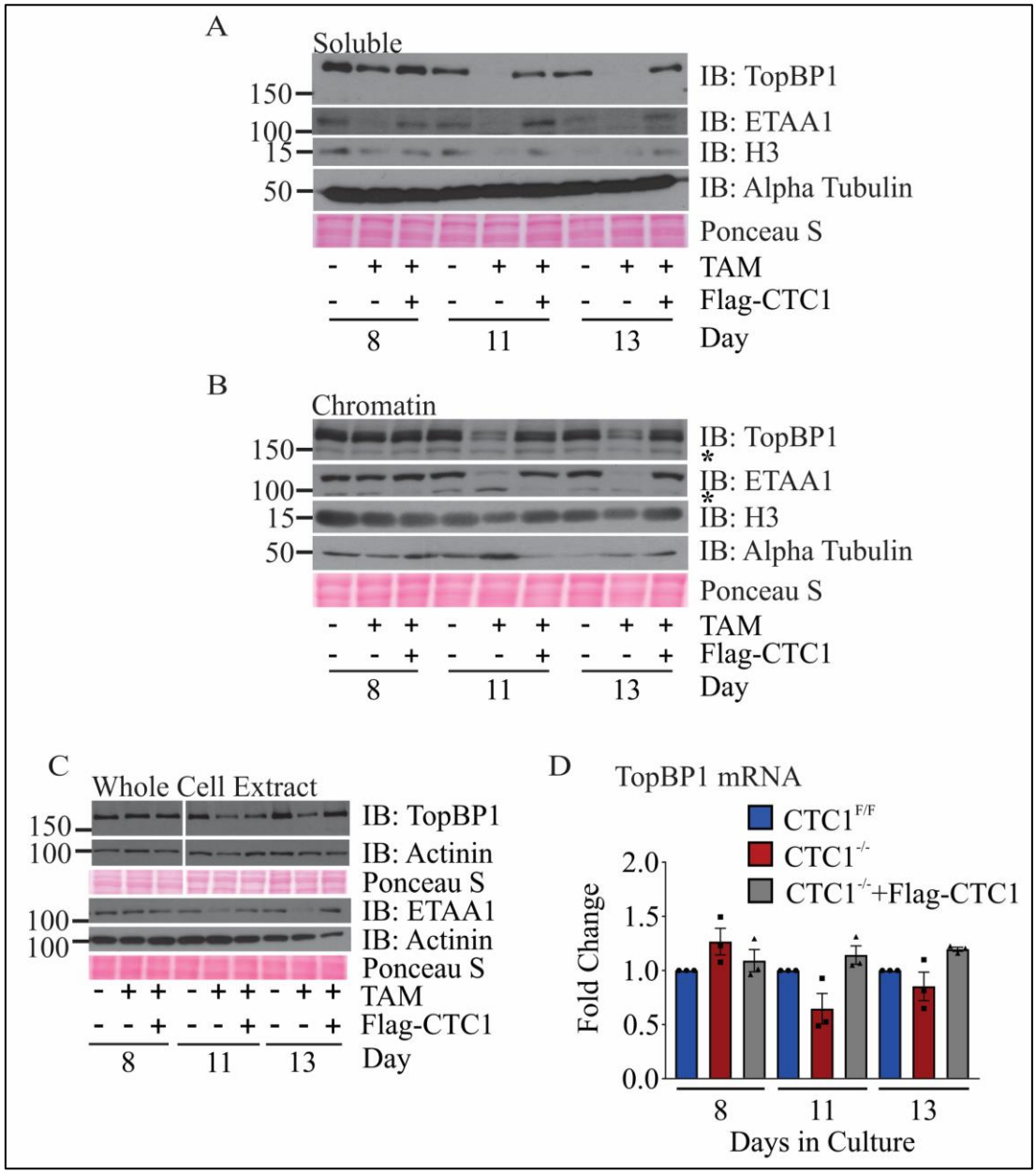

Figure 3.1 CTC1 deletion leads to decreased TopBP1. Western blots of soluble **(A)**, chromatin **(B)**, and **(C)** whole cell extractions at days 8, 11, and 13, as indicated. Ponceau S serves as a loading control for total protein. α-Tubulin and H3 serve as controls for the soluble and chromatin extracts, respectively. * Indicates non-specific bands. **(D)** Graph of the fold change in TopBP1 mRNA levels at days 8, 11, and 13 following TAM addition in HCT116 cells. CTC1-/-, and CTC1-/-+Flag-CTC1 fold change is normalized to the CTC1F/F sample on each day. Statistical analysis by *t* test did not find any samples that reached a p-value <0.05. (n=3 independent, biological experiments).

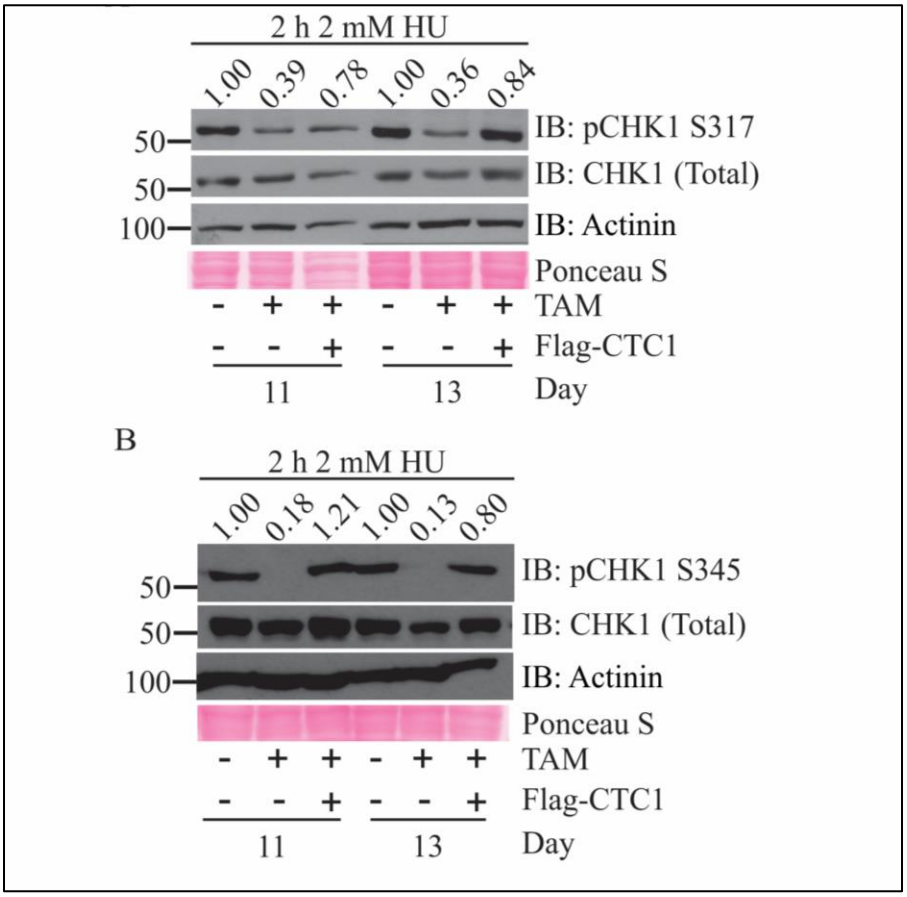

Figure 3.2 CTC1 promotes ATR-CHK1 signaling following HU treatment. (A-B) Western blots of pCHK1 S317 **(A)** or pCHK1S345 **(B)** from whole cell lysates after treatment with 2 mM HU for 2 h, as indicated. Quantification of pCHK1 signal intensity is indicated above the gel. Total CHK1 levels were used to normalize the pCHK1 signal.

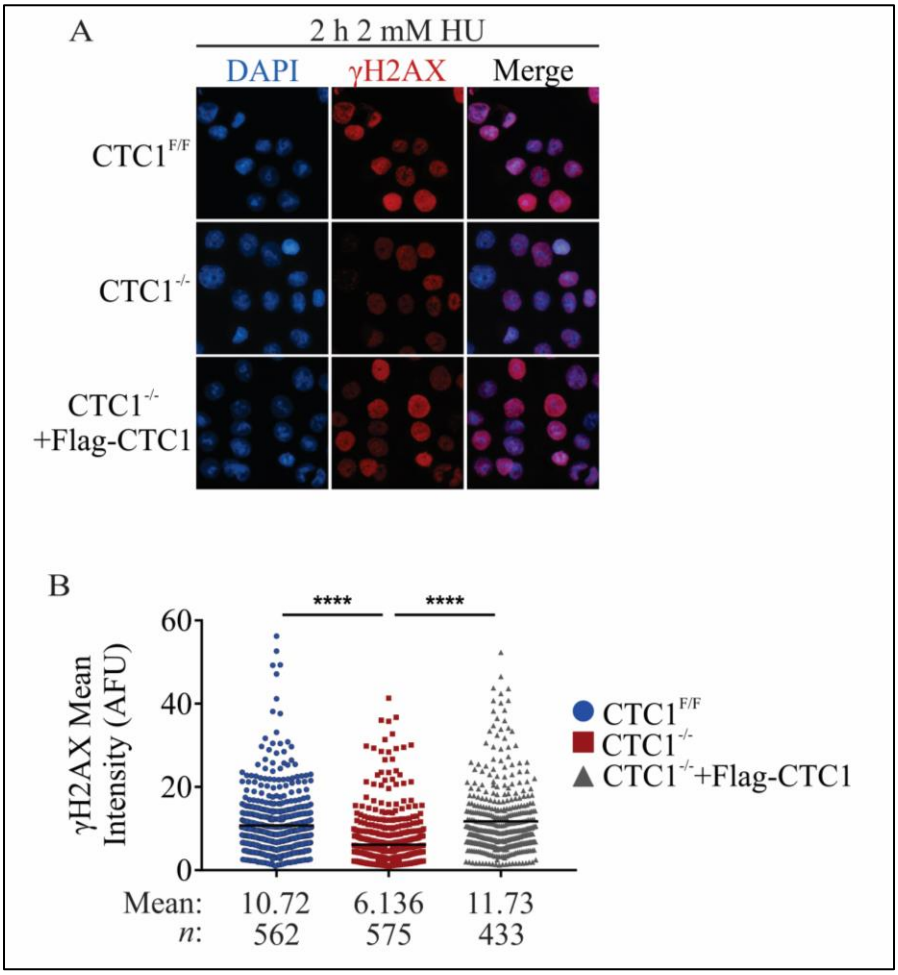

Figure 3.3 CTC1 promotes ATR signaling through γH2AX following HU treatment. Cells were treated with 2 mM HU for 24 h at 13 days after TAM addition. **(A)** Representative images of γH2AX signal. DAPI: blue, γH2AX: red. **(B)** Dot plots of mean γH2AX intensity per nucleus in arbitrary fluorescent units (AFU). Black line and numbers below the graph indicate the mean AFU (n=3 independent, biological replicates). P-values were calculated by an unpaired, two-tailed Mann-Whitney test (****$P \leq 0.0001$).

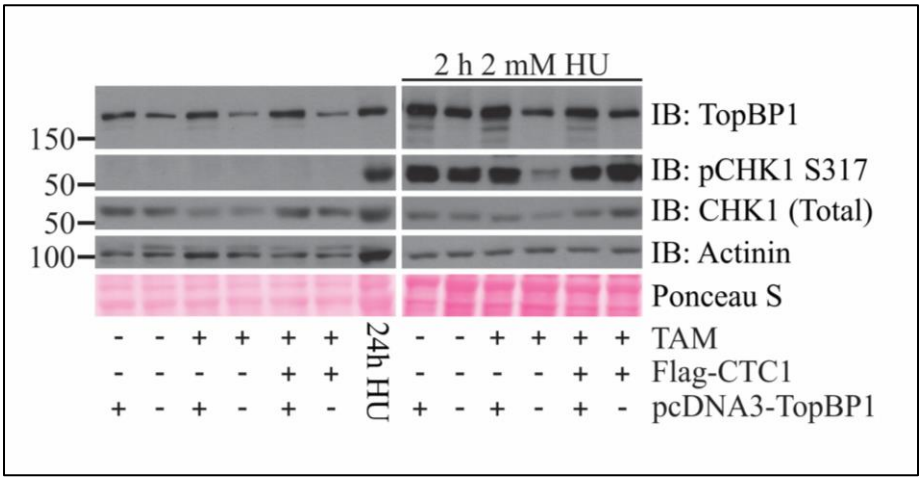

Figure 3.4 TopBP1 promotes ATR-CHK1 signaling in the absence of CTC1. Cells were transfected with pcDNA3-TopBP1 on day 8 and then collected on day 11. Western blot analysis of TopBP1 and pCHK1 S317 in whole cell lysates. For HU treated samples, cells were treated with 2 mM HU for 2 h just prior to collection. 24 h HU indicates $CTC1^{F/F}$ cells treated for 24 h with 2 mM HU and were used as a positive control for pCHK1. Total CHK1, Actinin and Ponceau S serve as loading controls.

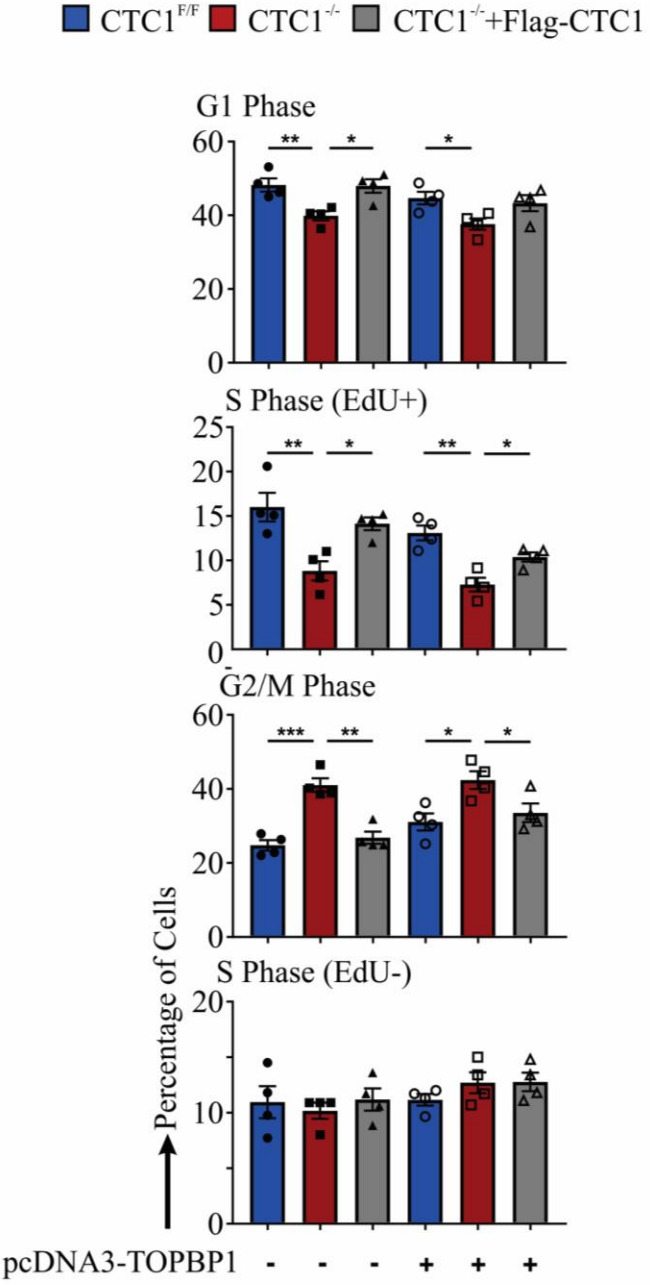

Figure 3.5 Exogenous TopBP1 expression does not increase the number of S-phase cells in CTC1$^{-/-}$ cells. Cell cycle profile analysis at 13 days after TAM addition with or without expression of exogenous Flag-TopBP1. (n=3 independent, biological replicates). Error bars indicate the ±SEM. P-values were calculated by an unpaired, two tailed *t* test (*$P \leq 0.05$, **$P \leq 0.01$, ***$P \leq 0.001$).

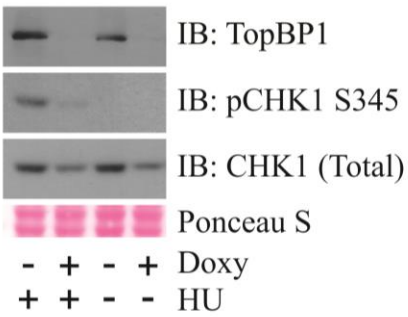

Figure 3.6 STN1 promotes TopBP1 stability and ATR-CHK1 signaling following HU treatment. Western blots of TopBP1 and pCHK1 S345 at 15 days after iCas9 deletion of STN1 (+Doxy). Samples were treated with or without 2 mM HU treatment for 2 h, as indicated. CHK1 and Ponceau S are loading controls.

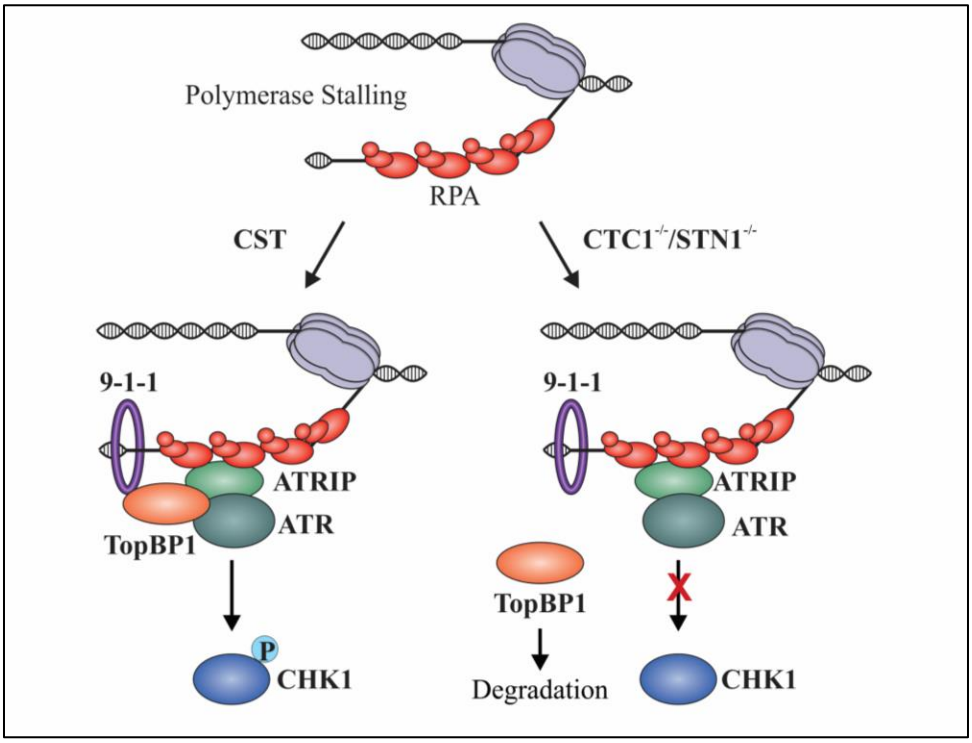

Figure 3.7 Model of CTC1 function in ATR-CHK1 activation following fork stalling. Following RPA binding, ATRIP-ATR and the 9-1-1 complex are recruited to the ssDNA damage. In the presence of CTC1 ($CTC1^{F/F}$), TopBP1 is then recruited for ATR-CHK1 activation and G2 arrest (left). However, when CTC1 is absent ($CTC1^{-/-}$), TopBP1 is destabilized leading to inhibition of CHK1 phosphorylation (right).

CHAPTER 4

STRUCTURE AND FUNCTIONAL ANALYSIS OF CTC1

4.1 INTRODUCTION

CTC1 promotes accurate and successful telomere replication (Chapter 2), and is a novel regulator of the ATR-CHK1 pathway (Chapter 3). However, it is unclear whether CST acts to rescue hyper-elongated G-overhangs to inhibit telomeric DNA damage signaling. Furthermore, little is still known about CST structure and how different domains affect cellular function.

Before the recent discovery of the cryo-EM structure of CST, CP patient mutations were used to try to separate different functions of CST through structural/function analysis. CTC1 mutations that cause CP have been identified across the CTC1 gene with the majority ocurring within the OB-fold domains [58]. Some phenotypes of these mutants overlap, such as the ability to interact with pol α, which is essential for CST stimulation of pol α activity. However, other functions of CTC1 are more localized to specific areas, such as the C-terminus which is important for CTC1-STN1 interaction, or OB-B and D which are important for preventing telomere elongation [93]. Engaging multiple OB-folds allows for dynamic and high affinity binding, and is proposed to facilitate "hand-off" of the DNA to other processing proteins depending on the needs of the cell [27]. For instance, after telomeres are elongated, CST promotes the inhibition of telomerase and stimulates pol α activity for fill-in of the C-strand to create duplex DNA and shorten the length of the G-overhang. This allows shelterin binding, t-loop formation, and protection of the telomere ends [58]. Since CST was shown to reverse resection at DSBs, we hypothesize that it could also do so at hyper-elongated telomeres [31, 121].

Thus far, we show that after CTC1 deletion, the telomere ends become over elongated and bound by RPA, leading to ATR localization to telomeres and activation of the DDR. Additionally, CTC1 regulates the ATR-CHK1 pathway by stabilizing TopBP1 levels in the cell. However, it is unclear whether CTC1 can also rescue these phenotypes to prevent genome instability. Therefore, we investigated the roles of CTC1 in activating and potentially reversing the telomeric DDR through a two-pronged approach. First, CTC1 was transiently expressed after these initial defects arise in $CTC1^{-/-}$ cells to determine whether $CTC1^{-/-}$ phenotypes can be rescued. Second, by using different CTC1 constructs with OB-fold mutations to assess the essential domains necessary for its various roles in promoting genome stability.

4.2 RESULTS

4.2A TRANSIENT CTC1 EXPRESSION PARTIALLY RESCUES RPA-γH2AX

During normal telomere replication, CST stimulates pol α activity to promote C-strand fill-in which provides a short G-overhang for POT1 to bind and inhibit ATR signaling. Previous studies and work presented here demonstrate that conditional deletion of CTC1 prevents C-strand fill-in resulting in over extended G-overhangs [37]. The endogenous POT1 pool is then exhausted and RPA accumulates on the telomeric ssDNA, thus promoting ATR activation and G2 arrest (Chapter 2). Since CST has a preference for G-rich sequences, we asked whether addback of CTC1 promotes pol α localization to the telomeres for C-strand fill-in to reverse the phenotypes of over elongated G-overhangs and ATR activation. We hypothesized that re-expressing CTC1 after the appearance of these phenotypes might reverse the over-extension of the G-overhang and rescue CTC1 KO related defects. CTC1 deletion results in decreased proliferation and partial G2 arrest

beginning 9 days after TAM treatment. Therefore, we transiently expressed pcDNA3-Flag-CTC1 for 48 h starting at 9 days after CTC1 KO. Flag-CTC1 expression was confirmed by IF with a transfection efficiency of about 30% (Figure 4.2). Flow cytometry analysis indicated that G2 arrest following CTC1 addback did not rescue the partial G2 arrest in $CTC1^{-/-}$ cells. Interestingly, addback of Flag-CTC1 resulted in increased G2 arrest and sub G1 population with both $CTC1^{F/F}$ and $CTC1^{-/-}$ backgrounds (Figure 4.2B). A possible explanation of this could be that CTC1 is needed in stoichiometric amounts to maintain the balance of genome stability.

Since CTC1 deletion results in over-elongated telomeres are bound by RPA and activate ATR signaling, we assessed pRPA and RPA-γH2AX colocalization by IF. We hypothesized that CTC1 addback could promote C-strand fill-in to prevent RPA binding and ATR signaling at telomeres. However, we found no significant changes in nuclei with 3 or more pRPA foci (Figure 4.8A), indicating that ATR is still activated. We next looked to see if CTC1 addback rescued telomeric RPA-γH2AX. We found a significant decrease in nuclei with 3 or more RPA-γH2AX foci after Flag-CTC1 expression (Figure 4.8B). While significant, it was not completely rescued to $CTC1^{F/F}$ levels. Although the RPA-γH2AX rescue is modest, this is an exciting result considering only a small subset of cells express Flag CTC1 (Figure 4.1). In future studies with this system, we will increase the transfection efficiency of the Flag-CTC1 construct to determine if this further decreases RPA-γH2AX foci. These preliminary results suggest that re-introducing CTC1 in $CTC1^{-/-}$ cells may rescue telomeric DDR through promoting C-strand fill-in and rescue of the over-extended G-overhangs.

4.2B CTC1 OB-FOLDS B-F ARE NECESSARY FOR PROPER CELL PROLIFERATION AND CELL CYCLE PROGRESSION

The use of OB-folds allows for high affinity and dynamic binding to different DNA substrates by CST [27-29, 62]. One explanation of this dynamic binding capability is that CTC1 has a core site that tightly binds G-rich ssDNA and then also secondary sites which can engage longer stretches of ssDNA [58]. Therefore, we hypothesize that the dynamic binding and/or high affinity binding of CTC1 to ssDNA is required for the localization of CST to telomeres or sites of genome-wide DNA damage or used in protein-protein interactions. To understand the role of the different OB-folds for CST function, we used four HCT116 $CTC1^{-/-}$ cell lines stably expressing CTC1 mutants with deletions of different OB-folds, which were graciously provided to us by Dr. Xuyang Feng. These mutants were created prior to the release of the cryo-EM structure of CST, using the predicted locations of the CTC1 OB-folds but align closely with the OB-fold predictions from the structure [58]. As seen in figure 4.4, these mutants target OB-folds B, C, D, and E/F as indicated. Like the HCT116 $CTC1^{F/F}$+Flag-CTC1 cell line used previously, all four mutant constructs are Flag-tagged to allow easy detection. We first analyzed the expression of the ΔOB-mutants by western blot (Figure 4.5A) and found that ΔOB-C, ΔOB-D, and ΔOB-E/F expressed at levels similar to full length Flag-CTC1. ΔOB-B levels, however, were lower than the others but are likely comparable with wild type CTC1 levels (see Figure 2.1).

After confirming expression of the ΔOB-mutants, we assessed cell proliferation and cell cycle progression in cells expressing CTC1 OB-fold mutants. We found that ΔOB-B and ΔOB-C did not rescue cell proliferation following CTC1 deletion. On the

other hand, ΔOB-D and ΔOB-E/F partially rescued cell proliferation. However, none of the mutants were able to rescue cell growth to levels of cells expressing full length Flag-CTC1 (Figure 4.5B). These results indicate that full length OB-C is essential for proper cell proliferation and OB-B could be important in normal cell growth. These findings suggest that the ability of CTC1 to properly promote genome stability is dependent on the presence of OB-folds B-F. However, we acknowledge that expression of the ΔOB-B mutant is lower than other rescue cell lines, and may not be at levels sufficient to restore function. Next, we examined the cell cycle by flow cytometry (Figure 4.6). Our preliminary results indicate that OB-B-F are all essential to prevent a partial G2 arrest (Figure 4.7). This suggests that the different OB-folds of CTC1 contribute to the inhibition of ATR-dependent G2 arrest.

4.2C CTC1 OB FOLDS C-F ARE DISPENSIBLE FOR TOPBP1 REGULATION

After conditional KO of CTC1, we observed a significant decrease in levels of the ATR-activating protein, TopBP1 (Figure 3.1). To test whether the OB-fold mutants were able to rescue TopBP1 levels in the CTC1 KO cells, we assessed TopBP1 levels in untreated and 2 h 2 mM HU treated cells. We found that expression of ΔOB-C, ΔOB-D, or ΔOB-E/F was sufficient to rescue TopBP1 expression to levels comparable to those in the $CTC1^{F/F}$ and $CTC1^{-/-}$+Flag-CTC1 (Figure 4.5) suggesting that the C-terminal domains are not involved in stabilizing TopBP1 levels.

4.3 DISCUSSION

CST promotes genome stability both at the telomeres and genome wide after DNA damage. Here, we were interested in whether CTC1 can rescue G-overhang elongation and began characterizing the roles of CTC1OB-folds in cell proliferation and

stabilizing TopBP1. In these preliminary studies, we found that CTC1 may promote C-strand fill-in of over elongated telomeric ssDNA reducing the amount of RPA-ssDNA and ATR-dependent DDR. Overall, this suggests that CTC1 may promote the protection of telomeres even after they have become over elongated through misregulation of telomerase activity. Future studies will assess whether CTC1 addback can rescue TopBP1 levels and ATR-CHK1 activation as well as whether specific OB-fold domains are required for the rescue of these phenotypes.

Through structural analysis of the different roles of CTC1 in genome stability, we saw that OB-folds B-F are essential for proper progression through the cell cycle and normal cell proliferation. OB-D-F were able to partially rescue cell growth, however this was still inhibited compared to $CTC1^{F/F}$. Additionally, we assessed the effects of OB-folds B-F on TopBP1 stability and found that OB-folds C-F are dispensable for the regulation of TopBP1. This result is surprising in particular in regard to the ΔOB-E/F mutant. OB-E contains the interacting site with the first STN1 wHTH domain, and as we saw previously, not only CTC1, but also STN1 deletion results in decreased TopBP1 expression. A few explanations for why these OB-folds are not necessary to maintain TopBP1 levels are as follows. First, CTC1-OB-G also interacts with STN1 through its singular OB-fold, and this may be sufficient to maintain CST complex formation. Second, CTC1 and STN1 may have separate mechanisms by which they maintain TopBP1 stability. Future work will continue to fine tune our understanding of the relation between CTC1 structure and function by examining CP patient mutations in studies similar to that done with the CTC1 OB-fold mutants.

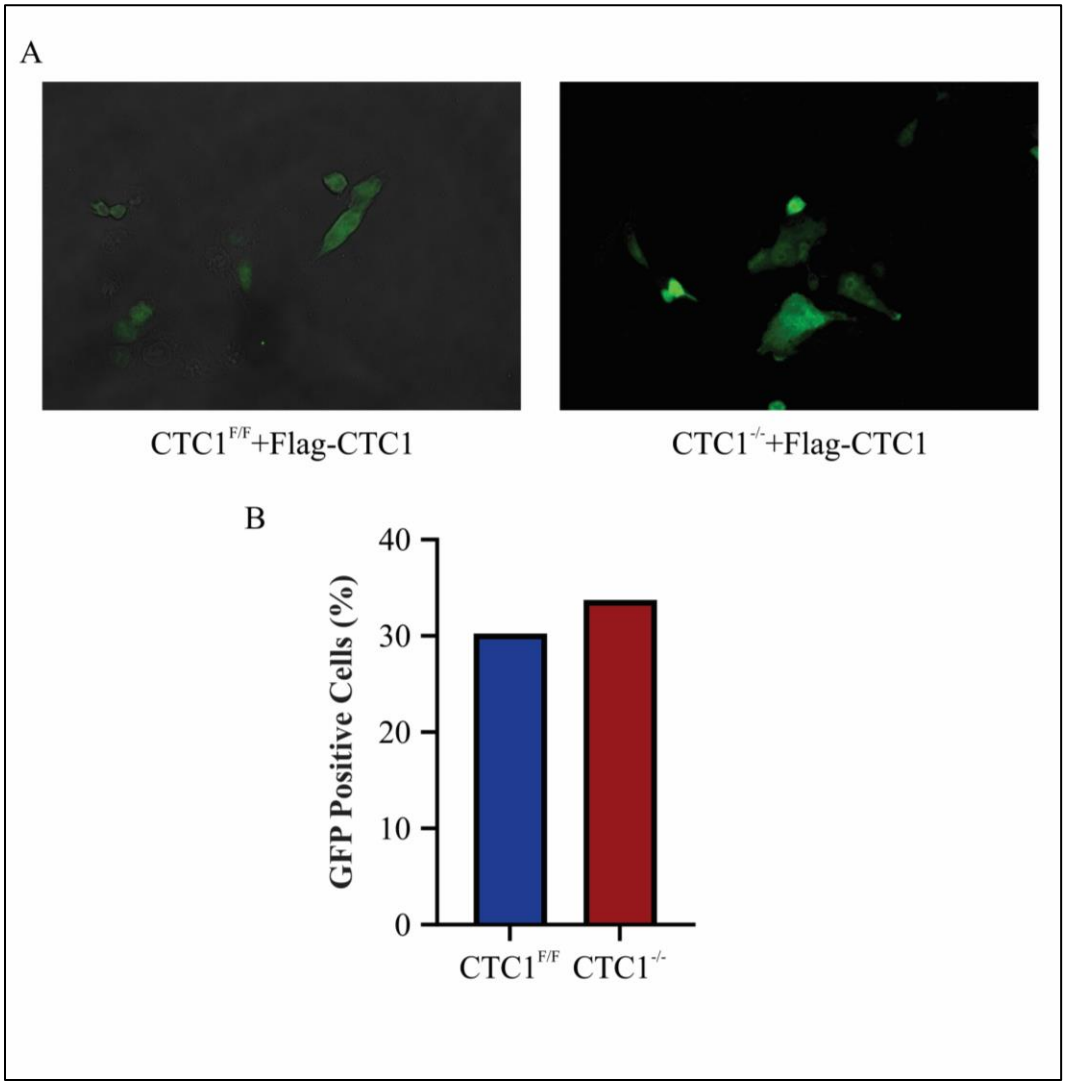

Figure 4.1 CTC1 addback transfection efficiency at day 11 in CTC1$^{-/-}$ cells. (A) Representative images of CTC1$^{F/F}$ and CTC1$^{-/-}$ cells after 48 h transfection with pcDNA3-Flag-CTC1. **(B)** Percentage of GFP positive cells, representing pcDNA3-Flag-CTC1 transfection efficiency. (n=1 biological replicate).

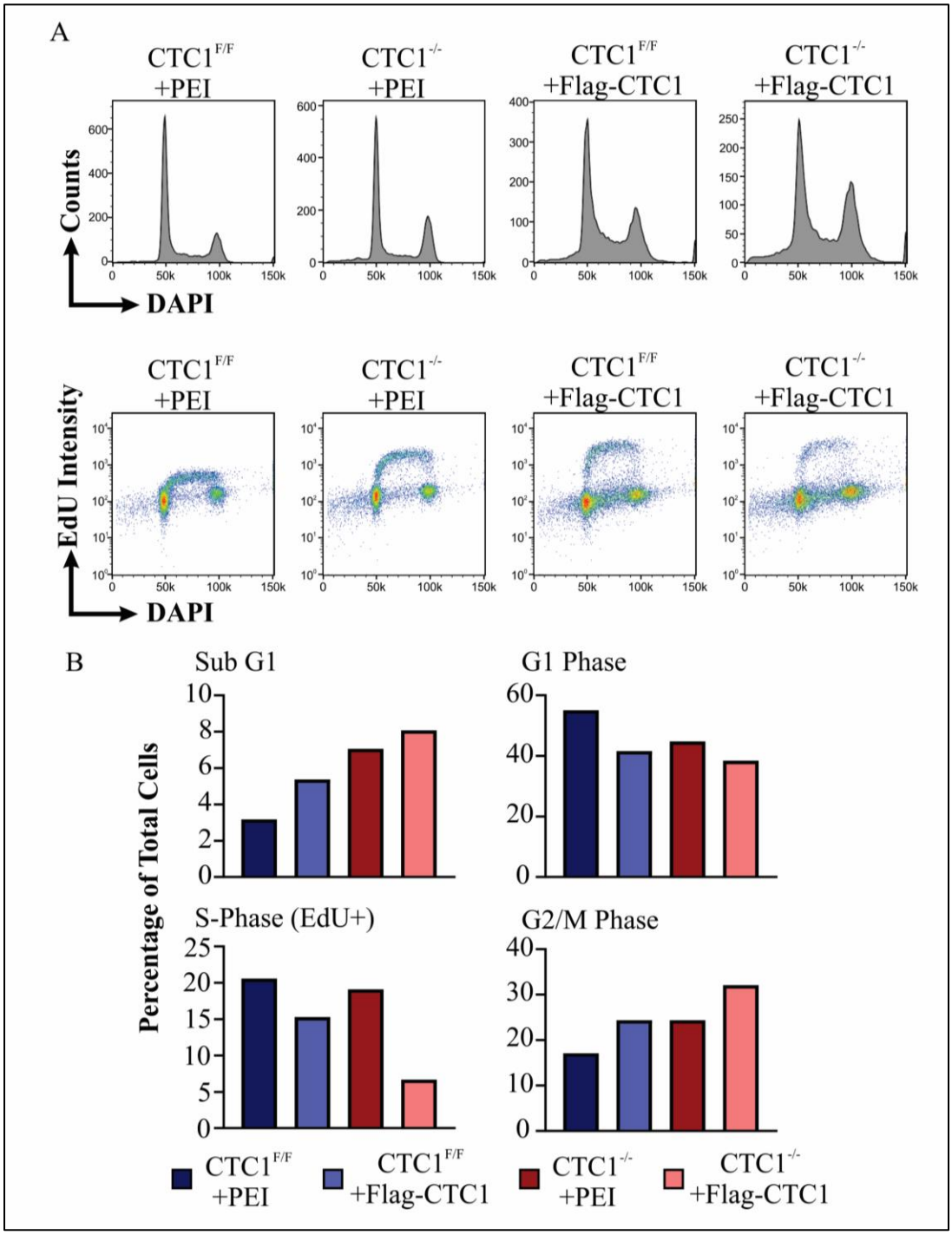

Figure 4.2 Flag-CTC1 transfection does not rescue CTC1 KO induced G2 arrest. (A) Representative histograms of flow analysis. Top panel: representative histograms from flow cytometry analysis showing DNA content versus cell count. Bottom panel: DNA content (DAPI) versus replicating cells (EdU+). **(B)** Cell cycle profile analysis at 11 days after TAM addition with 48 h exogenous pcDNA3-Flag-CTC1 (n=1 independent, biological replicate).

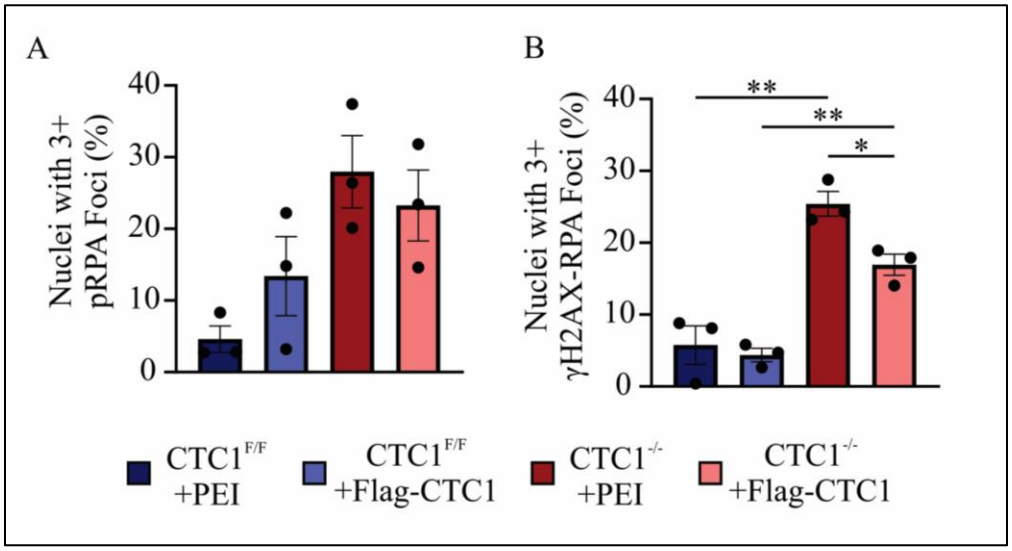

Figure 4.3 Exogenous CTC1 addback partially rescues γH2AX-RPA foci. (A) Percentage of nuclei with three or more pRPA foci 11 days after CTC1 KO with 48 h transfection. **(B)** Percentage of nuclei with greater than 3 co-localizing RPA-γH2AX foci. (n=3 independent, biological experiments). Error bars indicate the ±SEM. P-values were calculated by an unpaired, two tailed *t* test (*$P \leq 0.05$, **$P \leq 0.01$)

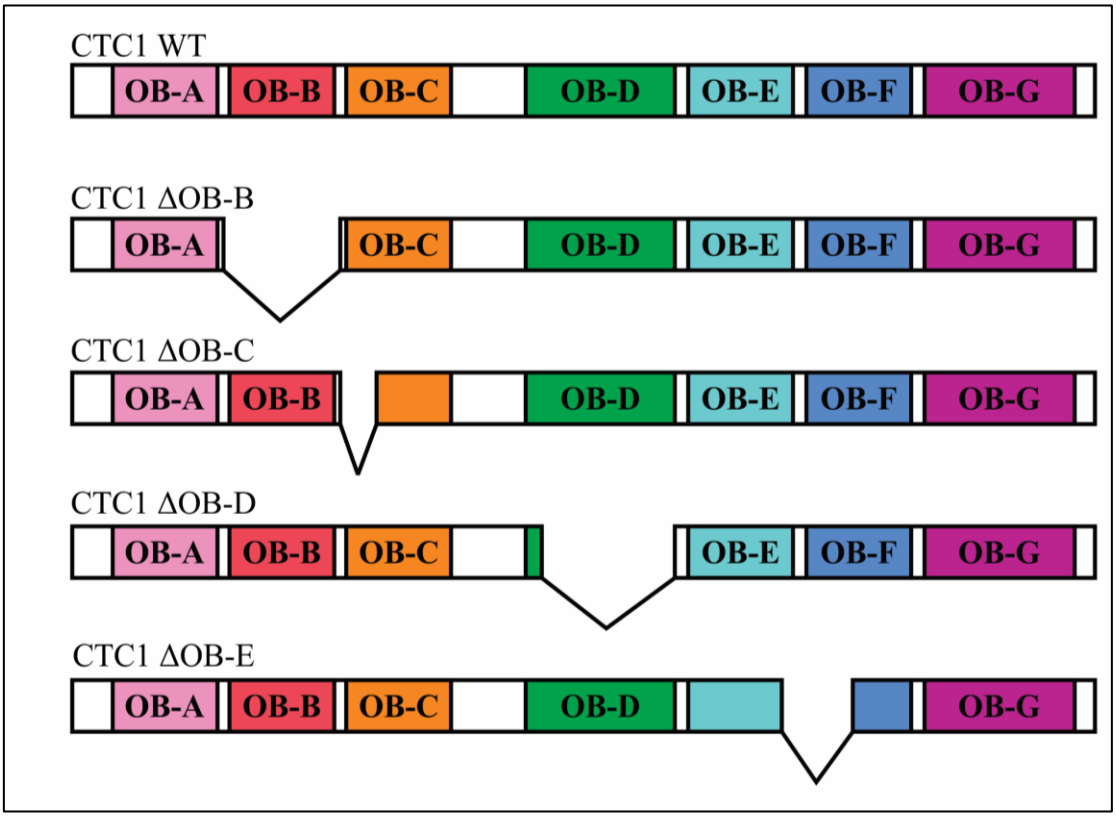

Figure 4.4 Schematic of ΔOB-Mutants in HCT116 CTC1$^{-/-}$ cells. For ΔOB-B amino acids 220-335, are deleted (all of OB-B). For ΔOB-C, aa 341-412 are deleted (the N-terminal portion of OB-C). For ΔOB-D, aa 609-702 are deleted (the majority of OB-D). For ΔOB-E/F, aa 851-921 are deleted (the C-terminus of OB-E and N-terminus of OB-F).

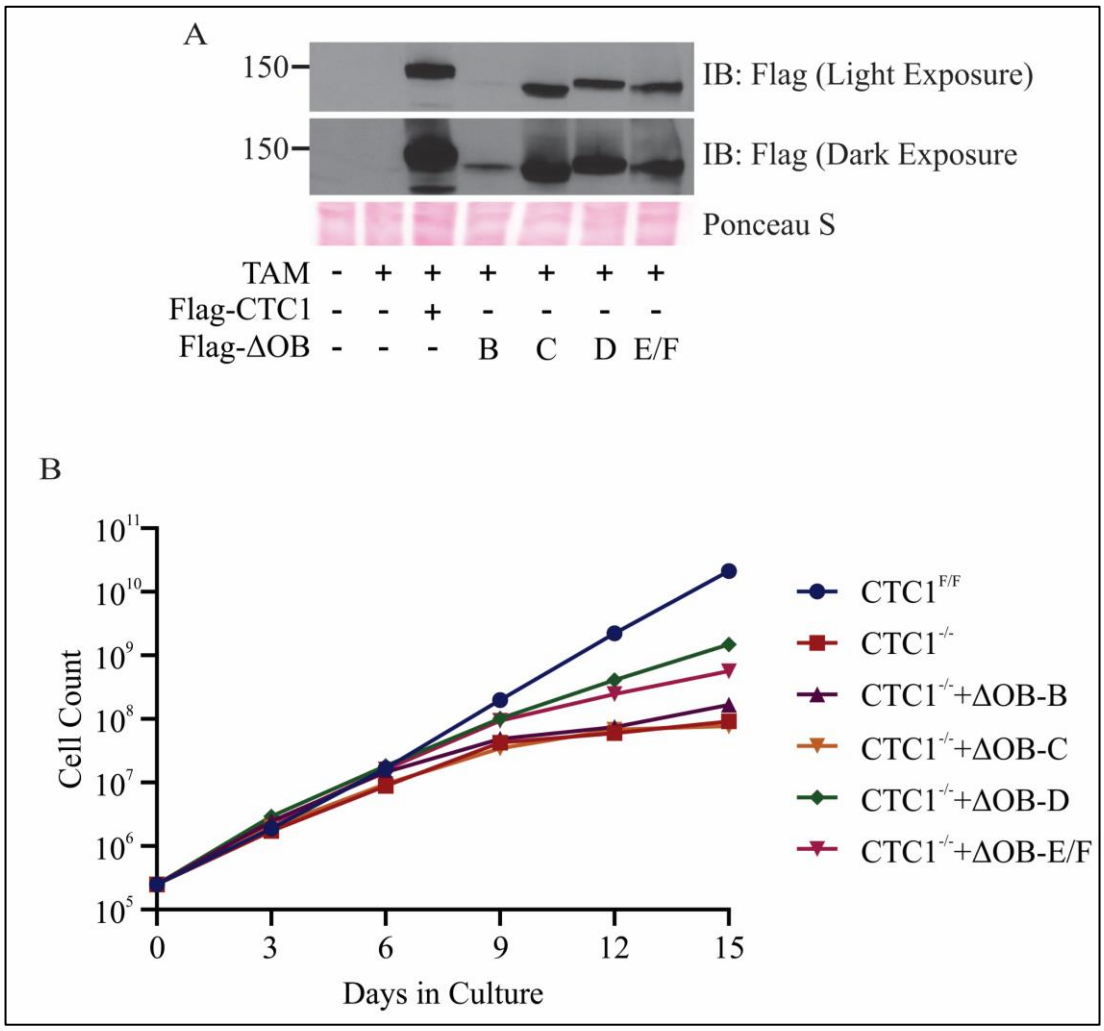

Figure 4.5 CTC1 OB-fold mutants partially rescue the CTC1 KO cell proliferation defect. (A) Western blot of Flag-tagged CTC1 WT and CTC1 OB-Mutants in HCT116 cells at day 11, as indicated. Ponceau S staining is a loading control. **(B)** Representative growth curve of CTC1 KO with Flag-CTC1 and Flag-OB-Mutants.

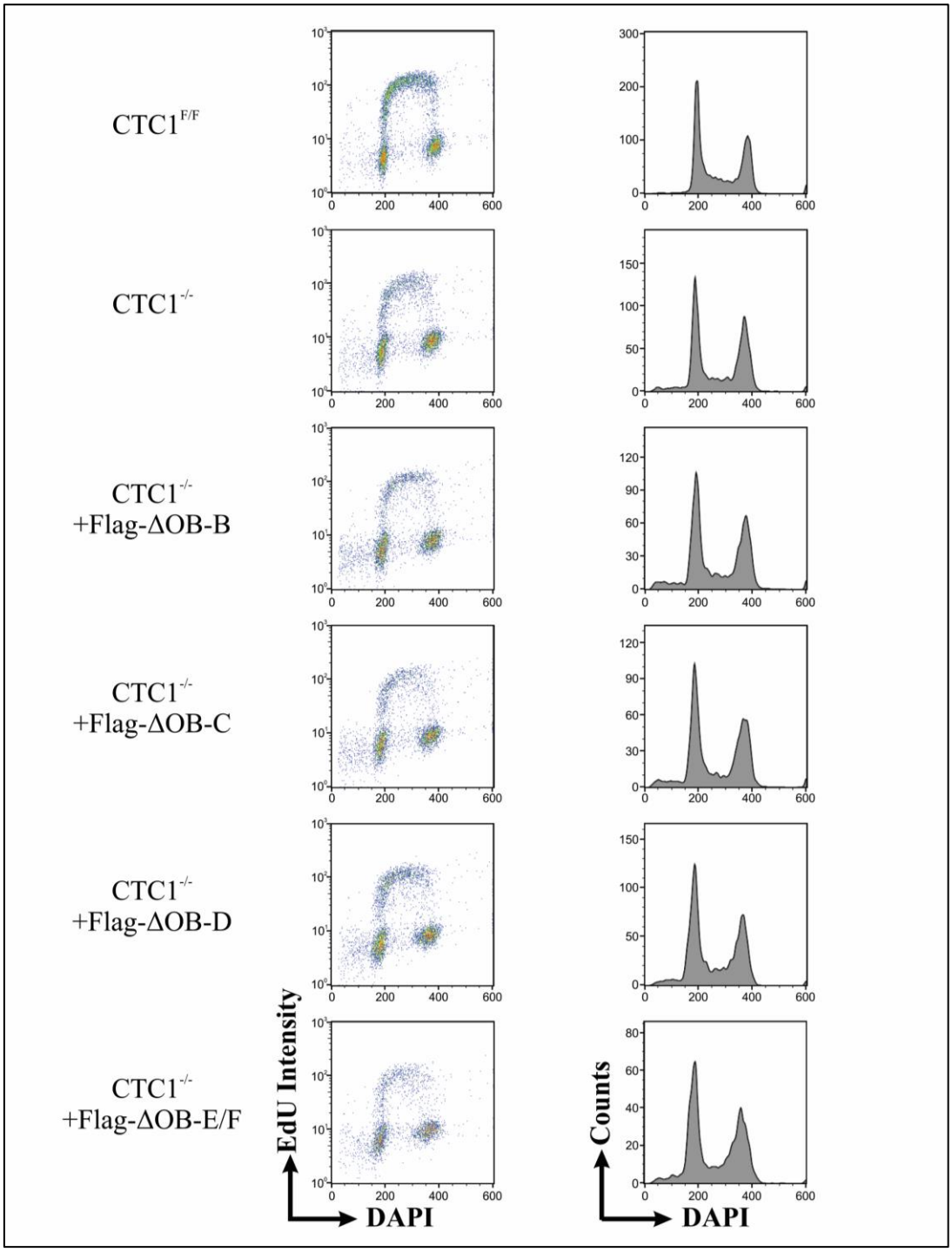

Figure 4.6 Cell cycle profile of CTC1$^{-/-}$ cells with OB-Mutant expression. Representative graphs from flow cytometry analysis. Left panel: DNA content (DAPI) versus replicating cells (EdU+). Right panel: representative histograms from flow cytometry analysis showing DNA content versus cell count.

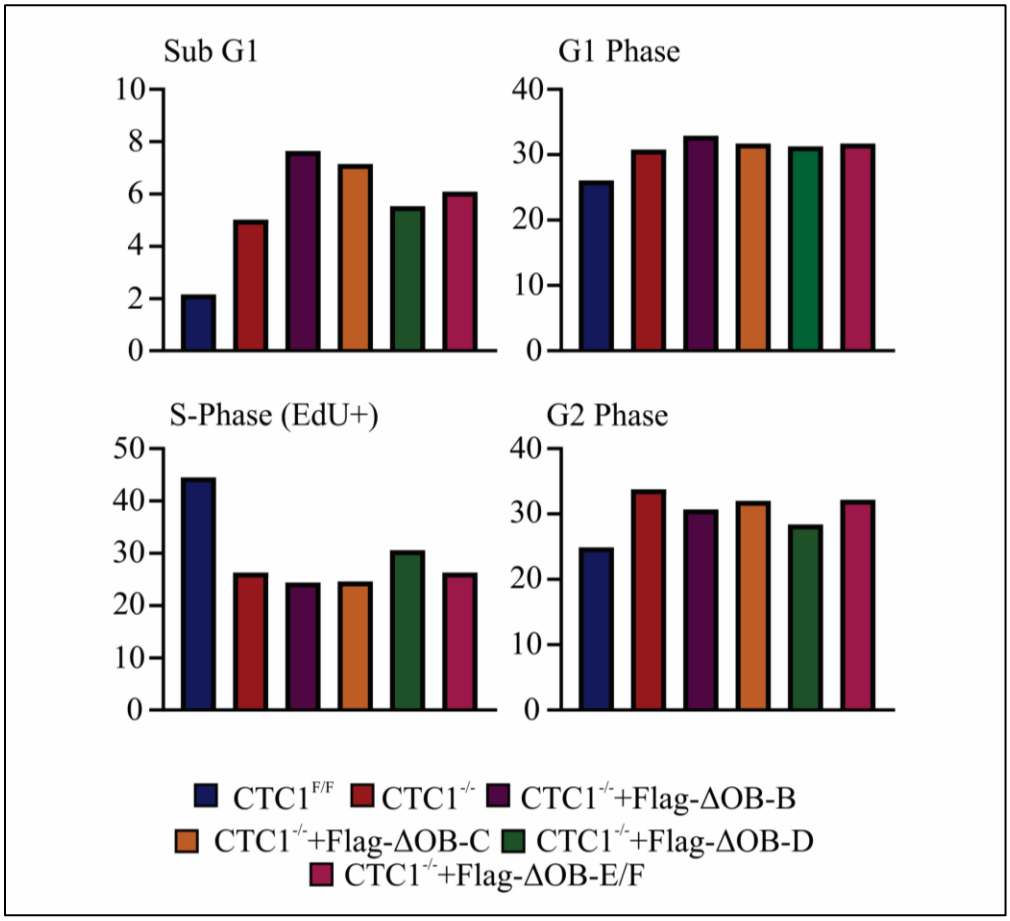

Figure 4.7 Addback of ΔOB-Mutants have limited effect on G2 arrest in CTC1$^{-/-}$ cells. Percentage of cells in each cell cycle phase, as indicated. (n=1 biological replicate).

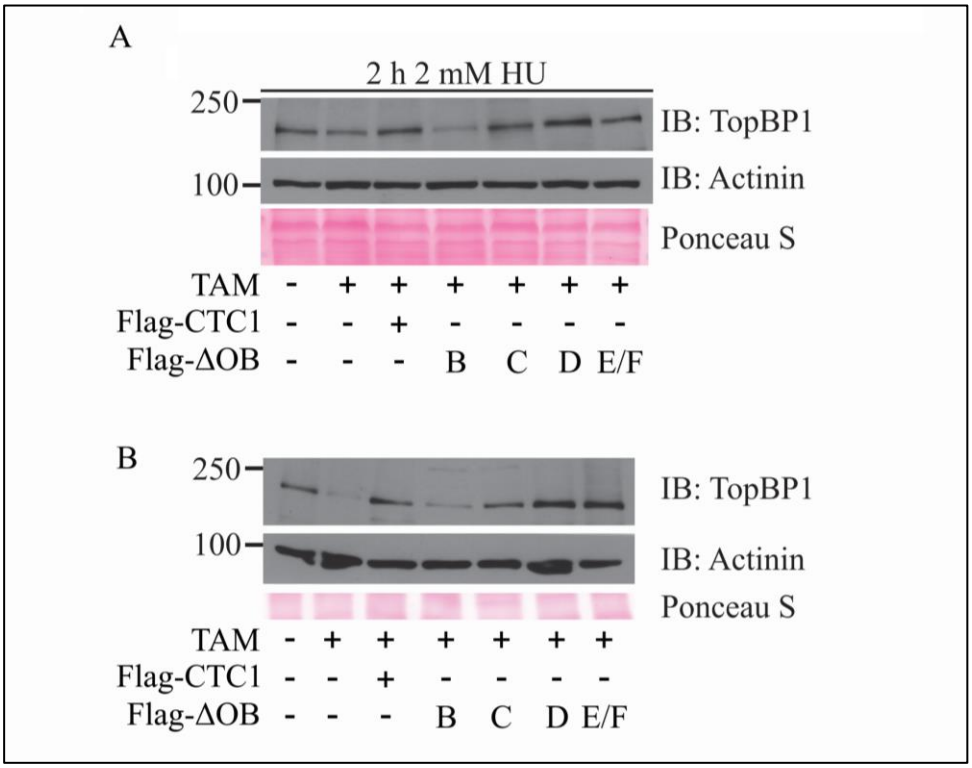

Figure 4.8 TopBP1 is partially rescued by expression of OB-fold mutants. (A) Western blot analysis of TopBP1 and pCHK1 S317 in whole cell lysates treated with 2 mM HU for 2 h just prior to collection. **(B)** Western blot analysis of TopBP1 in whole cell lysates. For **A and B,** extracts were collected at 11 days after TAM addition. Actinin and Ponceau S serve as loading controls.

CHAPTER 5

GENERAL CONCLUSIONS

Our understanding of the roles of CST has evolved over the years from its first discovery in yeast cells over 40 years ago [60, 61]. In *S. cerevisiae,* CST binds to the G-overhang and plays a primary role in end protection [122, 123]. However, in higher eukaryotes shelterin is the primary telomere capping protein[46]. For many years it was thought that CST had been lost in higher eukaryotes and replaced with the shelterin complex. However, in 2009, CST was discovered in plants and mammalian cells. In higher eukaryotes, STN1 and TEN1 share homology with their yeast counterparts, however, CTC1 and Cdc13 do not share homology [59, 62, 63]. This difference between the two CST complexes could possibly explain the more diverse roles of CST in higher eukaryotes versus *S. cerevisiae.* CST has conserved roles in inhibition of telomerase over-extension of the telomeres and in promoting C-strand fill in [45]. However, numerous studies have found that CST evolved additional telomere and non-telomeric functions. For instance, it promotes telomere replication through melting of secondary structures (G4s) [27, 54]. Genome-wide, CST can rescue replication fork stalling arising from endogenous and exogenous stresses, and aids in regulation of origin licensing [34, 45, 53]. Other evidence also indicates that CST is important for maintaining genome stability as CST depletion leads to anaphase bridges, chromatin cohesion loss, and micronuclei which may arise from telomeric or non-telomeric damage [63, 65]. Therefore, our main question was whether CST functions primarily at the telomere, genome-wide, or a combination of the two in order to prevent genome instability.

To get at this question we analyzed genome-wide DNA replication using DNA fiber analysis and found that CTC1 deletion does not affect replication speed, suggesting that CST has a more specialized role in promoting genome stability. A previous study

found that CTC1 deletion results in over-elongation of the G-overhang by kilobases in length [57]. Therefore, we wondered if the cell cycle arrest we see with CTC1 or STN1 deletion is instead due to the telomere defects. By overexpressing POT1 we found that the CTC1 KO induced growth defects were completely rescued. Under homeostatic conditions, telomerase adds ~10 telomeric hexanucleotide repeats before CST inhibits its activity and stimulates polα fill-in of the C-strand [55, 56]. However, we were curious as to whether CST can also work with polα to fill in on a much larger substrate, like those we see after CTC1 deletion. Our preliminary results suggest that adding back CTC1 after the telomeres have become elongated can partially rescue the over-elongated ssDNA. While further studies are required, this suggests that not only can CST prevent telomere over-elongation, but may also rescue consequences of telomere length regulation. Therefore, our work indicates that the genome instability we see in the absence of CST is likely due to dysregulation of the telomeres.

The overexpression of POT1 also rescued levels of telomeric RPA, therefore, we asked if the DDR goes through the canonical ATR pathway. ATR is the primary responder to ssDNA damage, and is localized to these damage sites through the interaction of ATRIP-ATR with RPA [2, 3, 8, 12]. However, this is not sufficient to fully activate ATR. TopBP1 is one of the two known ATR activating proteins and is independently localized to damage sites through its interaction with the 9-1-1 complex [16, 17]. After ATR is activated by TopBP1, it signals downstream to CHK1 and p53 [20-22]. We found that ATR is indeed localized to telomere-bound RPA and is responsible for the cell cycle defect we observed. However, we were surprised to find that ATR does not signal through the canonical ATR-CHK1 pathway. This suggests that

in response to long stretches of telomeric ssDNA, ATR doesn't signal to CHK1, but activates an unknown pathway. In support of this, the cell cycle arrest is ATR but not CHK1 or p53 dependent.

Since the canonical ATR-CHK1 pathway is not activated and is dependent on TopBP1 activation of ATR, we asked whether TopBP1 levels are compromised. TopBP1 is essential for cell survival, therefore we were shocked to find that TopBP1 levels are severely decreased in response to CTC1 or STN1 KO. We presumed that reintroducing TopBP1 would induce ATR-CHK1 signaling in response to over-elongated telomeres. However, we were surprised to find that even with sufficient levels of TopBP1, ATR was still unable to phosphorylate CHK1. This suggests that TopBP1 is not required to activate ATR in response to telomere damage and instead is activated and signals through a previously unknown pathway.

Our next question was whether the ATR-CHK1 pathway is also dysfunction in the event of genome-wide replication stress due to the decrease in TopBP1 stability or if this is a telomere specific response. Therefore, we induced replication for stalling resulting in stretches of ssDNA which we presumed would result in robust ATR-CHK1 signaling. However, we were surprised to find that CST also affects ATR signaling in response to genome wide replication stress by regulating TopBP1 stability. Unlike at the telomeres, restoring TopBP1 levels is sufficient to induce CHK1 phosphorylation in the absence of CST. Therefore, CST is essential for the activation of the canonical ATR-CHK1 signaling pathway in response to global DNA replication stress.

Our results suggest that there may be different pathways that ATR activates to respond to telomeric versus global DNA damage. This could possibly be due to the

limited substrates for the 9-1-1 complex to bind. 9-1-1 localizes to ds-ssDNA junctions, and the telomere, because it is the chromosome end, there is only one such junction to respond to kilobases worth of ssDNA. Another possibility is that shelterin binding blocks 9-1-1 localization [17]. These collectively could explain why even if we rescue TopBP1 levels, it would not affect telomeric ATR-CHK1 signaling because it is not involved in the telomeric ATR activation. Thus, there may be a yet to be discovered signaling cascade that is activated by ATR in response to telomere damage.

OB-folds function in protein-DNA and protein-protein interactions and proteins with multiple OB-folds can bind dynamically to their substrates. Therefore, we wondered how the multiple OB-fold domains of CTC1 affect its function. To this end we used OB-fold mutants with different domains deleted to asses cell proliferation and cell cycle progression. Our results indicate that each of the OB-folds is at least partially required for proper cell growth. Mutations in CTC1 underlie two telomeropathies, CP and DKC, with many of them falling within OB-fold domains. Therefore, future studies assessing the importance of these different domains will deepen our understanding of telomeropathies and the structure dependent functions of CST.

Overall, our results uncovered a novel link between the telomeric and non-telomeric roles of CST. For years, the different roles of CST have been viewed as two separate entities: telomere protection and genome-wide replication. However, this work indicates an essential link between the two. Unlike ATM and DNA-PK, ATR is essential in proliferating cells [1]. ATR promotes repair in the event of genome-wide replication stress, but also in responding to telomere over-elongation [1]. Our discovery that CST is essential to fully activate ATR not only in response to telomeric ssDNA, but also after

replication stress by stabilizing TopBP1 levels underscores the importance of CST in promoting genome stability. By manipulating these different, but synergistic roles of CST, we may be able to target the complex in diseases that hijack the DDR. The DDR is often dysregulated in cancer cells, and therefore they are reliant on maintaining a balance of continuous proliferation while preventing catastrophic levels of genome instability. Therefore, CST is a possible target which can tip the balance by possibly synergizing with ATR inhibitors to increase genome instability to a level unsustainable by cancer cells.

CHAPTER 6

MATERIALS AND METHODS

Cell Culture

HCT116 CTC1$^{F/F}$ and CTC1$^{F/F}$+Flag-CTC1 cells were generously provided by Dr. Carolyn Price [57] and were maintained in McCoy's 5A media supplemented with 10% fetal bovine serum and 1% penicillin/streptomycin at 37ºC with 5% CO_2. Cells were checked regularly for mycoplasma contamination. To induce Cre-ER mediated recombination of the CTC1 gene, a final concentration of 10 nM TAM was added to CTC1$^{F/F}$ and CTC1$^{F/F}$+Flag-CTC1 cells. The initial addition of TAM is indicated as day 0. At each passage, 10 nM TAM was again added to ensure CTC1 gene disruption. For siRNA knockdown, 5 nM ON-TARGETplus siRNA SMART pools to p53 (L-003329-00), ATM (L-003201-00-0005), ATR (L-003202-00-0005), CHK1 (L-003255-00-0005) or a non-targeting control (D-001810-10-05) (Dharmacon) were transfected into cells with Lipofectamine RNAiMAX (Thermo Fisher Scientific). siRNA treatment lasted 72 h and began on day 8 after TAM addition. For Flag-TopBP1 transfection, cells were plated 24 h before transfection in 100 mm dishes at 1x10^6 cells. 12.5 μg of pcDNA3-TopBP1 was mixed with 25 μl of Polyethylenimine (1 mg/ml) (Polysciences) in a total volume of 550 μl for each transfection. The pcDNA3-TopBP1 plasmid was generously provided by Dr. Weei-Chen Lin [124]. After 48 h, the cells were collected and whole cell protein extraction performed (see below).

Whole Cell Protein Extraction

Cell pellets were lysed, sonicated and nuclease-treated, as previously described [30]. The supernatant collected and protein concentration measured by BCA assay (Thermo Fisher). The samples were then mixed with SDS-PAGE loading buffer and analyzed by Western blot, as described below.

Subcellular Fractionation for Protein Extraction

Cell pellets were lysed in 200 µL Buffer A (10 mM HEPES pH 7.9, 10 mM KCl, 1.5 mM $MgCl_2$, 0.34 M Sucrose, 1 mM DTT, 0.1% Triton X-100, 1x phosphatase inhibitors [4 mM β-glycerophosphate, 4 mM sodium vanadate, and 20 mM sodium fluoride] and 1x protease inhibitors [1 µg/mL pepstatin A, 5 µg/mL leupeptin, 1 µg/mL E64, 2 µg/mL aprotinin, and 5 µg/mL antipain]) and incubated on ice for 10 min. Cell lysates were centrifuged at 4ºC 1300 *x g* for 5 min. The supernatant was transfered to a new tube and excess cell debris was removed by centrifugation at 20,000 *x g* for 15 min at 4ºC. The supernatant (souble fraction) was transfered to a new tube. Cell pellets containing nuclei were resuspended in 100 µl Buffer B (3 mM EDTA pH 8.0, 0.2 mM EGTA, 1 mM DTT, 1x phosphatase inhibitors, and 1x protease inhibitors) and incubated on ice for 30 min with mixing at 15 and 30 min. The samples were then centrifuged at 2,000 *x g* for 5 min at 4ºC and the supernatant containing the soluble nuclear fraction was transferred to a new tube. Cell pellets containing the chromatin bound fraction were resuspended in 100 µL Buffer A and then sonicated at 40% amplitude for 3 cycles of 10 seconds on and 5 seconds rest. Samples were then treated with Benzonase (0.0625 U/ µL; EMD Millipore) for 1 h on ice followed by centrifugation at 15,800 *x g* for 10 min at 4ºC and the supernatant saved as the chromatin fraction. Protein concentrations were determined with the BCA assay and samples analyzed by Western blot, as described below.

Western Blot Analysis

20-40 µg of protein were run by SDS-PAGE and transferred to a nitrocellulose membrane. All membranes were checked with Ponceau S staining for transfer efficiency

and total protein loading. Membranes to analyze CTC1 levels were blocked with 3% BSA in 1xPBS plus 0.1% Tween 20 (PBST) for at least 2 h, and all subsequent antibodies were diluted in 3% BSA-PBST. For analysis of CHK1 S317, membranes were blocked in 5% non-fat milk in 1xTBS plus 0.1% Tween 20 (TBST) for at least 2 h, and all subsequent antibodies were diluted in 5% non-fat milk-TBST. For all other western blots, membranes were blocked in 5% non-fat milk-PBST for at least 2 h. Primary antibodies were diluted in 5% non-fat milk-PBST and incubated at 4˚C overnight. The membranes were then washed 3 x for 10 min each in PBST (TBST for pCHK1 S317). Secondary antibodies were diluted in the solution indicated above for at least 2 h at room temperature. After incubation the blots were then developed with Western Lightning Plus ECL (Perkin Elmer) or ECL Prime (GE Healthcare).

Caspase-Glo 3/7 Assay

Active apoptosis was measured using the Promega Caspase-Glo 3/7 Assay (G8090), according to the manufacturer's instructions. DMSO or 5 μM VE-821 (ATRi) was added for 24 h, as indicated. Each treatment was performed in triplicate and at least three independent, biological replicates performed. The luciferase activity was measured on a Spectra Max i3 (Molecular Devices) and analyzed by Softmax Pro 6 (Molecular Devices).

Flow Cytometry

The cells were collected and washed with 1x PBS. After the supernatant was removed, 5 mL of ice-cold 100% methanol was added drop wise with gentle vortexing. Tubes were then placed at -20ºC for 10 min followed by centrifugation at 2000 *x g* for 5 min. The supernatant was removed and the cell pellets were washed with 5 mL 1x PBS

and centrifuged again at 2000 *x g* for 5 min. Cell pellets were then stored at 4ºC at least overnight.

To detect S-phase cells, EdU (50 μM) was added 30 min prior to collection. EdU was detected by Click-iT chemistry, according to the manufacturer's instructions (Thermo Fisher). Cells were resuspended in 250 μL of Click-iT reaction cocktail and incubated for 30 min at RT protected from light. 5 mL of 1% BSA-PBST was then added and samples were spun down at 1000 x *g* for 5 min and the supernatant removed. The cells were then resuspended in 650 μL of fresh DAPI Staining Solution (0.1% Triton X-100, 0.1 mg/mL RNase, 1 μg/mL DAPI diluted in 1 x PBS). The samples were spun at 50 *x g* for 30 s to remove cell clumps and debris through filter-capped tubes (Corning) and run on a BD LSR II Flow Cytometer in the Microscopy and Flow Cytometry Facility at the University of South Carolina, College of Pharmacy. At least 10,000 cells were analyzed per experiment.

RPA Flow Cytometry

Cells were collected and washed with 1x PBS. After the supernatant was removed, the cell pellets were resuspended in 500 μl 1x CSK buffer (10 mM HEPES pH 7.4, 300 mM sucrose, 100 mM NaCl, and 3 mM MgCl2 diluted in ddH2O) with 0.1% Triton-X and incubated at room temperature for 5 min. Then, with gentle vortexing, 5 mL of ice-cold 100% methanol was added to the tubes drop wise. Tubes were then placed at -20ºC for 10 min. Then 5 mL of 1% BSA-PBS was added to the samples followed by centrifugation at 2000 x g for 5 min. The supernatant was removed and the cell pellets were resuspended in 5 mL 1% BSA-PBS. Samples were then stored at 4ºC at least overnight. For analysis of chromatin-bound RPA, cells were centrifuged at 2000 x g for 5

min and the supernatant removed. The cell pellets were resuspended in 5 mL of 1% BSA-PBST and incubated at room temperature for 15 min. Samples were spun down at 1000 x g for 5 min. The supernatant was removed and the cell pellet was resuspended in 200 µL of RPA32 primary antibody diluted in 1% BSA-PBST (1:500). The samples were incubated with the primary antibody for at least 1 h at RT with mild vortexing halfway through incubation. 5 mL of 1% BSA-PBST was then added. Samples were spun down at 1000 x g for 5 min and the supernatant was removed. Cells were resuspended and incubated in 200 µL of goat α-mouse AlexaFluor 647 (1:500) in 1% BSA-PBST for at least 1 h at RT, protected from light, with mild vortexing halfway through incubation. Afterwards, 5 mL of 1% BSA-PBST was added and samples were spun down at 1000 x g for 5 min and the supernatant was removed.

DNA combing

Cells were labeled with IdU (50 µM) for 30 min, washed three times with 1x PBS and then labeled with CldU (100 µM) for 30 min. Cells were then collected, washed once with 1x PBS and diluted to ~3,300/µl. Agarose plugs were then made and prepared for DNA combing, as previously described (31127588). DNA fibers were combed on silanized coverslips according to the manufacturer's instructions (Genomic Vision). Coverslips were then baked at 80°C for 2 h, washed once with 1x PBS and denatured with 0.5 M NaOH/1 M NaCl for 8 min. Following two 1x PBS washes, the coverslips were blocked in 3% BSA/1x PBS for 30 min followed by incubation with two α-BrdU antibodies (Accurate Chemical [OBT0030] and BD [347580]) (1:100), each with specificity to either IdU or CldU, for 2 h at 37°C. After three PBST washes, goat α-mouse AlexaFluor 594 and goat α-rat AlexaFluor 488 (1:500) secondary antibodies were

incubated on the coverslips for 1 h at 37°C. Coverslips were washed three times with 1x PBST, dehydrated and mounted on slides with mounting media. Images were then taken under a 40x objective on an EVOS epifluorescence microscope (Thermo) and scored using ImageJ.

IF and IF-FISH

Cells were plated onto coverslips and allowed to grow for 24 hours to 50-70% confluency. 50 μM EdU was added for 30 min prior to collection. For detection of phosphorylated H2AX S140 (γH2AX), Histone H3 Ser10, and RPA32 Ser33, cells were fixed with 4% formaldehyde in 1 x PBS for 10 min at RT. After formaldehyde incubation, cells were rinsed twice with 1x PBS and then permeabilized with 0.5% Triton X-100 diluted in 1 x PBS for 10 min at RT. Slides were washed with 1 x PBS then stored 4˚C overnight in 1x PBS. For detection of chromatin-bound RPA32, cells were pre-extracted with 0.1% Triton X-100 in 1 x CSK buffer (10 mM HEPES pH 7.4, 300 mM Sucrose, 100 mM NaCl, 3 mM $MgCl_2$) for 5 min at room temperature. Slides were then washed once with 1 x PBS and fixed by adding 100% ice cold methanol. Slides were incubated at -20˚C for 10 min, washed with 1 x PBS and then stored at 4˚C overnight in 1x PBS. IF was then performed as previous described for γH2AX (1:5000), phosphorylated Histone H3 S10 (1:500), phosphorylated RPA32 S33 (1:1000) or RPA32 (1:500) [30]. Nuclear signal intensity of γH2AX was measured in ImageJ as previously described [30].

For IF-FISH, IF was performed for chromatin-bound RPA32, as described above. Telomere FISH was then performed, as previously described [125]. Briefly, after the last wash, following secondary antibody incubation, the coverslips were fixed with 2%

formaldehyde in 1x PBS for 10 min at RT. After two washes with 1x PBS, the coverslips were dehydrated and incubated with a telomeric G-strand PNA probe (AlexaFluor 488-$TTAGGG_3$; PNA Bio) in hybridization buffer (10 mM Tris pH 7.4, 70% formamide, 1% blocking reagent [Roche]) for 10 min at 80°C. Coverslips were then incubated at RT for 2-3 h followed by two washes in wash buffer (10 mM Tris pH 7.4, 70% formamide) for 15 min each. The coverslips were subsequently washed three times with 1x PBS, dehydrated and mounted on slides with mounting media containing 0.2 μg/ml DAPI. IF and IF-FISH images were then taken under 40x or 60x objectives on an EVOS epifluorescence microscope (Thermo). Foci and co-localizing foci were scored using ImageJ.

Antibodies and Chemical Inhibitors

Primary: CTC1 [57], STN1 (Abcam, 119263), Actinin (Santa Cruz, sc17829), α-Tubulin (Sigma, T-9026), ATM (Cell Signaling 2837), ATR (Cell Signaling 13934S), ATR T1989 (Cell Signaling 30632S), CHK1 (Bethyl, A300-298A), CHK1 S317 (Bethyl, A304-673A), CHK1 S345 (Cell Signaling, 2348T), p53 (Cell Signaling, 9282), p21 (Santa Cruz, sc-6246), H3 (Cell Signaling, 9715), pH3 S10 (Cell Signaling, 9706), Rad9 (Santa Cruz, sc-74464), RPA32 (Abcam, ab16850), pRPA32 S33 (Bethyl, A300-246A), TopBP1 (Bethyl, A300-111A), ETAA1 (kindly provided by Dr. David Cortez), γH2AX (Bethyl, A300-081A) and POT1 (Abcam, ab124784). Secondary: Thermo: anti-rabbit-HRP (32460); anti-mouse-HRP (32430); Molecular Probes: goat-anti-rabbit AlexaFluor 647 (A21244), goat-anti-mouse AlexaFluor 647 (A21235), goat-anti-mouse AlexaFluor 594 (A11032), goat-anti-rabbit AlexaFluor 594 (A11037). ATR inhibitor: VE-821 5 μM for 24 h (Selleckchem, S8007).

REFERENCES

1. Blackford, A.N. and S.P. Jackson, *ATM, ATR, and DNA-PK: The Trinity at the Heart of the DNA Damage Response.* Mol Cell, 2017. **66**(6): p. 801-817.
2. Saldivar, J.C., D. Cortez, and K.A. Cimprich, *The essential kinase ATR: ensuring faithful duplication of a challenging genome.* Nat Rev Mol Cell Biol, 2017. **18**(10): p. 622-636.
3. Brown, E.J. and D. Baltimore, *ATR disruption leads to chromosomal fragmentation and early embryonic lethality.* Genes Dev, 2000. **14**(4): p. 397-402.
4. de Klein, A., et al., *Targeted disruption of the cell-cycle checkpoint gene ATR leads to early embryonic lethality in mice.* Curr Biol, 2000. **10**(8): p. 479-82.
5. Byun, T.S., et al., *Functional uncoupling of MCM helicase and DNA polymerase activities activates the ATR-dependent checkpoint.* Genes Dev, 2005. **19**(9): p. 1040-52.
6. Raderschall, E., E.I. Golub, and T. Haaf, *Nuclear foci of mammalian recombination proteins are located at single-stranded DNA regions formed after DNA damage.* Proc Natl Acad Sci U S A, 1999. **96**(5): p. 1921-6.
7. Chen, R. and M.S. Wold, *Replication protein A: single-stranded DNA's first responder: dynamic DNA-interactions allow replication protein A to direct single-strand DNA intermediates into different pathways for synthesis or repair.* Bioessays, 2014. **36**(12): p. 1156-61.
8. Zou, L. and S.J. Elledge, *Sensing DNA damage through ATRIP recognition of RPA-ssDNA complexes.* Science, 2003. **300**(5625): p. 1542-8.
9. Lee, Y.C., et al., *RPA-Binding Protein ETAA1 Is an ATR Activator Involved in DNA Replication Stress Response.* Curr Biol, 2016. **26**(24): p. 3257-3268.
10. Bass, T.E., et al., *ETAA1 acts at stalled replication forks to maintain genome integrity.* Nat Cell Biol, 2016. **18**(11): p. 1185-1195.
11. Haahr, P., et al., *Activation of the ATR kinase by the RPA-binding protein ETAA1.* Nat Cell Biol, 2016. **18**(11): p. 1196-1207.
12. Kumagai, A., et al., *TopBP1 activates the ATR-ATRIP complex.* Cell, 2006. **124**(5): p. 943-55.
13. Thada, V. and D. Cortez, *Common motifs in ETAA1 and TOPBP1 required for ATR kinase activation.* J Biol Chem, 2019. **294**(21): p. 8395-8402.
14. Bass, T.E. and D. Cortez, *Quantitative phosphoproteomics reveals mitotic function of the ATR activator ETAA1.* J Cell Biol, 2019. **218**(4): p. 1235-1249.
15. Saldivar, J.C., et al., *An intrinsic S/G2 checkpoint enforced by ATR.* Science, 2018. **361**(6404): p. 806-810.
16. Delacroix, S., et al., *The Rad9-Hus1-Rad1 (9-1-1) clamp activates checkpoint signaling via TopBP1.* Genes Dev, 2007. **21**(12): p. 1472-7.

17. Lee, J., A. Kumagai, and W.G. Dunphy, *The Rad9-Hus1-Rad1 checkpoint clamp regulates interaction of TopBP1 with ATR.* J Biol Chem, 2007. **282**(38): p. 28036-44.
18. Acevedo, J., S. Yan, and W.M. Michael, *Direct Binding to Replication Protein A (RPA)-coated Single-stranded DNA Allows Recruitment of the ATR Activator TopBP1 to Sites of DNA Damage.* J Biol Chem, 2016. **291**(25): p. 13124-31.
19. Zhao, H. and H. Piwnica-Worms, *ATR-mediated checkpoint pathways regulate phosphorylation and activation of human Chk1.* Mol Cell Biol, 2001. **21**(13): p. 4129-39.
20. Liu, Q., et al., *Chk1 is an essential kinase that is regulated by Atr and required for the G(2)/M DNA damage checkpoint.* Genes Dev, 2000. **14**(12): p. 1448-59.
21. Tibbetts, R.S., et al., *A role for ATR in the DNA damage-induced phosphorylation of p53.* Genes Dev, 1999. **13**(2): p. 152-7.
22. Sorensen, C.S. and R.G. Syljuasen, *Safeguarding genome integrity: the checkpoint kinases ATR, CHK1 and WEE1 restrain CDK activity during normal DNA replication.* Nucleic Acids Res, 2012. **40**(2): p. 477-86.
23. Rundle, S., et al., *Targeting the ATR-CHK1 Axis in Cancer Therapy.* Cancers (Basel), 2017. **9**(5).
24. Bryan, C., et al., *Structure of the human telomeric Stn1-Ten1 capping complex.* PLoS One, 2013. **8**(6): p. e66756.
25. Lim, C.J., et al., *The structure of human CST reveals a decameric assembly bound to telomeric DNA.* Science, 2020. **368**(6495): p. 1081-1085.
26. Bhattacharjee, A., et al., *STN1 OB Fold Mutation Alters DNA Binding and Affects Selective Aspects of CST Function.* PLoS Genet, 2016. **12**(9): p. e1006342.
27. Bhattacharjee, A., et al., *Dynamic DNA binding, junction recognition and G4 melting activity underlie the telomeric and genome-wide roles of human CST.* Nucleic Acids Res, 2017. **45**(21): p. 12311-12324.
28. Hom, R.A. and D.S. Wuttke, *Human CST Prefers G-Rich but Not Necessarily Telomeric Sequences.* Biochemistry, 2017. **56**(32): p. 4210-4218.
29. Chen, L.Y., S. Redon, and J. Lingner, *The human CST complex is a terminator of telomerase activity.* Nature, 2012. **488**(7412): p. 540-4.
30. Wang, Y., et al., *Human CST suppresses origin licensing and promotes AND-1/Ctf4 chromatin association.* Life Sci Alliance, 2019. **2**(2).
31. Mirman, Z., et al., *53BP1-RIF1-shieldin counteracts DSB resection through CST- and Polalpha-dependent fill-in.* Nature, 2018. **560**(7716): p. 112-116.
32. Barazas, M., et al., *The CST Complex Mediates End Protection at Double-Strand Breaks and Promotes PARP Inhibitor Sensitivity in BRCA1-Deficient Cells.* Cell Rep, 2018. **23**(7): p. 2107-2118.
33. Chastain, M., et al., *Human CST Facilitates Genome-wide RAD51 Recruitment to GC-Rich Repetitive Sequences in Response to Replication Stress.* Cell Rep, 2016. **16**(7): p. 2048.
34. Stewart, J.A., et al., *Human CST promotes telomere duplex replication and general replication restart after fork stalling.* EMBO J, 2012. **31**(17): p. 3537-49.

35. Gu, P., et al., *CTC1 deletion results in defective telomere replication, leading to catastrophic telomere loss and stem cell exhaustion.* EMBO J, 2012. **31**(10): p. 2309-21.
36. Blackburn, E.H., *Structure and function of telomeres.* Nature, 1991. **350**(6319): p. 569-73.
37. Greider, C.W., *Telomeres.* Curr Opin Cell Biol, 1991. **3**(3): p. 444-51.
38. Makarov, V.L., Y. Hirose, and J.P. Langmore, *Long G tails at both ends of human chromosomes suggest a C strand degradation mechanism for telomere shortening.* Cell, 1997. **88**(5): p. 657-66.
39. McElligott, R. and R.J. Wellinger, *The terminal DNA structure of mammalian chromosomes.* EMBO J, 1997. **16**(12): p. 3705-14.
40. de Lange, T., *Shelterin-Mediated Telomere Protection.* Annu Rev Genet, 2018. **52**: p. 223-247.
41. Watson, J.D., *Origin of concatemeric T7 DNA.* Nat New Biol, 1972. **239**(94): p. 197-201.
42. Olovnikov, A.M., *A theory of marginotomy. The incomplete copying of template margin in enzymic synthesis of polynucleotides and biological significance of the phenomenon.* J Theor Biol, 1973. **41**(1): p. 181-90.
43. Frank, A.K., et al., *The Shelterin TIN2 Subunit Mediates Recruitment of Telomerase to Telomeres.* PLoS Genet, 2015. **11**(7): p. e1005410.
44. Pike, A.M., et al., *TIN2 Functions with TPP1/POT1 To Stimulate Telomerase Processivity.* Mol Cell Biol, 2019. **39**(21).
45. Stewart, J.A., et al., *Emerging roles of CST in maintaining genome stability and human disease.* Front Biosci (Landmark Ed), 2018. **23**: p. 1564-1586.
46. Giraud-Panis, M.J., et al., *CST meets shelterin to keep telomeres in check.* Mol Cell, 2010. **39**(5): p. 665-76.
47. Griffith, J.D., et al., *Mammalian telomeres end in a large duplex loop.* Cell, 1999. **97**(4): p. 503-14.
48. Drosopoulos, W.C., S.T. Kosiyatrakul, and C.L. Schildkraut, *BLM helicase facilitates telomere replication during leading strand synthesis of telomeres.* J Cell Biol, 2015. **210**(2): p. 191-208.
49. Sfeir, A., et al., *Mammalian telomeres resemble fragile sites and require TRF1 for efficient replication.* Cell, 2009. **138**(1): p. 90-103.
50. Huang, C., X. Dai, and W. Chai, *Human Stn1 protects telomere integrity by promoting efficient lagging-strand synthesis at telomeres and mediating C-strand fill-in.* Cell Res, 2012. **22**(12): p. 1681-95.
51. Kasbek, C., F. Wang, and C.M. Price, *Human TEN1 maintains telomere integrity and functions in genome-wide replication restart.* J Biol Chem, 2013. **288**(42): p. 30139-30150.
52. Boccardi, V., et al., *Stn1 is critical for telomere maintenance and long-term viability of somatic human cells.* Aging Cell, 2015. **14**(3): p. 372-81.
53. Wang, F., et al., *Human CST has independent functions during telomere duplex replication and C-strand fill-in.* Cell Rep, 2012. **2**(5): p. 1096-103.
54. Zhang, M., et al., *Mammalian CST averts replication failure by preventing G-quadruplex accumulation.* Nucleic Acids Res, 2019. **47**(10): p. 5243-5259.

55. Zhao, Y., et al., *Processive and distributive extension of human telomeres by telomerase under homeostatic and nonequilibrium conditions.* Mol Cell, 2011. **42**(3): p. 297-307.
56. Zhao, Y., et al., *Telomere extension occurs at most chromosome ends and is uncoupled from fill-in in human cancer cells.* Cell, 2009. **138**(3): p. 463-75.
57. Feng, X., et al., *CTC1-mediated C-strand fill-in is an essential step in telomere length maintenance.* Nucleic Acids Res, 2017. **45**(8): p. 4281-4293.
58. Lim, C.J. and T.R. Cech, *Shaping human telomeres: from shelterin and CST complexes to telomeric chromatin organization.* Nat Rev Mol Cell Biol, 2021. **22**(4): p. 283-298.
59. Casteel, D.E., et al., *A DNA polymerase-{alpha}{middle dot}primase cofactor with homology to replication protein A-32 regulates DNA replication in mammalian cells.* J Biol Chem, 2009. **284**(9): p. 5807-18.
60. Goulian, M. and C.J. Heard, *The mechanism of action of an accessory protein for DNA polymerase alpha/primase.* J Biol Chem, 1990. **265**(22): p. 13231-9.
61. Goulian, M., C.J. Heard, and S.L. Grimm, *Purification and properties of an accessory protein for DNA polymerase alpha/primase.* J Biol Chem, 1990. **265**(22): p. 13221-30.
62. Miyake, Y., et al., *RPA-like mammalian Ctc1-Stn1-Ten1 complex binds to single-stranded DNA and protects telomeres independently of the Pot1 pathway.* Mol Cell, 2009. **36**(2): p. 193-206.
63. Surovtseva, Y.V., et al., *Conserved telomere maintenance component 1 interacts with STN1 and maintains chromosome ends in higher eukaryotes.* Mol Cell, 2009. **36**(2): p. 207-18.
64. Simon, A.C., et al., *A Ctf4 trimer couples the CMG helicase to DNA polymerase alpha in the eukaryotic replisome.* Nature, 2014. **510**(7504): p. 293-297.
65. Wang, F., J. Stewart, and C.M. Price, *Human CST abundance determines recovery from diverse forms of DNA damage and replication stress.* Cell Cycle, 2014. **13**(22): p. 3488-98.
66. Noordermeer, S.M., et al., *The shieldin complex mediates 53BP1-dependent DNA repair.* Nature, 2018. **560**(7716): p. 117-121.
67. Vitor, A.C., et al., *Studying DNA Double-Strand Break Repair: An Ever-Growing Toolbox.* Front Mol Biosci, 2020. **7**: p. 24.
68. Ensminger, M. and M. Lobrich, *One end to rule them all: Non-homologous end-joining and homologous recombination at DNA double-strand breaks.* Br J Radiol, 2020. **93**(1115): p. 20191054.
69. Burma, S., B.P. Chen, and D.J. Chen, *Role of non-homologous end joining (NHEJ) in maintaining genomic integrity.* DNA Repair (Amst), 2006. **5**(9-10): p. 1042-8.
70. Sullivan, M.R. and K.A. Bernstein, *RAD-ical New Insights into RAD51 Regulation.* Genes (Basel), 2018. **9**(12).
71. Ranjha, L., S.M. Howard, and P. Cejka, *Main steps in DNA double-strand break repair: an introduction to homologous recombination and related processes.* Chromosoma, 2018. **127**(2): p. 187-214.
72. Briggs, T.A., et al., *Cerebroretinal microangiopathy with calcifications and cysts (CRMCC).* Am J Med Genet A, 2008. **146A**(2): p. 182-90.

73. Linnankivi, T., et al., *Cerebroretinal microangiopathy with calcifications and cysts.* Neurology, 2006. **67**(8): p. 1437-43.
74. Anderson, B.H., et al., *Mutations in CTC1, encoding conserved telomere maintenance component 1, cause Coats plus.* Nat Genet, 2012. **44**(3): p. 338-42.
75. Polvi, A., et al., *Mutations in CTC1, encoding the CTS telomere maintenance complex component 1, cause cerebroretinal microangiopathy with calcifications and cysts.* Am J Hum Genet, 2012. **90**(3): p. 540-9.
76. Bisserbe, A., et al., *Cerebro-retinal microangiopathy with calcifications and cysts due to recessive mutations in the CTC1 gene.* Rev Neurol (Paris), 2015. **171**(5): p. 445-9.
77. Netravathi, M., et al., *Whole exome sequencing in an Indian family links Coats plus syndrome and dextrocardia with a homozygous novel CTC1 and a rare HES7 variation.* BMC Med Genet, 2015. **16**: p. 5.
78. Romaniello, R., et al., *Cerebroretinal microangiopathy with calcifications and cysts associated with CTC1 and NDP mutations.* J Child Neurol, 2013. **28**(12): p. 1702-8.
79. Han, E., et al., *A unique case of coats plus syndrome and dyskeratosis congenita in a patient with CTC1 mutations.* Ophthalmic Genet, 2020. **41**(4): p. 363-367.
80. Liang, T., et al., *Ophthalmic findings and a novel CTC1 gene mutation in coats plus syndrome: a case report.* Ophthalmic Genet, 2021. **42**(1): p. 79-83.
81. Choudhury, A., et al., *Structural genomics approach to investigate deleterious impact of nsSNPs in conserved telomere maintenance component 1.* Sci Rep, 2021. **11**(1): p. 10202.
82. Passi, G.R., et al., *An Indian child with Coats plus syndrome due to mutations in STN1.* Am J Med Genet A, 2020. **182**(9): p. 2139-2144.
83. Acharya, T., et al., *Novel compound heterozygous STN1 variants are associated with Coats Plus syndrome.* Mol Genet Genomic Med, 2021: p. e1708.
84. Takai, H., et al., *A POT1 mutation implicates defective telomere end fill-in and telomere truncations in Coats plus.* Genes Dev, 2016. **30**(7): p. 812-26.
85. Simon, A.J., et al., *Mutations in STN1 cause Coats plus syndrome and are associated with genomic and telomere defects.* J Exp Med, 2016. **213**(8): p. 1429-40.
86. Keller, R.B., et al., *CTC1 Mutations in a patient with dyskeratosis congenita.* Pediatr Blood Cancer, 2012. **59**(2): p. 311-4.
87. Walne, A.J., et al., *Mutations in the telomere capping complex in bone marrow failure and related syndromes.* Haematologica, 2013. **98**(3): p. 334-8.
88. Holohan, B., W.E. Wright, and J.W. Shay, *Cell biology of disease: Telomeropathies: an emerging spectrum disorder.* J Cell Biol, 2014. **205**(3): p. 289-99.
89. Nelson, N.D. and A.A. Bertuch, *Dyskeratosis congenita as a disorder of telomere maintenance.* Mutat Res, 2012. **730**(1-2): p. 43-51.
90. Stanley, S.E. and M. Armanios, *The short and long telomere syndromes: paired paradigms for molecular medicine.* Curr Opin Genet Dev, 2015. **33**: p. 1-9.
91. Armanios, M. and E.H. Blackburn, *The telomere syndromes.* Nat Rev Genet, 2012. **13**(10): p. 693-704.

92. Gu, P. and S. Chang, *Functional characterization of human CTC1 mutations reveals novel mechanisms responsible for the pathogenesis of the telomere disease Coats plus.* Aging Cell, 2013. **12**(6): p. 1100-9.
93. Chen, L.Y., J. Majerska, and J. Lingner, *Molecular basis of telomere syndrome caused by CTC1 mutations.* Genes Dev, 2013. **27**(19): p. 2099-108.
94. Wang, Y., et al., *A gain-of-function senescence bypass screen identifies the homeobox transcription factor DLX2 as a regulator of ATM-p53 signaling.* Genes Dev, 2016. **30**(3): p. 293-306.
95. Angstadt, A.Y., et al., *A genome-wide approach to comparative oncology: high-resolution oligonucleotide aCGH of canine and human osteosarcoma pinpoints shared microaberrations.* Cancer Genet, 2012. **205**(11): p. 572-87.
96. Luo, Y.M., et al., *CTC1 increases the radioresistance of human melanoma cells by inhibiting telomere shortening and apoptosis.* Int J Mol Med, 2014. **33**(6): p. 1484-90.
97. Pinzaru, A.M., et al., *Telomere Replication Stress Induced by POT1 Inactivation Accelerates Tumorigenesis.* Cell Rep, 2016. **15**(10): p. 2170-2184.
98. Gyorffy, B., et al., *Online survival analysis software to assess the prognostic value of biomarkers using transcriptomic data in non-small-cell lung cancer.* PLoS One, 2013. **8**(12): p. e82241.
99. Feng, X., et al., *CTC1-STN1 terminates telomerase while STN1-TEN1 enables C-strand synthesis during telomere replication in colon cancer cells.* Nat Commun, 2018. **9**(1): p. 2827.
100. Chastain, M., et al., *Human CST Facilitates Genome-wide RAD51 Recruitment to GC-Rich Repetitive Sequences in Response to Replication Stress.* Cell Rep, 2016. **16**(5): p. 1300-1314.
101. Hendzel, M.J., et al., *Mitosis-specific phosphorylation of histone H3 initiates primarily within pericentromeric heterochromatin during G2 and spreads in an ordered fashion coincident with mitotic chromosome condensation.* Chromosoma, 1997. **106**(6): p. 348-60.
102. Marechal, A. and L. Zou, *RPA-coated single-stranded DNA as a platform for post-translational modifications in the DNA damage response.* Cell Res, 2015. **25**(1): p. 9-23.
103. McKinley, K.L. and I.M. Cheeseman, *Large-Scale Analysis of CRISPR/Cas9 Cell-Cycle Knockouts Reveals the Diversity of p53-Dependent Responses to Cell-Cycle Defects.* Dev Cell, 2017. **40**(4): p. 405-420 e2.
104. McKinley, K.L., *Employing CRISPR/Cas9 genome engineering to dissect the molecular requirements for mitosis.* Methods Cell Biol, 2018. **144**: p. 75-105.
105. Wan, M., et al., *OB fold-containing protein 1 (OBFC1), a human homolog of yeast Stn1, associates with TPP1 and is implicated in telomere length regulation.* J Biol Chem, 2009. **284**(39): p. 26725-31.
106. Liu, G., et al., *Replication fork stalling and checkpoint activation by a PKD1 locus mirror repeat polypurine-polypyrimidine (Pu-Py) tract.* J Biol Chem, 2012. **287**(40): p. 33412-23.
107. Churikov, D. and C.M. Price, *Pot1 and cell cycle progression cooperate in telomere length regulation.* Nat Struct Mol Biol, 2008. **15**(1): p. 79-84.

108. Denchi, E.L. and T. de Lange, *Protection of telomeres through independent control of ATM and ATR by TRF2 and POT1.* Nature, 2007. **448**(7157): p. 1068-71.
109. Kratz, K. and T. de Lange, *Protection of telomeres 1 proteins POT1a and POT1b can repress ATR signaling by RPA exclusion, but binding to CST limits ATR repression by POT1b.* J Biol Chem, 2018. **293**(37): p. 14384-14392.
110. Mailand, N., et al., *Rapid destruction of human Cdc25A in response to DNA damage.* Science, 2000. **288**(5470): p. 1425-9.
111. Jin, J., et al., *SCFbeta-TRCP links Chk1 signaling to degradation of the Cdc25A protein phosphatase.* Genes Dev, 2003. **17**(24): p. 3062-74.
112. Guo, C., et al., *Interaction of Chk1 with Treslin negatively regulates the initiation of chromosomal DNA replication.* Mol Cell, 2015. **57**(3): p. 492-505.
113. Liu, S., et al., *Claspin operates downstream of TopBP1 to direct ATR signaling towards Chk1 activation.* Mol Cell Biol, 2006. **26**(16): p. 6056-64.
114. Cortez, D., *Preventing replication fork collapse to maintain genome integrity.* DNA Repair (Amst), 2015. **32**: p. 149-157.
115. Petermann, E., et al., *Hydroxyurea-stalled replication forks become progressively inactivated and require two different RAD51-mediated pathways for restart and repair.* Mol Cell, 2010. **37**(4): p. 492-502.
116. Wardlaw, C.P., A.M. Carr, and A.W. Oliver, *TopBP1: A BRCT-scaffold protein functioning in multiple cellular pathways.* DNA Repair (Amst), 2014. **22**: p. 165-74.
117. Herold, S., et al., *Negative regulation of the mammalian UV response by Myc through association with Miz-1.* Mol Cell, 2002. **10**(3): p. 509-21.
118. Honda, Y., et al., *Cooperation of HECT-domain ubiquitin ligase hHYD and DNA topoisomerase II-binding protein for DNA damage response.* J Biol Chem, 2002. **277**(5): p. 3599-605.
119. Feng, H., et al., *CK2 kinase-mediated PHF8 phosphorylation controls TopBP1 stability to regulate DNA replication.* Nucleic Acids Res, 2020. **48**(19): p. 10940-10952.
120. Lyu, K., A. Kumagai, and W.G. Dunphy, *RPA-coated single-stranded DNA promotes the ETAA1-dependent activation of ATR.* Cell Cycle, 2019. **18**(8): p. 898-913.
121. Ghezraoui, H., et al., *53BP1 cooperation with the REV7-shieldin complex underpins DNA structure-specific NHEJ.* Nature, 2018. **560**(7716): p. 122-127.
122. Grandin, N., S.I. Reed, and M. Charbonneau, *Stn1, a new Saccharomyces cerevisiae protein, is implicated in telomere size regulation in association with Cdc13.* Genes Dev, 1997. **11**(4): p. 512-27.
123. Grandin, N., C. Damon, and M. Charbonneau, *Ten1 functions in telomere end protection and length regulation in association with Stn1 and Cdc13.* EMBO J, 2001. **20**(5): p. 1173-83.
124. Liu, K., et al., *Regulation of p53 by TopBP1: a potential mechanism for p53 inactivation in cancer.* Mol Cell Biol, 2009. **29**(10): p. 2673-93.
125. Cesare, A.J., C.M. Heaphy, and R.J. O'Sullivan, *Visualization of Telomere Integrity and Function In Vitro and In Vivo Using Immunofluorescence Techniques.* Curr Protoc Cytom, 2015. **73**: p. 12 40 1-12 40 31.

APPENDIX A

CELL CYCLE PERMISSIONS TO USE ACCEPTED MAUSCRIPT

This contains portions of an Accepted Manuscript of an article published by Taylor & Francis in Cell Cycle on [2020 Dec], available online: http://www.tandfonline.com/[doi:10.1080/15384101.2020.1849979]

APPENDIX B

FRONTIERS IN BIOSCIENCE REPRINT PERMISSIONS

This contains portions of a Published Manuscript of an article published by Frontiers in Frontiers in Bioscience on [2018 Mar], available online: https://www.bioscience.org/2018/v23/af/4661/fulltext.htm

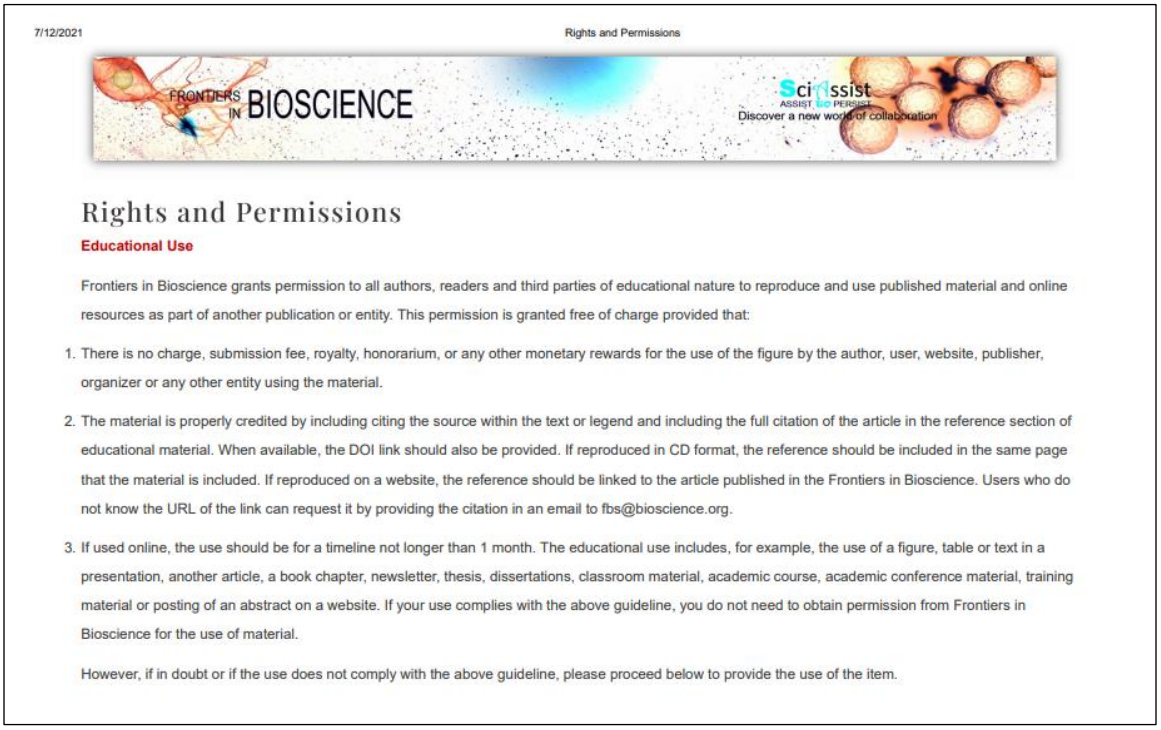

7/12/2021 Rights and Permissions

FRONTIERS IN BIOSCIENCE

SciAssist
ASSIST TO PERSIST
Discover a new world of collaboration

Rights and Permissions

Educational Use

Frontiers in Bioscience grants permission to all authors, readers and third parties of educational nature to reproduce and use published material and online resources as part of another publication or entity. This permission is granted free of charge provided that:

1. There is no charge, submission fee, royalty, honorarium, or any other monetary rewards for the use of the figure by the author, user, website, publisher, organizer or any other entity using the material.
2. The material is properly credited by including citing the source within the text or legend and including the full citation of the article in the reference section of educational material. When available, the DOI link should also be provided. If reproduced in CD format, the reference should be included in the same page that the material is included. If reproduced on a website, the reference should be linked to the article published in the Frontiers in Bioscience. Users who do not know the URL of the link can request it by providing the citation in an email to fbs@bioscience.org.
3. If used online, the use should be for a timeline not longer than 1 month. The educational use includes, for example, the use of a figure, table or text in a presentation, another article, a book chapter, newsletter, thesis, dissertations, classroom material, academic course, academic conference material, training material or posting of an abstract on a website. If your use complies with the above guideline, you do not need to obtain permission from Frontiers in Bioscience for the use of material.

However, if in doubt or if the use does not comply with the above guideline, please proceed below to provide the use of the item.

APPENDIX C

FRONTIERS IN CELL AND DEVELOPMENTAL BIOLOGY REPRINT PERMISSIONS

This contains portions of a Provisionally Accepted Manuscript of an article published by Frontiers in Frontiers in Cell and Developmental Biology on [2021 July], available online: https://www.frontiersin.org/articles/10.3389/fcell.2021.708763/abstract

1. Frontiers Policies

1.1. Open Access and Copyright

All Frontiers articles from July 2012 onwards are published with open access under the CC-BY Creative Commons attribution license (the current version is CC-BY, version 4.0). This means that the author(s) retains copyright, but the content is free to download, distribute, and adapt for commercial or non-commercial purposes, given appropriate attribution to the original article.

Upon submission, the author(s) grants Frontiers a license to publish, including to display, store, copy, and reuse the content. The CC-BY Creative Commons attribution license enables anyone to use the publication freely, given appropriate attribution to the author(s) and citing Frontiers as the original publisher. The CC-BY Creative Commons attribution license does not apply to third-party materials that display a copyright notice to prohibit copying. Unless the third-party content is also subject to a CC-BY Creative Commons attribution license, or an equally permissive license, the author(s) must comply with any third-party copyright notices.